ÉCOLE DE TECHNOLOGIE SUPÉRIEURE
UNIVERSITÉ DU QUÉBEC

THESIS PRESENTED TO
ÉCOLE DE TECHNOLOGIE SUPÉRIEURE

IN PARTIAL FULFILLMENT OF THE REQUIREMENTS FOR
THE DEGREE OF DOCTOR OF PHILOSOPHY
Ph.D.

BY
Olivier DUVAL

LOCALIZATION AND COOPERATIVE COMMUNICATION METHODS FOR COGNITIVE RADIO

MONTREAL, FEBRUARY 20, 2013

BOARD OF EXAMINERS

THIS THESIS HAS BEEN EVALUATED

BY THE FOLLOWING BOARD OF EXAMINERS:

M. François Gagnon, Thesis Director
Département de génie électrique à l'École de technologie supérieure

M. Jean Belzile, Thesis co-Director
Département de génie électrique à l'École de technologie supérieure

M. Eric Paquette, Committee President
Département de Génie Logiciel et des TI à l'École de technologie supérieure

M. Chahé Nerguizian, External Examiner
Département de génie électrique à l'École Polytechnique de Montréal

M. Ghyslain Gagnon, Examiner
Département de génie électrique à l'École de technologie supérieure

THIS THESIS WAS PRESENTED AND DEFENDED

IN THE PRESENCE OF A BOARD OF EXAMINERS AND PUBLIC

ON JANUARY 14^{TH}, 2013

AT ÉCOLE DE TECHNOLOGIE SUPÉRIEURE

ACKNOWLEDGEMENTS

To Jeanne, for her considerate support at every waking minute.

To François & Francine for closely following their son in his adventures since the beginning.

To my supervisor, professor François Gagnon, for letting me choose a new research path and for showing me how to navigate in the unknown.

To professor Ghyslain Gagnon, for his kindness, generosity and clever feedbacks; things are always simpler than they look.

To professor Vijay Bhargava, for welcoming me and reminding me how important it is to dose grunt work and soft skills well.

To Christian Talbot, for his help on the extensive field tests this work required, even in snow-covered fields.

To Ziaul, Gaurav, Hamid and Anjana for their friendship, their hard work, and for old times' sake.

LOCALIZATION AND COOPERATIVE COMMUNICATION METHODS FOR COGNITIVE RADIO

Olivier DUVAL

ABSTRACT

We study localization of nearby nodes and cooperative communication for cognitive radios.

Cognitive radios sensing their environment to estimate the channel gain between nodes can cooperate and adapt their transmission power to maximize the capacity of the communication between two nodes. We study the end-to-end capacity of a cooperative relaying scheme using orthogonal frequency-division modulation (OFDM) modulation, under power constraints for both the base station and the relay station. The relay uses amplify-and-forward and decode-and-forward cooperative relaying techniques to retransmit messages on a subset of the available subcarriers. The power used in the base station and the relay station transmitters is allocated to maximize the overall system capacity. The subcarrier selection and power allocation are obtained based on convex optimization formulations and an iterative algorithm. Additionally, decode-and-forward relaying schemes are allowed to pair source and relayed subcarriers to increase further the capacity of the system. The proposed techniques outperforms non-selective relaying schemes over a range of relay power budgets.

Cognitive radios can be used for opportunistic access of the radio spectrum by detecting spectrum holes left unused by licensed primary users. We introduce a spectrum holes detection approach, which combines blind modulation classification, angle of arrival estimation and number of sources detection. We perform eigenspace analysis to determine the number of sources, and estimate their angles of arrival (AOA). In addition, we classify detected sources as primary or secondary users with their distinct second-orde one-conjugate cyclostationarity features. Extensive simulations carried out indicate that the proposed system identifies and locates individual sources correctly, even at -4 dB signal-to-noise ratios (SNR).

In environments with a high density of scatterers, several wireless channels experience non-line-of-sight (NLOS) condition, increasing the localization error, even when the AOA estimate is accurate. We present a real-time localization solver (RTLS) for time-of-arrival (TOA) estimates using ray-tracing methods on the map of the geometry of walls and compare its performance with classical TOA trilateration localization methods. Extensive simulations and field trials for indoor environments show that our method increases the coverage area from 1.9% of the floor to 82.3 % and the accuracy by a 10-fold factor when compared with trilateration. We implemented our ray tracing model in C++ using the CGAL computational geometry algorithm library. We illustrate the real-time property of our RTLS that performs most ray tracing tasks in a preprocessing phase with time and space complexity analyses and profiling of our software.

Keywords: Cooperative Communications, Cognitive Radio, Ray-Tracing, Localization

MÉTHODES DE LOCALISATION ET DE COMMUNICATION COOPÉRATIVE POUR LA RADIO COGNITIVE

Olivier DUVAL

RÉSUMÉ

Une étude sur des applications de la radio cognitive pour la localisation et l'identification de radios à courte distance et les communications coopératives entre plusieurs radios est présentée.

Les radios cognitives analysant leur environnement pour estimer le gain du canal entre les nœuds peuvent coopérer et adapter leur puissance de transmission afin de maximiser la capacité du lien de communication entre deux nœuds. La capacité de communication entre deux noeuds coopérant avec un relais et utilisant une modulation orthogonal frequency-division frequency modulation OFDM, sous des contraintes de puissance d'émission pour la station de base et la station relais est étudiée. Le relais utilise une technique de relais par amplification et retransmission pour retransmettre des messages à un sous-ensemble de sous-porteuses disponibles. La puissance utilisée dans la station de base et les émetteurs des stations relais est distribuée de telle sorte que la capacité globale du système est optimisée. La sélection de sous-porteuse et l'attribution de puissance sont obtenues sur la base de formulations d'optimisation convexe et d'un algorithme itératif. De plus, des modèles de relais par décodage et retransmission incluent la possibilité de joindre les sous-porteuses de source à d'autres sous-porteuses relayées pour augmenter la capacité du système. Les technique proposées offre de meilleures performances de capacité que des méthodes de relais non sélectives pour une gamme de budgets de puissance du relais.

Les radios cognitives peuvent être utilisées pour un accès opportuniste au spectre radiofréquentiel en détectant les trous laissés vacants par des utilisateurs primaires licensés dans ces bandes. Nous introduisons une approche de détection de trous spectraux, qui combine la classification de modulation aveugle, l'estimation de l'angle d'arrivée (AOA) et la détection du nombre de sources. Nous effectuons une analyse des sous-espace propres pour déterminer le nombre de sources, et pour estimer leurs AOA. De plus, nous classons les sources détectées entre utilisateurs primaires ou secondaires avec leurs caractéristiques cyclostationnarires de second ordre et conjugué primaire. De nombreuses simulations réalisées indiquent que le système proposé identifie et localise les sources individuelles correctement, même à un rapport signal à bruit de -4 dB.

Dans les environnements impliquant une forte densité d'obstacles, plusieurs canaux sans fil n'ont pas de ligne de vue directe (NLOS), ce qui augmente considérablement l'erreur de localisation, même lorsque l'estimation d'AOA est exacte. Nous présentons un estimateur de localisation en temps réel (RTLS) basé sur des estimés de temps d'arrivée (TOA) en utilisant des méthodes de tracé de rayons sur la carte de la géométrie des murs et nous comparons ses performances avec les méthodes classiques de localisation de trilatération de temps d'arrivée. De nombreuses simulations et des essais sur le terrain pour de tels environnements intérieurs

montrent que notre méthode permet d'augmenter la zone de couverture de 1,9 % de la surface à 82,3 % et la précision d'un facteur de 10 par rapport à la trilatération.

Nous avons implémenté notre modèle de tracé de rayons en C++ en utilisant la bibliothèque CGAL d'algorithmes de géométrie computationelle. Nous démontrons, par une analyse théorique de la complexité spatiale et temporelle de l'algorithme et par un profilage de notre logiciel, comment nous pouvons maintenir la propriété "temps réel" de notre RTLS en effectuant la plupart des tâches associées au tracé de rayons dans une phase de prétraitement.

Mots-clés: Communication coopérative, Radio cognitive, Tracé de rayons, Localisation

CONTENTS

LIST OF TABLES

Page

LIST OF FIGURES

LIST OF ABBREVIATIONS

AOA	Angle Of Arrival
AWGN	Additive White Gaussian Noise
BPSK	Binary Phase Shift Keying
BS	Base Station
CC	Cyclic Cumulant
CDF	Cumulative Distribution Function
CF	Cyclic Frequency
CIR	Channel Impulse Response
CR	Cognitive Radio
ELVIS	Emitter Localization and VISualization
ETS	École de technologie supérieure
GPS	Global Positioning System
LOS	Line Of Sight
GSM	Global System for Mobile Communications
KKT	Karush–Kuhn–Tucker
MC	Modulation Classifier
MPSK	M-ary Phase Shift Keying
MS	Mobile Station
MUSIC	MUltiple SIgnal Classification
NLOS	Non Line Of Sight

OFDM	Orthogonal Frequency-Division Multiplexing
OFDMA	Orthogonal Frequency-Division Multiple Access
PSK	Phase Shift Keying
RMS	Root Mean Square
RMSE	Root Mean Square Error
RSS	Received Signal Strength
RT	Ray Tracing
RTLS	Real-Time Localisation Solver
SCLD	Single Carrier Linear Digital
SNR	Signal to Noise Ratio
TOA	Time Of Arrival
TWVP	Through Wall Visibility Polygon
UWB	Ultra Wide Band
VP	Visibility Polygon

INTRODUCTION

In the last 30 years, consumer demand for wireless communication devices has exploded into a more than one trillion dollars market for the mobile industry alone. Since the development of the first generation of mobile telephony, the scarcity of radio-frequency spectrum has been a major issue limiting the use of mobile devices for voice and data. Technological breakthroughs such as frequency reuse, code-division-multiple-access modulation schemes, and voice compression have helped expand mobile technology to billions of users worldwide. The recent development of smart phones and its internet access, as well as its numerous popular software applications has increased the demand for data traffic. The capacity of a communication channel is a limit on the data transmission that can be achieved with arbitrarily small error probability. Wireless communication systems with a higher capacity can then sustain more data traffic and potentially more subscribers, and produce larger profits for their operators.

A survey has shown that spectrum usage ranges from 15% to 85% in licensed bands under 6 GHz, while the rest of this licensed spectrum is wasted in many low traffic periods, frequency bands and areas known as spectrum holes [Cabric *et al.* (2004)]. Opportunistic access to these spectrum holes has been proposed as a method to further increase the spectrum available to wireless communication networks. Cognitive radios use sensors to analyze the changing radio environment in their vicinity and can adapt to these changes by modifying their data rates, transmission power, modulation scheme, and other parameters.

The first technology based on cognitive radios, IEEE 802.22, aims at reusing television broadcast bands to establish wireless regional area networks [Cordeiro *et al.* (2005)].

In this work, three aspects of wireless communications related to cognitive radio capabilities are studied: low-power communications, line-of-sight (LOS) localization & identification of uncooperative mobile nodes and non-line-of-sight (NLOS) localization in environments deeply cluttered with scatterers.

Transmission power is an important factor in the design and regulations governing the deployment of most radio devices worldwide. Mobile devices are battery-powered and their power

resources are limited, and several technological breakthroughs have targeted lowering battery usage while maintaining communication capabilities. Regulation agencies such as the Federal Communication Commission in the United States or the Canadian Radio-Television Telecommunication Council have also defined spectrum masks to which radio transmitting devices must comply prior to obtaining permits to operate in these countries. Low-power technologies such as Ultra-wideband tackle these two issues by limiting the transmission power to very low levels, but transmitting on large portions of the radio spectrum. A drawback for low-power communications is the lowering of communication capacity at ranges larger than several tens of meters in most cases. Cooperating wireless communication mobile devices or fixed repeaters acting as relays can help tackle this limitation.

Objective of the Thesis

This thesis aims at investigating several concepts permitting the practical integration of cognitive radios. Mainly, the objective is to propose constructive OFDM schemes and to exploit localisation to maximize the spectrum efficiency of communication strategies for real-world radio scenarios. The aim is constructive in the sense that the algorithms should be tractable and usable in real-time by small devices.

List of Contributions

The list of contributions of this thesis is intimately linked to the publications:

a. An optimal subcarrier and power allocation algorithm for OFDM relay links [Duval *et al.* (2010) and Boostanimehr *et al.* (2010)];

b. An angle-of-arrival and cyclostationarity feature detection method to localize and identify nearby radio nodes that offers high probability of localization and detection, even with channels with signal-to-noise ratios under -4 dB [Duval *et al.* (2008)];

c. A two-dimensional ray tracing software for calculating specular reflections on multiple obstacles [Duval *et al.* (2012)];

d. A real-time localization solver (RTLS) based on ray-tracing calculations improving the accuracy by a ten-fold factor and coverage from 2% to 81% in deeply occluded areas [Duval *et al.* (2012)].

Thesis Organization

This thesis aims at spectral spectrum holes identification end exploitation. Each chapter follows results published in [Duval *et al.* (2010) and Boostanimehr *et al.* (2010)] [Duval *et al.* (2008)], as well as ray-tracing investigation results submitted for publication.

The global cognitive radio scenario uniting the research topics reported in this thesis is detailed in chapter 1. This chapter also includes a litterary review on these topics.

In chapter 2, cooperative transmission power optimization methods are presented for several scenarios. In multiple-carrier cooperative communications networks, the power and subcarriers frequencies are shared between a source and a relay node. We propose power and subcarrier allocation methods that increases the capacity of state-of-the-art relay-assisted communications links.

Spatial spectrum holes offer another dimension for cognitive radios networks to increase their communication capacity without interfering with primary users. Radio devices equipped with antenna arrays, such as 802.11n or more recent versions of Wi-Fi technology, can adjust their radiation pattern to avoid interfering with primary users and maximize their transmission power in the direction of spatial spectrum holes. By doing so, the spectrum that would normally be wasted can now be used by cognitive radio operators to generate significant revenues by providing more services to end users. A prior step in this endeavour is to locate the position of nearby primary users.

Localization of mobile targets is a technological problem that has attracted a large amount of attention since its first use in air defense in the late 1930's. In the last 75 years, localization technology developers have reduced the costs and improved on the accuracy and coverage of military and civilian positioning systems. Nowadays, radar applications are used worldwide

in both civilian and military air traffic control and surveillance, and commercial applications of the global positioning system (GPS) are available worldwide. Nevertheless, a unified localization method able to position mobile devices accurately for indoor environments is not yet available.

Localization methods applied in the cognitive radio context do not count on the cooperation of primary users, and therefore can not take advantage of GPS receivers. However, since spatial spectrum hole cognitive radio systems require the use of antenna arrays, this equipment can also be used to estimate the angle of arrival (AOA) of transmission coming from primary users.

Since primary users do not cooperate with cognitive radios systems, their location has to be estimated before any spectrum hole can be exploited. However, several competing cognitive radio systems can field radio devices in the same area, which do not cooperate with each other. Since spectrum holes are only defined by primary users, nearby cognitive radio nodes must not be confused with primary users to identify all spatial spectrum holes.

In chapter 3 we present a joint localization and identification method for cognitive radios. In general, nodes in wireless communication networks do not have a direct path, and in some cases, a NLOS condition occurs which can potentially cause large positioning errors in real-time localization solvers (RTLS). However, commercial RTLS offer the possibility of including the map of these obstacles to help in improving their localization accuracy. We have developed a complete two-dimensional RTLS software using ray tracing techniques to exploit the geometry of these obstacles to cancel their effect on the localization accuracy. The developed software is presented in chapter 4 and improves the localization accuracy by a factor of ten over methods using no obstacles maps in heavily occluded areas. We also show that using the obstacles map increases the coverage area for one considered RTLS scenario from 2% to 81% of the floorplan.

CHAPTER 1

COGNITIVE RADIO CONCEPT AND LITTERATURE REVIEW

This chapter covers a general literature review of topics covered in this work. Every chapter will then offer a more detailed and contained literature review that will introduce each specific topic more thoroughly.

Digital communication systems include a transmitter device, a receiver device and a channel, and several basic blocks as shown on figure 1.1 [Proakis (2000)], on which the source encoder and decoder are used to reduce the impact of noise in the channel to the probability of error in transmitted messages. The modulator and demodulator pair is used to convert the information bits into parameters - frequency, amplitude, or phase - of one or multiple carrier waves. Radio communication systems operate on wireless channels and their access to the channel includes several radio-frequency analog electronic components, including antennas, filters and amplifiers, following technology-specific topologies.

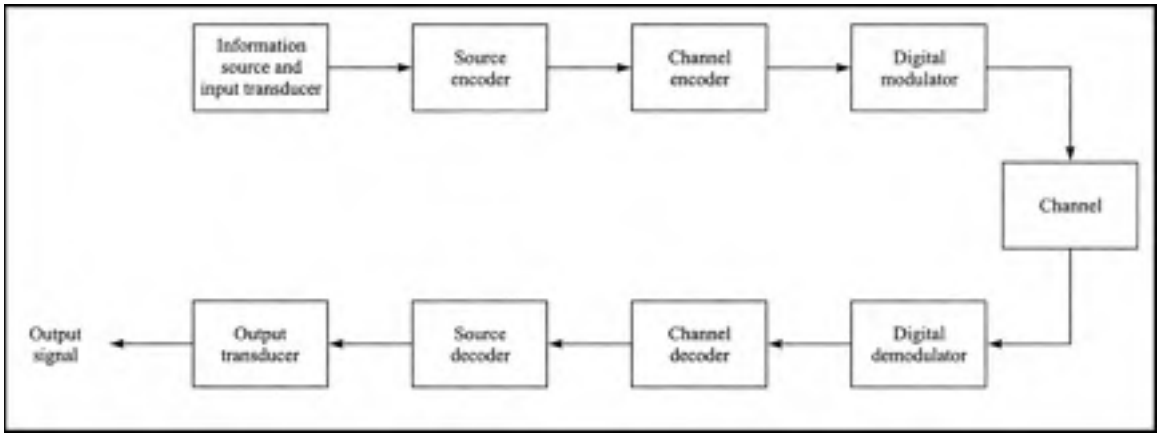

Figure 1.1 Basic elements of a digital communication system.

Software-defined radios include high performance analog-to-digital and digital-to-analog converters and replace some analog components with programs embedded on digital-signal-processors and field-programmable gate array circuits (Fig. 1.2 [Luo (2011)]). This technology offers a

greater flexibility than its analog counterpart, for its frequency of operation or filter characteristics can be modified by uploading a firmware update even when it is deployed on the field.

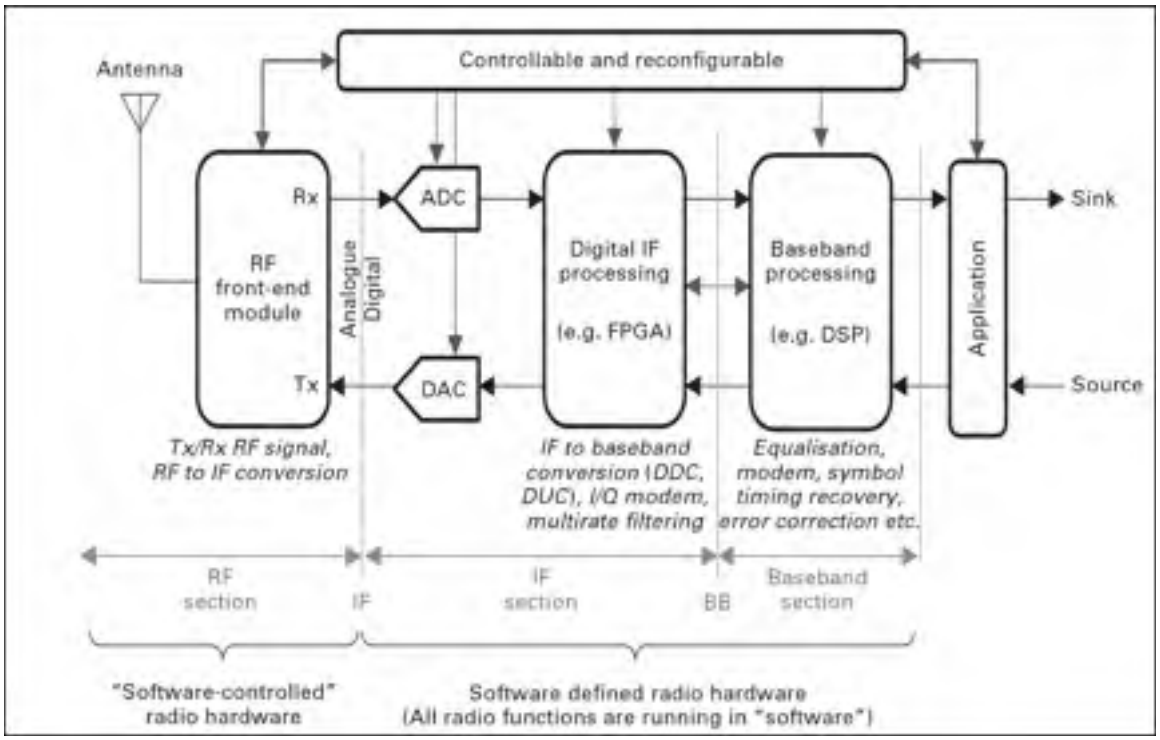

Figure 1.2 Basic elements of a software-defined radio architecture.

Cognitive radio is a concept that emerged as an extension of software-defined radio [Mitola (2000)] for radios using information about their environment to adapt their behavior for various ends.

Figure 1.3 [Haykin (2005)] illustrates the basic elements of the cognition cycle: sensors on the radio measure radio-frequency stimuli, another block is used to analyze the radio scene. A notable scene analysis object is the spectrum hole: a portion of licensed radio spectrum that is temporarily left unused by primary users, and which can be reused by cognitive radios. Another scene analysis element is the interference temperature, which is used for interference-controlled spectrum access cognitive policies. A cognitive radio can transmit in a frequency band if and only if it can guarantee that transmitting will not cause interference temperature to cross a pre-defined interference temperature threshold at primary users level [Haykin (2005); Bhargava and Hossain (2007)]. Under this opportunistic spectrum access scenario, the cogni-

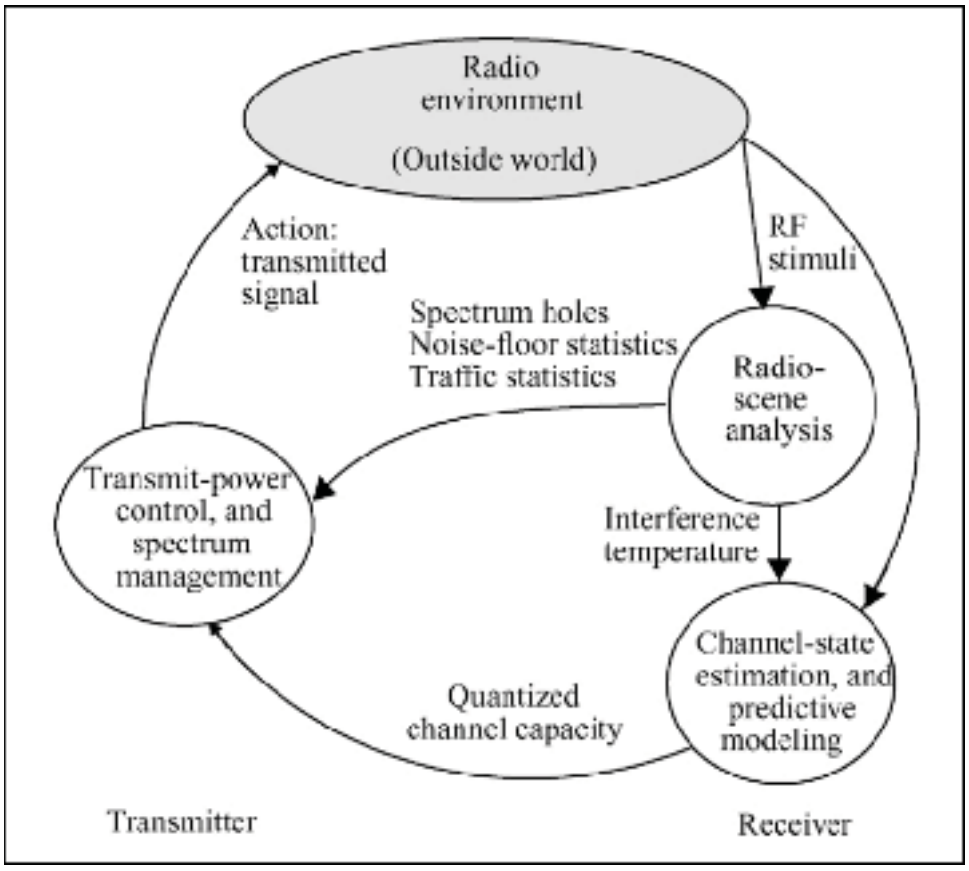

Figure 1.3 Basic cognition cycle.

tive radio plays a secondary user role, while nodes taking part in a licensed network play the role of primary users.

1.1 Basic Cognitive Radio Scenario

Several dimensions of the spectrum can be exploited by cognitive radios to communicate without causing harmful interference to primary users: time, frequency, space, interference temperature and others. In this work, we aim at exploiting the spatial dimension and interference temperature.

Figure 1.4 illustrates the location of primary users and cognitive radios for our basic scenario where friendly and competing cognitive radios, as well as primary users compete for radio spectrum at the same time and in the same frequency bands; only interference and spatial

spectrum holes can be exploited by cognitive radios to communicate. Apart from cooperative cognitive radio belonging to the same network, other cognitive networks can compete to seize spectrum holes, and do not require the same protection from interference as primary users do.

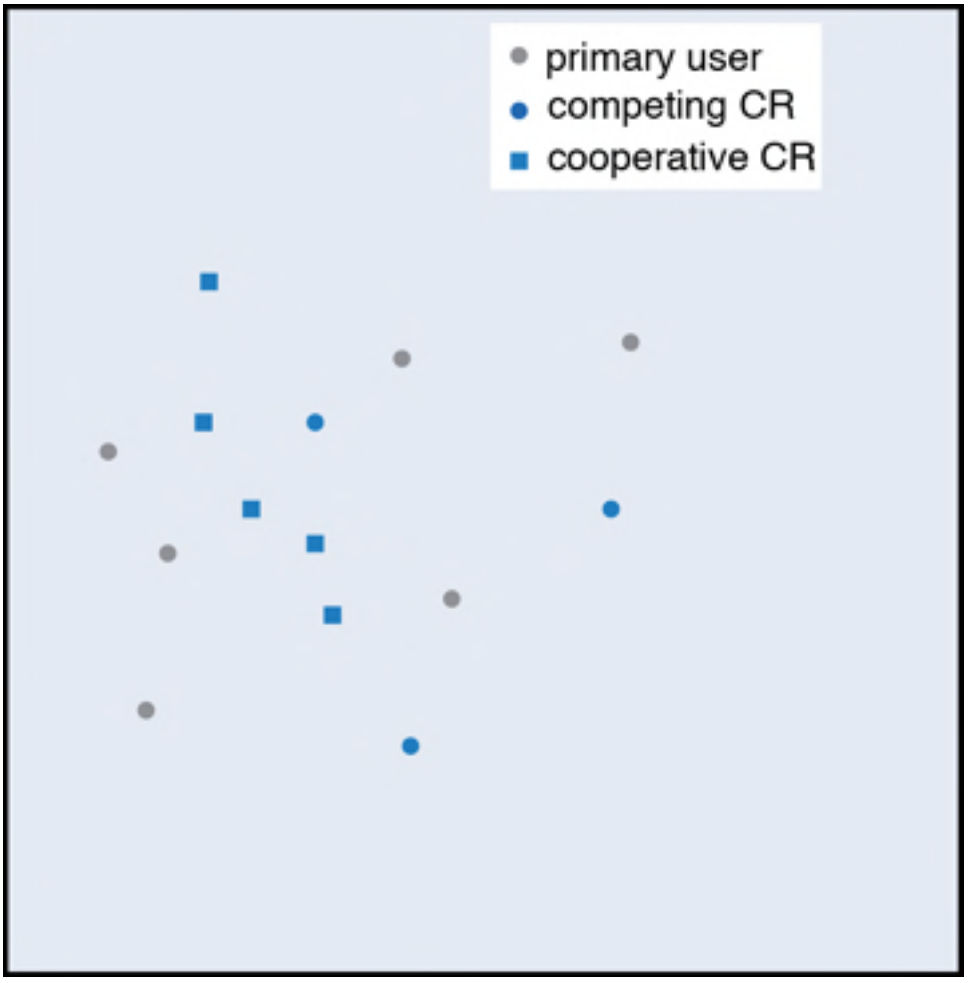

Figure 1.4 Cognitive Radio Basic Scenario.

1.2 Low Power Operation

One way to reduce the interference to primary users operating in the same bands as cognitive radios is to limit their transmission power to very low level and use wide frequency band, as in underlay schemes like ultra-wideband networks [Bansal *et al.* (2010)]. These power limitations could greatly limit the communication capacity of cognitive radio networks. Nevertheless, using a relay node, two nodes can improve their communication capacity under severe power

limitations. Figure 1.5 illustrates three cooperative nodes: a source node uses a relay node to communicate with a destination node.

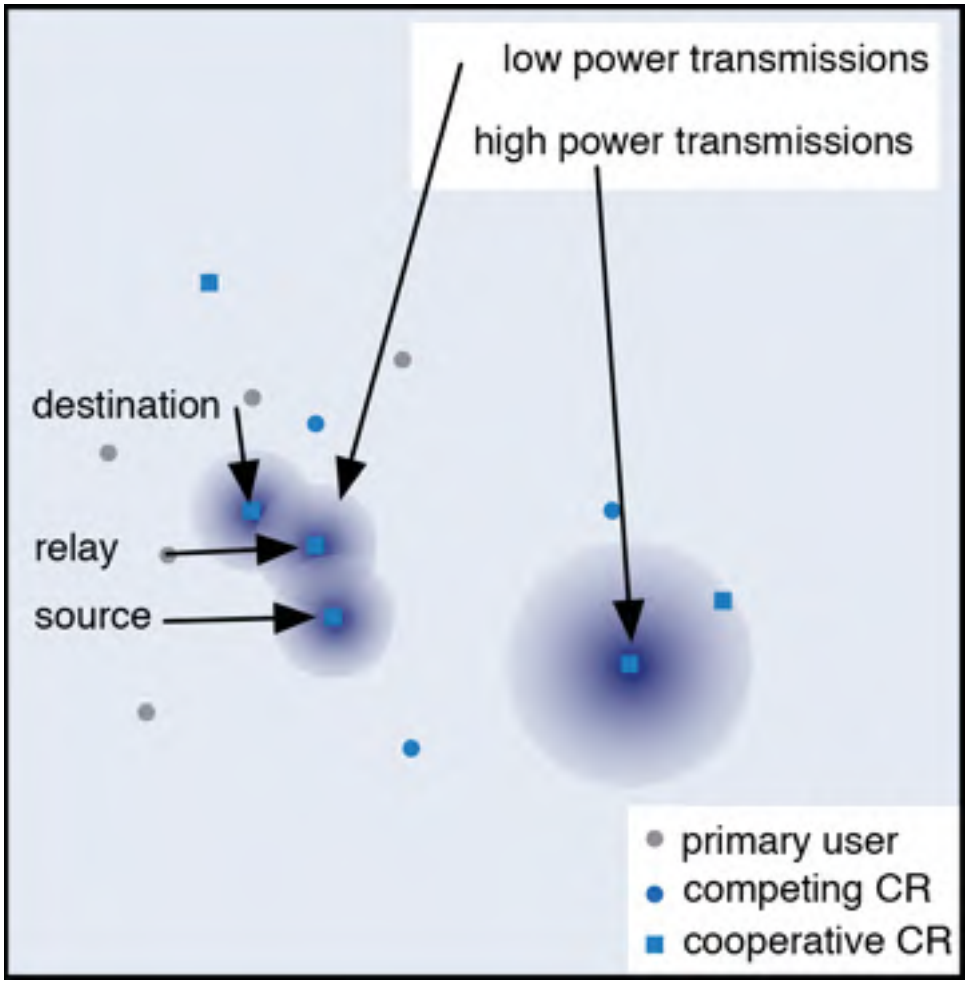

Figure 1.5 Low power communications in the vicinity of primary users.

Many wideband wireless channels experiment frequency-selective fading, and allocating more power to subcarriers with higher channel gains can improve their communication capacity. We consider an OFDM modulation scheme where a source and a relay node share N_{FFT} subcarriers using half-duplex signalling. Under this scenario, the source and relay nodes have different power budgets P_S and P_R to be divided among the channel's subcarriers.

Research on communications with relay links have been pioneered by [Van Der Meulen (1971)] and theoretical bounds for the capacity of relay additive white gaussian noise channels (AWGN)

have been derived by [Cover and Gamal (1979)]. More recently, the capacity for other AWGN relaying schemes has been studied: with feedback [Marina *et al.* (2008)], linear relaying [Del Coso and Ibars (2009)] and orthogonal channels [Liang and Veeravalli (2005), Liang *et al.* (2007), Liang and Kramer (2007)]

Several authors have derived the capacity of non-relaying channels experiencing frequency-selective Rayleigh fading. Resource allocation plays an important part in the capacity of these channels, as power is allocated to timeslots and frequency bands with higher channel gains [Li and Goldsmith (2001), Caire *et al.* (1999), Biglieri *et al.* (1998), Goldsmith and Varaiya (1997)].

Different signalling schemes have been studied for fading relay channels: decode-and-forward [del Coso and Ibars (2005), Siriwongpairat *et al.* (2006), Gunduz and Erkip (2007), Farhadi and Beaulieu (2008)], turbo codes [Hu and Duman (2007)], amplify-and-forward [Issariyakul and Krishnamurthy (2009)], stability [Jose *et al.* (2009)], multi-user [Rankov and Wittneben (2007)].

As it is the case for non-relaying channels, power allocation is a major component for maximizing the capacity of fading relay channels [Host-Madsen and Zhang (2005), Yu and Lui (2006), Hammerstrom and Wittneben (2007), Louveaux *et al.* (2008)]. In multiple carrier relay channels, resource allocation can include power and subcarrier selection [Li and Liu (2006), Bakanoglu *et al.* (2007), Hsu *et al.* (2011)].

Using the channel impulse response information on multi-carriers communications schemes, in chapter 2 we study schemes capable of maximizing the capacity of a wireless link by allocating power and frequency bands to the source and relay nodes. By carefully selecting the subcarriers on which the relay transmits and distributing the transmission power on these subcarriers, we obtain near-optimal capacity, and compare communication capacity with non-selective relaying methods as the ones described in this section.

We have developed a joint power and subcarrier allocation optimization method for amplify-and-forward cooperative communication scheme for fading relay channels using available channel state information.

1.3 Primary Users LOS-AOA Localization and Identification

Cognitive radios equipped with antenna arrays can direct their antenna transmission patterns away from primary users receivers to minimize the interference to primary users [Mouhamadou *et al.* (2006)]. In order to accomplish this task, cognitive radios must estimate the position of nearby users and direct their transmission power in directions unoccupied by primary users [Nasif (2009)]. Nearby radios can be other unlicensed cognitive radios, competing for the same spectrum, on which no interference regulations are enforced. By identifying competing cognitive radios, more spatial spectrum holes can be made available. Figure 1.6 illustrates a cognitive radio directing its power to an area only occupied by other unlicensed cognitive radios, cooperative or not.

Classical mobile localization methods include received signal strength (RSS), time-of-arrival (TOA) or angle-of-arrival (AOA) [Pahlavan and Levesque (2005)]. The AOA estimation has been studied for line-of-sight (LOS) multipath environments [Klukas and Fattouche (1998)], and applied for Global System for Mobile Communications (GSM) systems [Cesbron and Arnott (1998)]. Realistic primary user nodes deployment scenarios include more than one node to be detected and localized by a cognitive radio network. Fortunately, radios equipped with antenna arrays can improve on the detection of the number of nearby mobiles [Zhang *et al.* (1989), Hu *et al.* (1999a)].

Using higher-order statistical tests performed on signals emitted from nearby radios, it is possible to classify the different modulation schemes employed [Dobre *et al.* (2007)]. and more specifically, distinguish between single-carrier and multiple-carriers linear modulation schemes [Punchihewa *et al.* (2007)].

In cognitive radio networks, the interference to primary users is strictly enforced, while the interference to competing cognitive radios is not. Using nearby radios' modulation scheme

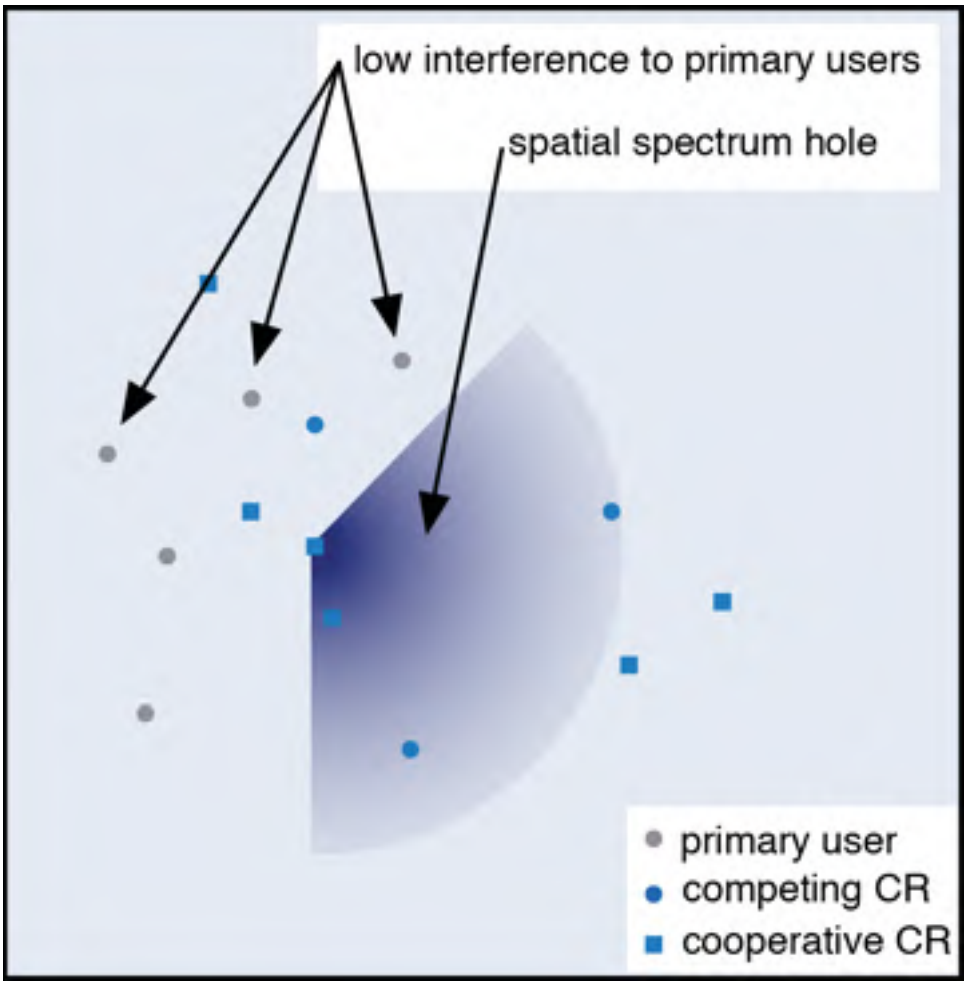

Figure 1.6 Exploiting a spatial spectrum hole with an antenna array-equipped CR.

pattern, it is then possible to mitigate whether they are primary users or competing cognitive radios. In chapter 3, we propose a joint angle-of-arrival (AOA) localization method for line-of-sight (LOS) environments combined with a modulation pattern identification method to localize primary users.

1.4 NLOS Localization using Ray Tracing

When obstacles such as walls block the direct path between nodes (Fig. 1.7), the resulting NLOS channel distorts RSS, TOA and AOA estimations, causing large localization errors in LOS estimators. Using a map showing the geometry of these obstacles can help in reducing

the impact of these distortions by tracing the path of waves reaching a cognitive radio receiver bouncing on walls back to their transmitter.

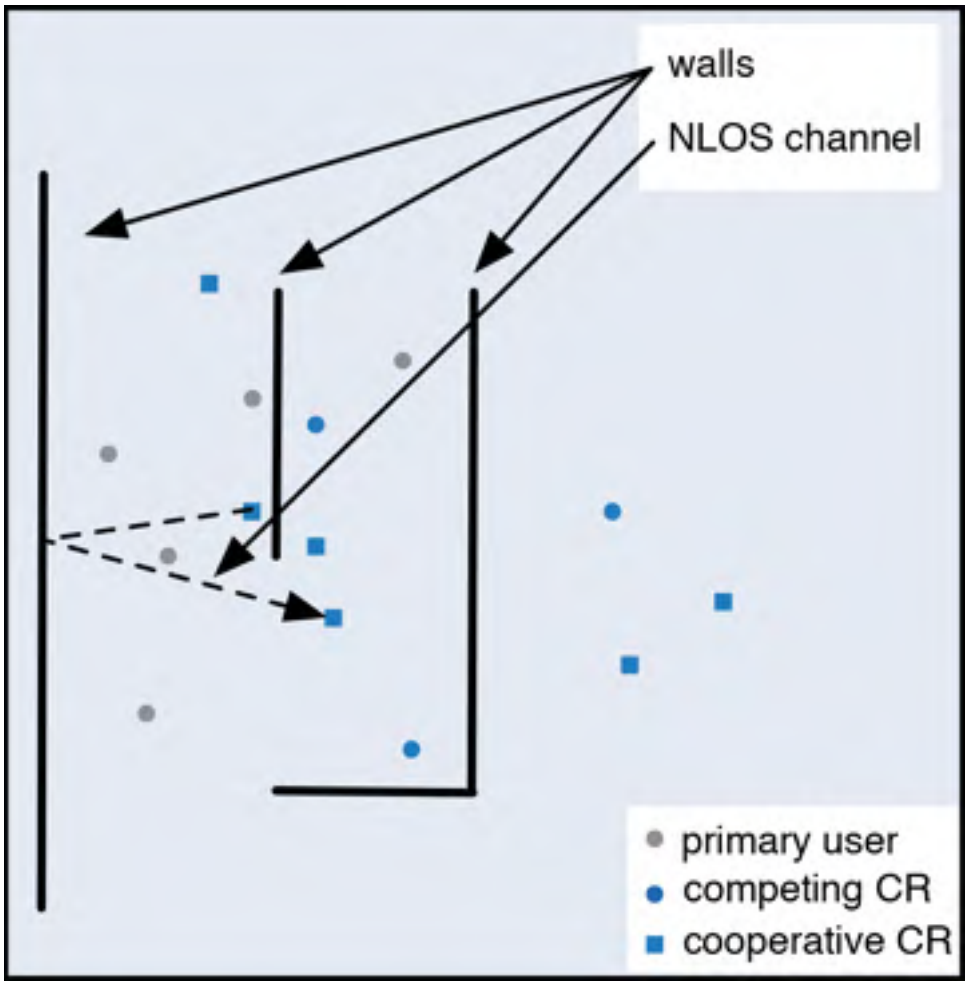

Figure 1.7 NLOS channels caused by the presence of obstacles.

In general, indoor wireless channels experience a large number of multipaths [Saleh and Valenzuela (1987)], which largely distort the channel impulse response. In order to resolve some of the strongest multipaths for indoor environments, channel bandwidths as wide as several hundreds of MHz like for ultra-wide band (UWB) communication channels can be necessary [Yousef and Sayed (2002), Yu *et al.* (2009) Jourdan *et al.* (2008), Denis *et al.* (2005), Gezici *et al.* (2005)]. When these conditions are respected, the first peak in the channel impulse response can be interpreted as the "time-of-arrival". Advanced sampling techniques can be used to further increase the resolution of the TOA estimate [Li and Pahlavan (2004), Zhao *et al.*

(2006a), Humphrey and Hedley (2008)]. However, even these methods cannot cope with the undetected node problem that arises in NLOS channels and cause large distance biases [Alavi and Pahlavan (2003a), Alavi and Pahlavan (2003b), Alavi *et al.* (2005), Alavi and Pahlavan (2006)].

Cooperation between dense radios network nodes can increase the precision and robustness of localization results [Patwari *et al.* (2005), Jia and Buehrer (2011)]. Measurements of RSS in 802.11 networks obtained at a specific site can also be used to train a localization estimation algorithm [Haeberlen *et al.* (2004), Mitilineos *et al.* (2009)].

When the obstacle density is high compared to the sensor density and when field measurements are not available, the map of the obstacles' location and shape can be used to reduce their impact on the localization error. Since cognitive radios are expected to access information on their environment, they can exploit the map of scatterers surrounding the base stations in their networks [Zhao *et al.* (2007b), Zhao *et al.* (2007a), Zhao *et al.* (2006b)], provided this map offers sufficient information on the obstacles' properties [Wahl *et al.* (2007)].

Ray launching techniques modelling individual rays rather than groups of rays [Lawton and McGeehan (1994)] can become particularly complex as the covered space and the obstacles density grow. Acceleration techniques have been presented that help reduce this complexity for specific tasks [Wölfle *et al.* (1997), Wölfle *et al.* (1999), Aguado Agelet *et al.* (2000), Ji *et al.* (2001), Hoppe *et al.* (2003)]. Ray tracing can be made progressive, offering a trade-off between calculation time and accuracy, with partial results available at any step [Chen *et al.* (2004)].

Ray tracing is primarily a computer graphics method for rendering the propagation of light waves scattering on surfaces and reaching an observer [Keller (1978), Sack and Urrutia (2000)]. The computational complexity of these methods can be prohibitive for some applications, and a significant research effort has been deployed to make it more efficient. Hierarchical space partitions [Samet and Webber (1988)] or occluder fusion [Wonka *et al.* (2000)] can reduce the complexity of visibility queries.

Space partition is an important factor in the complexity of ray tracing techniques and several partitioning methods have been developed for ray tracing [Van Bilsen and Stolk (2008), Ize *et al.* (2007)].

Radio ray tracing methods aim at modelling the propagation of radio frequency waves on obstacles, and are both faster and less precise than finite difference Maxwell equations solvers [Wagen and Rizk (2003)]. Still, classical radio ray tracing methods are usually too computationally demanding for real-time applications in mobile devices. Several ray tracing models have been developed over the years, and their models concord with field measurements [Aguado *et al.* (1997), Yang *et al.* (1998), Zhang *et al.* (1998)].

The effects of obstacles on the propagation of radio waves are modelled with a collection of specular reflections, transmissions and diffractions, and diffuse scattering [Ullmo and Baranger (1999), Bladel (2007)]. Ray tracing models for transmission through walls have been developped and tested [Grubisic *et al.* (2006)]. Diffraction can be modelled with the uniform theory on diffraction [Walfisch and Bertoni (1988), Kouyoumjian and Pathak (1974)], which is shown to be accurate by several field experiments [Kanatas *et al.* (1997)].

Diffuse scattering models add to the accuracy of ray tracing models at the cost of more computational complexity [Durgin *et al.* (2002), Degli-Esposti *et al.* (2007)]. The calculation of the visibility queries around observer points is particularly complex for diffusion scattering models [Prasant and Sarkar (2003)]. Applications of ray tracing models for MIMO models have also been developed and tested against field measurements [Ng *et al.* (2004), Ng *et al.* (2007)].

Ray tracing methods can be extended from electromagnetic field propagation modelling to the characterization of wireless channels. Site-specific information on the location and shape of obstacles can improve on the accuracy of empirical models [Kaya *et al.* (2009), Clarke (2002), Iskander and Yun (2002)].

Ray-tracing aided localization methods have been proposed for 802.11 indoor networks [El-Kafrawy *et al.* (2010), Atia *et al.* (2012)], UWB [Yang and Naitong (2005)] or using hybrid

AOA/TDOA estimates [Bishop *et al.* (2008), Gentile *et al.* (2008)] or hybrid AOA/RSS [Tayebi *et al.* (2009)].

Ray tracing methods have been presented to improve the accuracy of wireless channel models, but their acceleration is still a major research topic, especially for real-time application like localization solvers. In chapter 4 we propose a ray tracing acceleration technique for the localization of mobile nodes in environments with a large density of scatterers. We use field-gathered channel sounding data to show that it can achieve high localization accuracy in real-time.

CHAPTER 2

POWER AND SUBCARRIER ALLOCATION METHODS FOR RELAY LINKS

2.1 Introduction

In recent years, cooperative communications techniques have been proposed to improve coverage, enhance capacity and combat shadowing in wireless communication networks, such as cellular networks or mesh networks. Relay cooperative techniques exploit cooperative diversity by means of providing several copies of a signal, which experience independent channel gains, in order to further overcome channel fading [Pabst *et al.* (2004), Laneman *et al.* (2004), Nabar *et al.* (2004)].

We study the parallel relay channel which has three nodes: a source S, a relay R, and a destination node D, as shown on Fig. 2.1. The wireless medium is divided into N_{FFT} subcarriers, each with index k. The gains for the source-to-relay, relay-to-desintation and source-to-destination channels are h_{sr}, h_{rd} and h_{sd}, respectively.

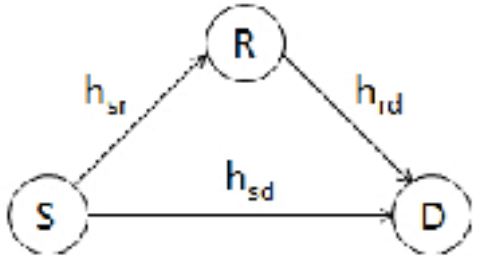

Figure 2.1 The relay channel.

Two fundamental relaying methods have been defined in [Laneman *et al.* (2004)]: amplify-and-forward (AF), where the relay retransmits an amplified version of the transmitted signal including noise and channel degradations, without reading its content; and decode-and-forward (DF) where the relay reads the message completely, encodes a new one and transmits it to the destination.

Resource allocation methods for orthogonal frequency-division multiplexing (OFDM) without cooperation have been studied thoroughly [Wong *et al.* (1999); Rhee and Cioffi (2000)]. Cooperative communications in the OFDM context have been shown to improve the achievable downlink communication rate between a base station and a destination node, using a single relay that performs relaying on all available subcarriers [Hammerstrom and Wittneben (2006)]. When considering selective subcarrier relaying in the OFDM context, we will need to identify which subcarriers to use for relaying (i.e., subcarrier selection). This technique was proven to improve rate [Vandendorpe *et al.* (2008a)] for decode-and-forward relaying systems.

Several researchers have included selective relaying in their power allocation schemes. The work in [Pischella and Belfiore (2008)] does select subchannels but the joint problem of subcarrier and power allocation in orthogonal frequency-division multiple access (OFDMA) was not treated. Subcarrier selection and bit-loading algorithms based on power gains, as presented in [Gui and Cimini (2008)], do not consider the capacity loss when the base station does not transmit in the second timeslot. [Ma *et al.* (2008)] used a selective subchannel relaying bit-loading scheme, but the power allocation problem was not considered.

Several researchers have studied cooperative communication optimization problems where a centralized control unit with knowledge of the channel state information can allocate power to the transmitters at source and relay nodes in order to fulfill an objective under a set of constraints. Early research in cooperative communications has shown that energy efficient transmitters operating in relay networks help extending battery life Laneman and Wornell (2000). Other investigations on power allocation for relay networks have relied on the sum power constraints shared by source and relay nodes to minimize outage probability [Hasna and Alouini (2003)] rather than power constraints distributed to each individual nodes. Using distributed constraints can be described as more practical in the mobile communications context, as each mobile device has access to its own battery source power.

In this work, we are interested in capacity maximization objectives, which several researchers reached under similar sum power constraints [Jingmei *et al.* (2004), Qi *et al.* (2004), Ying *et al.*

(2007) and Li *et al.* (2008)]. Individual power constraints, however, represent practical systems more faithfully, because geographically separated nodes have independent power sources.

Current research has considered individual power constraints for capacity maximization power allocation [Hammerstrom and Wittneben (2006), Louveaux *et al.* (2008) and Vandendorpe *et al.* (2008b)], but did not consider another dimension of the problem: frequency selective fading. Early power allocation problems [Hasna and Alouini (2003)] have considered flat fading for AF [Jingmei *et al.* (2004)] and DF [Qi *et al.* (2004)] relaying schemes. Frequency selective channels under OFDM modulation, which consider constant channel gains in narrow subcarriers, have been studied in [Ying *et al.* (2007), Vandendorpe *et al.* (2008b)]. In cooperative power allocation for OFDM modulated transmitters, most researchers decide to relay on all subcarriers [Ying *et al.* (2007), Li *et al.* (2008)], but choosing to relay on only some subcarriers offer better capacity performance in general [Hammerstrom and Wittneben (2006), Vandendorpe *et al.* (2008b)]. Also, the relay node has an opportunity to transmit on a given subcarrier, messages that were received on a different subcarrier. This *pairing* technique improves capacity in systems under sum power constraints [Qi *et al.* (2004) and Ying *et al.* (2007)], but is only mentioned as a potential benefit for individual power constrained problems [Hammerstrom and Wittneben (2006)].

In this chapter, we study joint power and subcarrier allocation schemes for frequency selective relay channels under OFDM modulation. We propose selective subcarrier allocation schemes for AF systems and subcarrier pairing for DF systems under individual power constraints at the source and relay transmitters.

For AF schemes, we show that by carefully selecting the subcarriers on which relaying should be performed and using a capacity improvement criterion, we are able to improve end-to-end system capacity when compared to that in the relay system proposed in [Hammerstrom and Wittneben (2006)]. For DF schemes, we show that by using convex and integer optimization methods, we can allocate subcarrier and power resources in an optimal manner.

We show the AF and DF system models in sections 2.2 and 2.3, and numerical results for both schemes in section 2.4.

2.2 Amplify and Forward Model

A base station transmits to a single mobile user using OFDM modulation schemes, and can use a single mobile as a relay station. Then, we consider the capacity for every frequency separated subcarrier, k. Each time period is separated in two time slots, where the base station transmits a message in the first time slot. In the second timeslot, we define the relay decision as μ_k, where $\mu_k = 1$ means that the relay station amplifies and forwards the message sent by the base station in timeslot 1. In bands with $\mu_k = 0$ the transmission is solely undertaken by the source node in two successive time slots, and the relay node is not transmitting at all:

$$\mu_k = \begin{cases} 0, & \text{if subcarrier } k \text{ is not used by the relay} \\ 1, & \text{if subcarrier } k \text{ is used by the relay.} \end{cases} \tag{2.1}$$

We assume that there are N_{FFT} subcarriers in the OFDM system. The gain of the kth subcarrier's channel between source and destination is $h_{sd,k}$, between source and relay is $h_{sr,k}$, and between relay and destination is $h_{rd,k}$. We assume that these channel gains are slow-varying, and are therefore constant for both transmission and relaying timeslots. We assume that the source sends data with power $p_{S,k}$ on the kth subcarrier, and the relay amplifies the message by a factor g_k using power $p_{R,k}$ on the kth subcarrier:

$$g_k = \sqrt{\frac{p_{R,k}}{p_{S,k}|h_{sr,k}|^2 + \sigma_r^2}}. \tag{2.2}$$

The noise variance at the relay within one OFDM subcarrier is σ_r^2 and at the destination is σ_d^2. The SNR ρ_k for subcarrier k is then [Hammerstrom and Wittneben (2006)]

$$\begin{aligned} \rho_k &= \frac{p_{S,k}|h_{rd,k}g_k h_{sr,k}|^2}{\sigma_d^2 + \sigma_r^2|g_k h_{rd,k}|^2} + \frac{p_{S,k}|h_{sd,k}|^2}{\sigma_d^2} \\ &= \frac{p_{S,k}a_k \cdot p_{R,k}b_k}{1 + p_{S,k}a_k + p_{R,k}b_k} + p_{S,k}c_k \end{aligned} \tag{2.3}$$

where $a_k = \frac{|h_{sr,k}|^2}{\sigma_r^2}$, $b_k = \frac{|h_{rd,k}|^2}{\sigma_r^2}$, and $c_k = \frac{|h_{sd,k}|^2}{\sigma_d^2}$ represent the signal gain to noise ratios for the source-relay, relay-destination and source-destination channels, respectively. Figure 2.2 illustrates the overall received signal and noise powers at receiver rx_k.

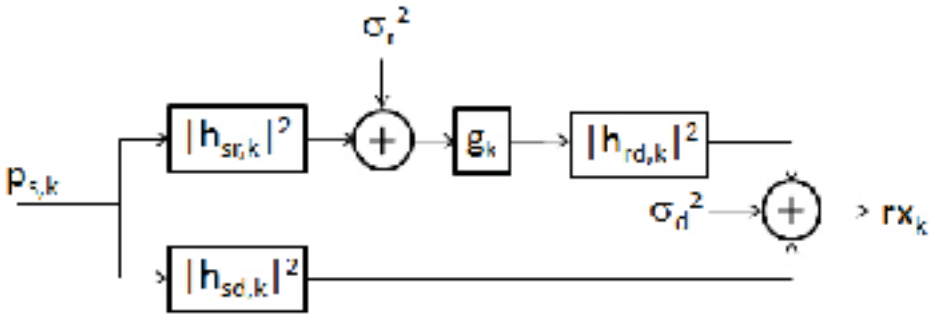

Figure 2.2 Relaying system model.

We assume that the base station has total information on channel gains and noise variance at the relay and destination receivers, i.e. a_k, b_k, c_k are known $\forall k \in \{1, 2, \ldots, N_{FFT}\}$. The source and relay powers are constrained by power budget P_S and P_R, respectively:

$$\mathbf{1}^T \mathbf{p}_S = P_S \tag{2.4}$$

$$\mathbf{1}^T \mathbf{p}_R = P_R. \tag{2.5}$$

The capacity for a relay communication in the kth subcarrier is given by

$$C_{R,k} = \mu_k \frac{1}{2} \log_2(1 + \rho_k) \tag{2.6}$$

for which the $1/2$ factor represents the half duplex relaying process, and the μ_k factor represents the relaying decision. The capacity for the non-relaying process is given by:

$$C_{S,k} = (1 - \mu_k) \log_2(1 + p_{S,k} c_k). \tag{2.7}$$

If $\mu_k = 0$, transmission over that subchannel is solely undertaken by the source node without any involvement of the relay node in two successive time slots. Combining (2.6) and (2.7), the overall capacity using selective subcarrier relaying in the k-th subcarrier is given by:

$$C_{I,k} = \mu_k \frac{1}{2} \log_2(1 + \rho_k) + (1 - \mu_k) \log_2(1 + p_{S,k} c_k). \tag{2.8}$$

Our objective is to determine the relay decision μ_k, the power allocations for the base station $p_{S,k}$ and the relay station $p_{R,k}$ for all subcarriers k which offer the optimal global capacity C_I:

$$C_I = \sum_{k=1}^{N_{FFT}} C_{I,k}. \tag{2.9}$$

2.2.1 Subcarrier and Power Allocation: Preprocessing Heuristic and Optimization Formulations

Being a proper integer problem, we solve the subcarrier selection and power allocation problem in two recursive steps that we repeat until convergence is obtained. As will be demonstrated in section 2.4, only a few iterations are required to converge to a suboptimal capacity. In the next section, we describe the first of these steps, namely, the subcarrier selection and power allocation at the relay.

2.2.1.1 Subcarrier Selection and Power Allocation at the Relay

In this first step, given a base station power vector $\mathbf{p_S}$, we calculate estimates of both $\mathbf{p_R}$ and $\boldsymbol{\mu}$. Let us first rewrite (2.8) by grouping the μ_k dependent factors in a single log expression as follows:

$$C_{I,k} = \frac{1}{2} \log_2 \left[\left(\frac{(1 + \rho_k)}{(1 + p_{S,k} c_k)^2} \right)^{\mu_k} \right] + \log_2(1 + p_{S,k} c_k). \tag{2.10}$$

Then clearly, the first term of (2.10) must be larger than 0 for the relaying process to increase capacity in subcarrier k. Let $\Xi(p_{R,k}, p_{S,k})$ represent the capacity increase brought by relaying on subcarrier k:

$$\Xi(p_{R,k,}, p_{S,k}) = \frac{1 + \rho_k}{(1 + p_{S,k} c_k)^2}. \tag{2.11}$$

For power allocation at the relay, we fix source power $p_{S,k}$ and consider

$$\Xi(p_{R,k,}) = \frac{d_1 p_{R,k} + d_2}{d_3 p_{R,k} + d_4}, \quad \text{where} \tag{2.12}$$

$$\begin{aligned} d_1 &= b_k(p_{S,k}a_k + p_{S,k}c_k + 1) \\ d_2 &= p_{S,k}^2 a_k c_k + p_{S,k}a_k + p_{S,k}c_k + 1 \\ d_3 &= b_k(p_{S,k}c_k + 1)^2 \\ d_4 &= (p_{S,k}a_k + 1)(p_{S,k}c_k + 1)^2. \end{aligned}$$

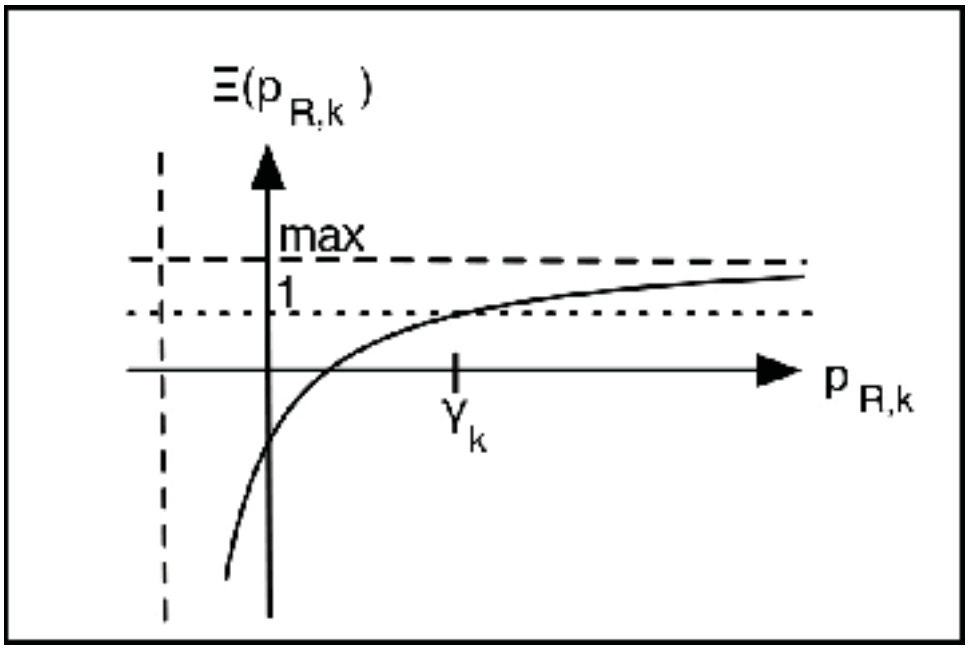

Figure 2.3 Relaying capacity gain function.

Eq. (2.12) represents a rational function which is plotted in Fig. 2.3. The asymptotes of this curve are defined as

$$\begin{aligned} \text{(vertical)} : p_{R,k} &= \frac{-p_{S,k}a_k - 1}{b_k} \\ \text{(horizontal)} : \Xi(p_{R,k}) &= \frac{p_{S,k}a_k + p_{S,k}c_k + 1}{(p_{S,k}c_k + 1)^2}. \end{aligned}$$

In order to obtain gain in capacity, the horizontal asymptote has to be larger than 1, so that at least some values of $0 < p_{R,k} < P_R$ can actually improve capacity. In other words, the following condition has to be satisfied in order to improve capacity through relaying:

$$a_k > c_k(p_{S,k}c_k + 1). \tag{2.13}$$

For every subcarrier k that does not satisfy condition (2.13), we set $\mu_k = 0$, $\gamma_k = 0$ and $P_{R,k} = 0$. Our problem is then to assign power to the remaining subcarriers that do satisfy it. We define the point $\{\gamma_k = p_{R,k} | \, \Xi(p_{R,k}) = 1\}, \gamma_k \in \boldsymbol{\gamma}$ as the minimum value of $p_{R,k}$ that improves capacity, where

$$\gamma_k = \frac{c_k(p_{S,k}a_k + 1)(p_{S,k}c_k + 1)}{b_k(a_k - c_k(p_{S,k}c_k + 1))}. \tag{2.14}$$

Table 2.1 Symbols for the AF Optimization Problem

Description	**Symbol Name**	
	Source	Relay
Power Budget	P_S	P_R
Power Vector	$\mathbf{p}_S$	$\mathbf{p}_R$
Power Vector's Element k	$p_{S,k}$	$p_{R,k}$
Vector for Minimal Power to Improve Capacity	nil	$\boldsymbol{\gamma}$
Vector for Relay Selection	nil	$\boldsymbol{\mu}$
Source-relay power gain to noise ratio	**a**	
Relay-destination power gain to noise ratio	**b**	
Source-destination power gain to noise ratio	**c**	

Therefore, for all subcarriers for which we want to perform relay, we must select $\mu_k = 1$ and set $p_{R,k} > \gamma_k$ so that we can obtain a gain in capacity. In order to calculate global capacity, which satisfies these constraints, we define a pre-processing heuristic. First, we make sure that we can improve capacity in all subcarriers, while respecting global power constraints by successively setting $\mu_k = 0$ for the subcarrier with largest $\mu_k \cdot \gamma_k$ until $\boldsymbol{\mu}^T\boldsymbol{\gamma} \leq P_R$.

Then, we calculate $\mathbf{p}_R$ that maximizes capacity, we set $\mu_k = 0$ for the subcarrier with largest $\mu_k \cdot \gamma_k$ and recalculate $\mathbf{p}_R$ that maximizes capacity as long as this iterative process increases capacity. This heuristic simplifies the complexity of μ_k selection process from a combinatorial to a linear complexity. This ordering based on γ comes at the performance cost of dropping some bands with relatively high $d1/d3$ ratios.

A complete version of this heuristic is detailed in Section 2.2.2 and in the flowchart in Fig. (2.4). We determine the value of $\mathbf{p}_R$ which maximizes capacity using convex optimization techniques [Boyd and Vandenberghe (2004)] to obtain the optimal power allocation for all subcarriers for which $\mu_k = 1$. The optimization problem is formulated as follows:

$$\begin{aligned} \text{minimize} \quad & -\sum_{\{\forall k|\mu_k=1\}} \log_2 \Xi(\mathbf{p}_{R,k}) \\ \text{subject to} \quad & \boldsymbol{\gamma} - \mathbf{p}_R \preceq 0 \\ & \mathbf{1}^T \mathbf{p}_R - P_R = 0. \end{aligned} \tag{2.15}$$

The Karush–Kuhn–Tucker (KKT) conditions for this convex optimization problem are given by

$$\begin{aligned} \gamma_k - p_{R,k} &\leq 0 \\ \mathbf{1}^T \mathbf{p}_R - P_R &= 0 \\ \lambda_k &\geq 0 \\ \lambda_k(\gamma_k - p_{R,k}) &= 0 \\ -\lambda_k + \nu - \frac{1}{ln2} \frac{p_{S,k} a_k b_k (p_{S,k} a_k + 1)}{p_{R,k}^2 w_1 + p_{R,k} w_2 + w_3} &= 0 \\ \text{with } w_1 = b_k^2 (p_{S,k} a_k + p_{S,k} c_k + 1), & \\ w_2 = b_k (p_{S,k} a_k + 1)(2 p_{S,k} c_k + p_{S,k} a_k + 2) \quad & \text{and} \\ w_3 = (p_{S,k} a_k + 1)^2 (p_{S,k} c_k + 1). & \end{aligned} \tag{2.16}$$

The solution is given by

$$p^*_{R,k} = \min\left\{\gamma_k, \frac{p_{S,k}a_k + 1}{b_k(p_{S,k}a_k + p_{S,k}c_k + 1)}[\cdot]\right\}$$
$$[\cdot] = \frac{p_{S,k}a_k}{2}\sqrt{1 + \frac{4b_k(1 + p_{S,k}a_k + p_{S,k}c_k)}{\nu \ln(2) p_{S,k}a_k(p_{S,k}a_k + 1)}}$$
$$- (2p_{S,k}c_k + p_{S,k}a_k + 2). \tag{2.17}$$

The parameter ν is chosen such that the power constraint $\mathbf{1}^T\mathbf{p}_R = P_R$ is fulfilled.

2.2.1.2 Power Allocation at the Source

Using the relay decision μ^*_k and power $p^*_{R,k}$ calculated in the previous section, we then determine the source power allocation $p^*_{S,k}$ for all subcarriers k. In all relaying subcarriers ($\mu^*_k = 1$), the source power must be chosen so that we maintain the capacity increase function $\Xi(p_{R,k} = p^*_{R,k}, p_{S,k}) > 1$, which after several algebraic manipulations, reduces to the following:

$$p_{S,k} < \Gamma_k$$
$$\Gamma_k = \frac{\sqrt{(\cdot)} - (a_k + c_k(p^*_{R,k}b_k + 1))}{2a_kc_k}$$
$$(\cdot) = (a_k + c_k(p^*_{R,k}b_k + 1))^2 - 4a_k(p^*_{R,k}b_k(c_k - a_k) + c_k), \quad \text{for} \quad a_k > c_k. \tag{2.18}$$

The $a_k > c_k$ condition is already verified by (2.13) for every relaying subcarrier, with $\mu_k = 1$. The power allocation is performed in a similar fashion as in the previous section. Using the subcarrier selection $\boldsymbol{\mu}$ and relay power $\mathbf{p}_R$ vectors found in Section 2.2.1.1 we obtain the

marginally optimal source power vector by solving the following optimization problem:

$$\begin{aligned} \text{minimize} - & \sum_{k=1}^{N_{FFT}} C_{I,k} \\ \text{subject to} \quad & -\mathbf{p}_S \preceq 0 \\ & \boldsymbol{\mu}^T(\mathbf{p}_S - \boldsymbol{\Gamma}) \preceq 0 \\ & \mathbf{1}^T\mathbf{p}_S - P_S = 0. \end{aligned} \tag{2.19}$$

Solving the KKT conditions in a similar manner as in Section 2.2.1.1, we obtain

$$p^*_{S,k} = \begin{cases} \frac{1}{\nu ln(2)} - \frac{1}{c_k}, & \text{for } \mu_k = 0 \\ \max\left(\Gamma_k, \frac{1}{a_k}\left[-1 + \frac{b_k p_{R,k}}{2}(\cdot)\right]\right), & \text{for } \mu_k = 1 \end{cases} \tag{2.20}$$

where $(\cdot) = -1 + \sqrt{1 + \frac{2a_k}{\nu ln(2) b_k p_{R,k}}}$. Assuming that when relaying occurs, $h_{s,d} << 1$, so we can ignore the 2nd term in (2.3). The parameter ν is chosen so that the sum power constraint $\mathbf{1}^T\mathbf{p}_S = P_S$ is fulfilled.

2.2.2 Iterative Algorithm for Optimizing Subcarrier Selection and Power Allocation

We now perform the selective subcarrier and power allocation using the expressions derived in the previous section. In this section, we provide a more detailed algorithmic description of our method. Given power budgets P_R and P_S for the relay and the base station, N_{FFT} subcarriers, the power allocation is performed using the following iterative steps:

1: **procedure** POWER ALLOCATION
2: initialize: $p_{S,k} = P_S/N_{FFT}, \forall k$
3: **while** convergence is not attained **do**
4: calculate $\mathbf{p}_R$ and $\boldsymbol{\mu}_k$ using $\mathbf{p}_S$ using the algorithm described below
5: find $\mathbf{p}_S$ that maximizes capacity with current $\boldsymbol{\mu}$ and $\mathbf{p}_R$ using (2.20)

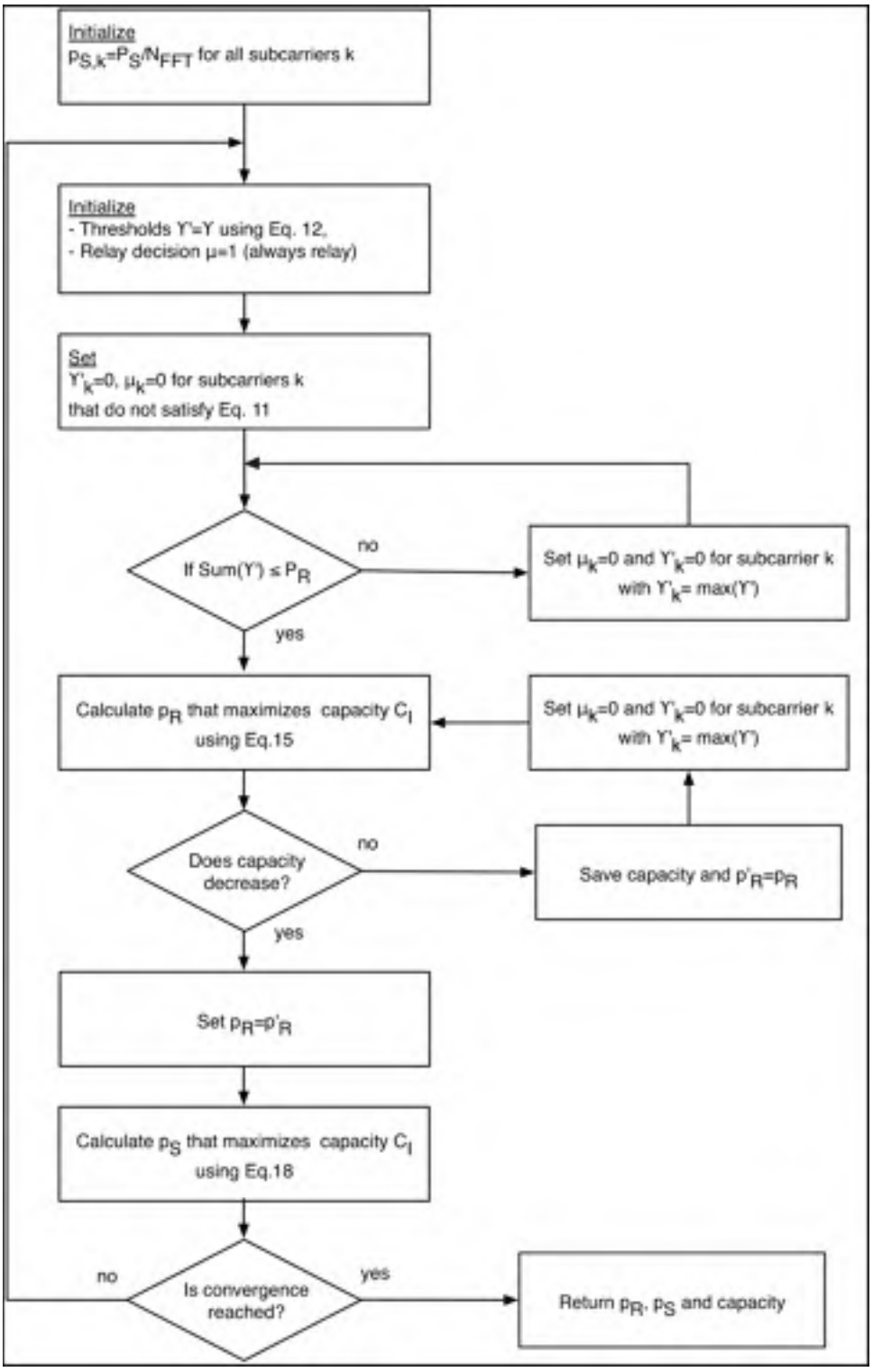

Figure 2.4 Flow chart for power allocation.

The calculation of $\mathbf{p}_R$ and $\boldsymbol{\mu}$ is performed as follows:

procedure RELAY POWER AND FREQUENCY ALLOCATION
  initialize: $\boldsymbol{\gamma}' = \boldsymbol{\gamma}$ using (2.14) and $\boldsymbol{\mu} = \mathbf{1}$
  set $C_I' = -1$, $\mu_k = 0$, $\boldsymbol{\gamma}_k'$ and $p_{R,k} = 0, \forall\, k \,|\, a_k \leq c_k(P_{S,k}c_k + 1)$
  while $\mathbf{1}^T\boldsymbol{\gamma}' > P_R$ **do**
    set $\mu_k = 0$ and $\gamma_k = 0$, for $\{k \,|\gamma_k = \max(\boldsymbol{\gamma}')\}$
  repeat
    calculate $\mathbf{p}_R$ that maximizes capacity with current $\boldsymbol{\mu}$ using (2.17)
    set this maximized capacity as C_I
    if $C_I < C_I'$ **then**
      return $\boldsymbol{\mu}$, $\mathbf{p}_R = \mathbf{p}_R'$ and $C_I = C_I'$
    set $C_I' = C_I$ and $\mathbf{p}_R' = \mathbf{p}_R$
    set $\mu_k = 0$ and $\gamma_k = 0$, for $\{k \,|\gamma_k = \max(\boldsymbol{\gamma}')\}$
  until $\boldsymbol{\gamma} = \mathbf{0}$ and $\boldsymbol{\mu} = \mathbf{0}$
  return $\boldsymbol{\mu}$, $\mathbf{p}_R$ and C_I

A flowchart of the algorithm is shown in Fig. 2.4. The combination of $\mathbf{p}_S$, $\mathbf{p}_R$ and $\boldsymbol{\mu}$ that maximizes capacity can then be calculated. In section 2.4, we show performance evaluation results for this algorithm show the capacity and convergence rate for this algorithm.

2.3 Decode-and-Forward Models

In a wireless OFDM network operating on frequency selective channels, a source wishes to send data to a destination, using the assistance of a relay, as shown in Fig. 2.5. The channel's bandwidth is divided into $N = N_{FFT}$ subcarriers, and a transmission period lasts two time slots. We define the gain of the i^{th} subcarrier's channel between source and destination as $h_{sd,i}$, source and relay $h_{sr,i}$, and relay and destination $h_{rd,i}$. We assume these channel gains do not vary during a period of two time slots.

In the first time slot, data is broadcasted by source to relay and destination on all subcarriers, with power $\mathbf{p}_S^{(1)}$. In the second time slot, on the M subcarriers that have been selected for

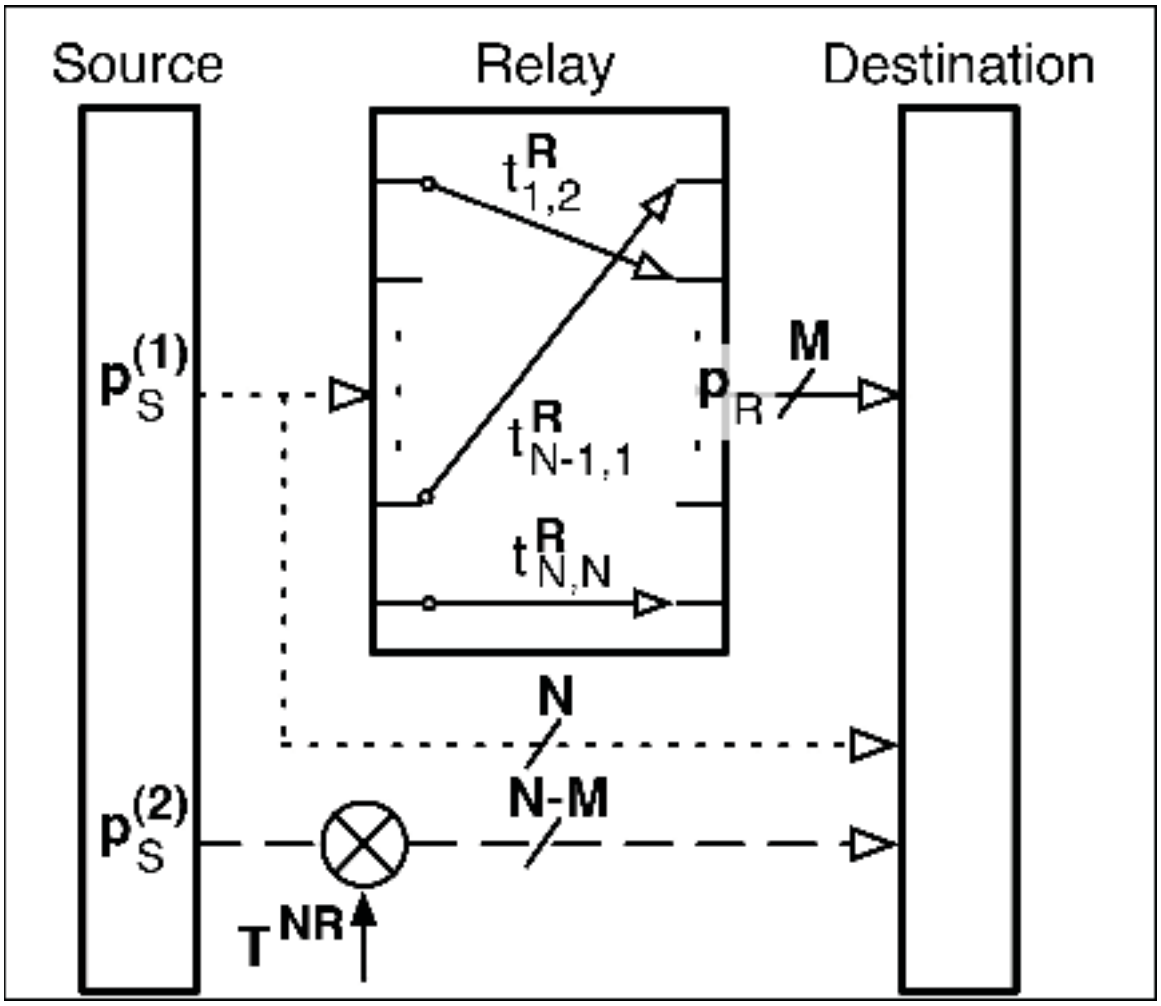

Figure 2.5 Decode-and-forward system model.

relaying, the relay decodes, permutes and retransmits data with power $\mathbf{p}_R$. On the remaining N-M subcarriers, the source transmits new data with power $\mathbf{p}_S^{(2)}$. Therefore, the relay might use a different subcarrier as the one used by the source for a given message.

We define a $N_{FFT} \times N_{FFT}$ relay pairing matrix as $\mathbf{T}^R$ with elements $t^R_{i,j}$. The permutations occur from subcarrier i in the first time slot to subcarrier j in the second time slot if they are *paired*, which is denoted by elements $t^R_{i,j} = 1$. Similarly, the non-relay pairing $N_{FFT} \times N_{FFT}$ matrix $\mathbf{T}^{NR}$ has elements $t^{NR}_{i,j} = 1$ if the subcarrier j is used to transmit a new message from the source. All other elements $t^R_{i,j} = 0$ and $t^{NR}_{i,j} = 0$.

Then, after a two time slot period, the destination exploits maximum ratio combining to retrieve the relayed messages. If we assume noise variance at the relay within one OFDM subcarrier to be σ_r^2 and σ_d^2 at the destination, the capacity on relaying pairs and non-relaying pairs will be [Laneman *et al.* (2004)]:

$$C_R(i,j) = \frac{1}{2}\min\left\{\log(1+a_i p_{S,i}^{(1)}), \log(1+c_i p_{S,i}^{(1)} + b_j p_{R,j})\right\} \tag{2.21}$$

$$C_{NR}(i,j) = \frac{1}{2}\log(1+c_i p_{S,i}^{(1)}) + \frac{1}{2}\log(1+c_j p_{S,j}^{(2)}) \tag{2.22}$$

where $a_i = |h_{sr,i}|^2/\sigma_r^2$, $b_i = |h_{rd,i}|^2/\sigma_d^2$, and $c_i = |h_{sd,i}|^2/\sigma_d^2$. Our objective is to solve the following optimization problem which involves joint optimization of pairing, selecting, allocating power to the source in the first time slot, and allocating power to relay and source in the second time slot:

$$\begin{aligned}
&\underset{\mathbf{p}_S^{(1)}, \mathbf{p}_S^{(2)}, \mathbf{p}_R, t_{i,j}^R, t_{i,j}^{NR}}{\text{minimize}} \\
&-\sum_{i=1}^{N_{FFT}} \sum_{j=1}^{N_{FFT}} \{t_{i,j}^R \cdot C_R(i,j) + t_{i,j}^{NR} \cdot C_{NR}(i,j)\} \\
&\text{s.t.} \quad \sum_{i=1}^{N_{FFT}} (t_{i,j}^R + t_{i,j}^{NR}) = 1, \forall j \in \{1,2,\ldots,N_{FFT}\} \\
&\quad \sum_{j=1}^{N_{FFT}} (t_{i,j}^R + t_{i,j}^{NR}) = 1, \forall i \in \{1,2,\ldots,N_{FFT}\} \\
&\quad t_{i,j}^R, t_{i,j}^{NR} \in \{0,1\}, \forall i,j \in \{1,2,\ldots,N_{FFT}\} \\
&\quad \mathbf{p}_{S,i}^{(1)}, \mathbf{p}_{S,i}^{(2)}, \mathbf{p}_R \succeq 0 \\
&\quad \mathbf{1}^T \mathbf{p}_S^{(1)} = P_S, \mathbf{1}^T \mathbf{p}_S^{(2)} = P_S, \mathbf{1}^T \mathbf{p}_R = P_R
\end{aligned} \tag{2.23}$$

We solve this problem in two parts, the second one being power allocation, but we first discuss pairing and selection in the next section.

2.3.1 Pairing and selection

The pairing and selection is equivalent to determining the optimal $\mathbf{T}^R$ and $\mathbf{T}^{NR}$ matrices, which is an integer programming problem that often proves to be unsolvable without a complex enumeration of possibilities. This is very complex in practical applications. In this paper, an algorithm based on Hungarian method [Kuhn (1955)] is proposed in order to treat this issue.

Pairing algorithms are investigated in [Ying *et al.* (2007)] and [Li *et al.* (2008)], where the proposed solutions are based on ordering the subchannel gains: the best source-relay gain is paired with the best relay-destination. For instance, [Ying *et al.* (2007)] orders source-relay subcarriers according to $a_i - c_i$ and relay-destination subcarriers according to b_j. These pairing algorithms are only optimal when selection is unavailable, i.e. when relaying occurs on all subcarriers. Consequently, this ordering method cannot be used to achieve optimal subcarrier selection.

Proof. Pairing matrices following a $a_i - c_i$ order are not optimal when selection is allowed.

Consider 2 subcarriers, indexed 1 and 2, for which channel gain to noise power ratios respect the following constraints:

$\nearrow$	a_1	a_2	b_1	b_2	c_1	c_2
a_1		$<$	$<$	$>$	$>$	$>>$
a_2			$<$	$>$	$>$	$>>$
b_1				$>$	$>$	$>>$
b_2					$>$	$>>$
c_1						$>$

then, the ordered pairing method results in: $\{a_1, b_2\}_1^R, \{a_2, b_1\}_2^R$ and the Hungarian pairing method in: $\{a_2, b_2\}_1^R, \{c_1\}_2^{NR}$ If there are any conditions which satisfy $C_R(a_1, b_2) + C_R(a_2, b_1) < C_R(a_2, b_2) + C_{NR}(c_1)$ then the ordered pairing can not be optimal in general.

Reasonably straightforward algebra results in the following conditions:

$$c_1(c_1 + 2) > a_2$$

which is true, for example, with numerical values

$\{a_1, a_2, b_1, b_2, c_1, c_2\}$=$\{895, 1047, 2612, 514, 58, 5\}$.

□

In terms of selection, [Qi *et al.* (2004)] and [Ying *et al.* (2007)] introduced a straightforward algorithm for DF relaying systems for which a particular pair is used for relaying if $a_i, b_j > c_i$. Otherwise, the direct link offers a better capacity. However, this algorithm is based upon a sum power constraint; and as discussed earlier, individual power constraints are more realistic to depict practical applications.

To overcome the two shortcomings mentioned above, we present a unified algorithm based on the Hungarian method to deal with the pairing and selection problem jointly. First we define the following matrices:

$$\mathbf{D}(i,j) = \begin{cases} C_R(i,j) & C_R(i,j) > C_{NR}(i,j) \\ C_{NR}(i,j) & \text{otherwise} \end{cases} \tag{2.24}$$

$$\mathbf{F}(i,j) = \begin{cases} 1 & C_R(i,j) > C_{NR}(i,j) \\ -1 & \text{otherwise} \end{cases} \tag{2.25}$$

The integer programming problem is then reduced to an assignment problem on $\mathbf{D}$ that gives $\mathbf{T} = \mathbf{T}^R + \mathbf{T}^{NR}$ and can be solved by applying the Hungarian method. This method can be described as a series of recursive matrix row and column subtractions. First, the lowest cost element in the assignment matrix is identified, and its corresponding row and column are removed from the matrix, then, the same process is applied to the reduced matrix until all assignments are determined. The $\mathbf{T}^R$ and $\mathbf{T}^{NR}$ matrices can be extracted from matrix $\mathbf{T}$ using

Table 2.2 Symbols for the DF Optimization Problem

Description	Symbol Name	
	Source	Relay
Power Budget	P_S	P_R
Power Vector	$\mathbf{p}_S$	$\mathbf{p}_R$
Power Vector's Element k	$p_{S,k}$	$p_{R,k}$
Source-relay power gain to noise ratio	$\mathbf{a}$	
Relay-destination power gain to noise ratio	$\mathbf{b}$	
Source-destination power gain to noise ratio	$\mathbf{c}$	
Pairing Matrix	$\mathbf{T}$	

the pre-calculated flag matrix $\mathbf{F}$. The computational complexity of the Hungarian method is $\Theta(N^3)$, which is one order of magnitude faster than the bruteforce method, which requires testing all $\Theta(N^4)$ combinations before solving the assignment problem.

The pairing and selection method described above has a useful property that will be used in section 2.3.2:

Proposition 1: A pair (i, j) selected for relaying has $a_i > c_i$.

Proof: If a pair (i, j) is selected by Hungarian, it immediately follows that $C_R(i, j) \geq C_{NR}(i, j)$. Therefore:

$$\frac{1}{2}\log\left(1 + min\left\{a_i p_{S,i}^{(1)}, c_i p_{S,i}^{(1)} + b_j p_{R,j}\right\}\right) > \frac{1}{2}\log\left(1 + c_i p_{S,i}^{(1)}\right) + \frac{1}{2}\log\left(1 + c_j p_{S,j}^{(2)}\right) \tag{2.26}$$

The second term in the right hand side in (2.26) is always positive, and does not affect the inequality. And, if the inequality holds, it means that it is held for both terms in the min function. So, we have $\frac{1}{2}\log\left(1 + a_i p_{S,i}^{(1)}\right) > \frac{1}{2}\log\left(1 + c_i p_{S,i}^{(1)}\right)$ and it suggests $a_i > c_i$.

After pairing and selection, the second part of the problem defined in (2.23) is power allocation.

2.3.2 Power allocation

Once the pairing and selection problem is solved using techniques developed in section 2.3.1, we use the resulting $\mathbf{T}^R$ and $\mathbf{T}^{NR}$ matrices to define two sets of (i,j) index pairs as follows:

$$S_R = \{(i,j)|t_{i,j}^R = 1\} \ : \qquad \{(i,j)|p_{R,j} \geq 0, p_{S,j}^{(2)} = 0\} \tag{2.27}$$

$$S_{NR} = \{(i,j)|t_{i,j}^{NR} = 1\} : \qquad \{(i,j)|p_{R,j} = 0, p_{S,j}^{(2)} \geq 0\} \tag{2.28}$$

Now the problem can be reformulated as follows:

$$\begin{aligned} \underset{\mathbf{p}_S^{(1)}, \mathbf{p}_S^{(2)}, \mathbf{p}_R}{\text{minimize}} \quad & -\sum_{(i,j)\in S_R} \min\{\log(1+a_i p_{S,i}^{(1)}), \log(1+c_i p_{S,i}^{(1)} + b_j p_{R,j})\} \\ & -\sum_{(i,j)\in S_{NR}} \{\log(1+c_i p_{S,i}^{(1)}) + \log(1+c_j p_{S,j}^{(2)})\} \\ s.t. \quad & \mathbf{p}_S^{(1)}, \mathbf{p}_S^{(2)}, \mathbf{p}_R \succeq 0 \\ & \mathbf{1}^T \mathbf{p}_S^{(1)} = P_S, \mathbf{1}^T \mathbf{p}_S^{(2)} = P_S, \mathbf{1}^T \mathbf{p}_R = P_R \end{aligned} \tag{2.29}$$

The objective function in (2.29) is separable in $\mathbf{p}_S^{(2)}$. Note also that $\mathbf{p}_S^{(2)}$ is not coupled by constraints. Thus, we can break problem (2.29) into two sub-problems:

Sub-Problem 1: Cooperative water-filling:

$$\begin{aligned} \underset{\mathbf{p}_S^{(1)}, \mathbf{p}_R}{\text{minimize}} \quad & -\sum_{(i,j)\in S_R} \min\{\log(1+a_i p_{S,i}^{(1)}), \log(1+c_i p_{S,i}^{(1)} + b_j p_{R,j})\} \\ & -\sum_{(i,j)\in S_{NR}} \{\log(1+c_i p_{S,i}^{(1)})\} \\ s.t. \quad & \mathbf{p}_S^{(1)}, \mathbf{p}_R \succeq 0 \\ & \mathbf{1}^T \mathbf{P}_S^{(1)} = P_S, \mathbf{1}^T \mathbf{P}_R = P_R \end{aligned} \tag{2.30}$$

Sub-Problem 2: Classical water-filling:

$$\begin{aligned} \underset{\mathbf{p}_S^{(2)}}{\text{minimize}} \quad & -\sum_{(i,j)\in S_{NR}} \log(1+c_j p_{S,j}^{(2)}) \\ s.t. \quad & \mathbf{p}_S^{(2)} \succeq 0 \\ & \mathbf{1}^T \mathbf{p}_S^{(2)} = P_S \end{aligned} \tag{2.31}$$

Using the Karush-Kuhn-Tucker (KKT) conditions [Boyd and Vandenberghe (2004)], the solution of classical water-filling sub-problem is as follows:

$$p_{S,j}^{(2)} = \begin{cases} 0 & (i,j) \in S_R \\ \max\left\{0, \frac{1}{\nu_S^{(2)}} - \frac{1}{c_j}\right\} & (i,j) \in S_{NR} \end{cases} \tag{2.32}$$

where the constant $\nu_S^{(2)}$ is chosen such that the constraint $\mathbf{1}^T \mathbf{p}_S^{(2)} = P_S$ is satisfied.

For solving the cooperative sub-problem water-filling, we first investigate its convexity by introducing new variable w.

$$\begin{aligned} \underset{\mathbf{p}_S^{(1)}, \mathbf{p}_R}{\text{minimize}} \quad & -\sum_{(i,j)\in S_R} \log(1+w_i) - \sum_{(i,j)\in S_{NR}} \log(1+c_i p_{S,i}^{(1)}) \\ s.t. \quad & w_i \le a_i p_{S,i}^{(1)},\ (i,j) \in S_R \\ & w_i \le c_i p_{S,i}^{(1)} + b_j p_{R,i}, (i,j) \in S_R \\ & w_i \ge 0,\ (i,j) \in S_R \\ & p_{S,i}^{(1)} \ge 0, (i,j) \in S_{NR} \\ & \mathbf{1}^T \mathbf{p}_S^{(1)} = P_S, \mathbf{1}^T \mathbf{p}_R = P_R \end{aligned} \tag{2.33}$$

The cooperative water-filling sub-problem is equivalent to (2.33), and the convexity of (2.33) is obvious, because, the objective function is a summation over convex functions, and constraints are all affine and linear [Boyd and Vandenberghe (2004)]. Now we solve the problem in two steps:

Step 1: We set the source powers to be constant and optimize the relay power by writing the KKT conditions:

$$p_{R,j} = \begin{cases} \min\left\{\max\left\{0, \frac{1}{\nu_R} - \frac{c_i p_{S,i}^{(1)}+1}{b_j}\right\}, \frac{a_i-c_i}{b_j} p_{S,i}^{(1)}\right\}, \\ \qquad\qquad (i,j) \in S_R \\ 0 \qquad\qquad (i,j) \in S_{NR} \end{cases} \tag{2.34}$$

in which, the constant ν_R is chosen such that the constraint $\mathbf{1}^T \mathbf{p}_R = P_R$ is satisfied. As stated before in proposition 1, if a pair (i,j) is in the set S_R, then $a_i - c_i > 0$. And in turn, $\left(\frac{a_i-c_i}{b_j}\right) p_{S,i}^{(1)}$ is a positive constant.

Step 2: We set the relay powers to be constant and optimize the source power by writing the KKT conditions:

$$p_{S,i}^{(1)} = \begin{cases} \min\left\{\max\left\{0, \frac{1}{\nu_S^{(1)}} - \frac{1}{a_i}\right\}, \frac{b_j}{a_i-c_i} p_{R,j}\right\}, \\ \qquad\qquad (i,j) \in S_R \\ \max\left\{0, \frac{1}{\nu_S^{(1)}} - \frac{1}{c_i}\right\}, (i,j) \in S_{NR} \end{cases} \tag{2.35}$$

in which, the constant $\nu_S^{(1)}$ is chosen such that the constraint $\mathbf{1}^T \mathbf{p}_S^{(1)} = P_S$ is satisfied. Again, according to proposition 1, $\frac{b_j}{a_j-c_j} p_{R,j}$ is a positive constant.

Finally, these two steps can be conducted alternatively until convergence is reached. Simulation results show that this process converges quickly to an optimal point.

2.4 Numerical Results

2.4.1 Amplify-and-Forward

We evaluate the proposed subcarrier relay selection technique using different relay positions and power budgets, and we compare the resulting capacity with the one we can obtain with non-relaying and all-subcarriers relaying schemes. For all the numerical evaluations, we adjust P_S to obtain a nominal average signal-to-noise ratio $\rho_k = 0$ dB in all source-to-destination, non-

relaying links as in [Hammerstrom and Wittneben (2006)]. The fading channel gain follow a complex normal distribution as defined in [Hammerstrom and Wittneben (2006)]:

$$h_{n,k} \sim CN\left(0, \frac{1}{L(1+d)^{\alpha}}\right) \tag{2.36}$$

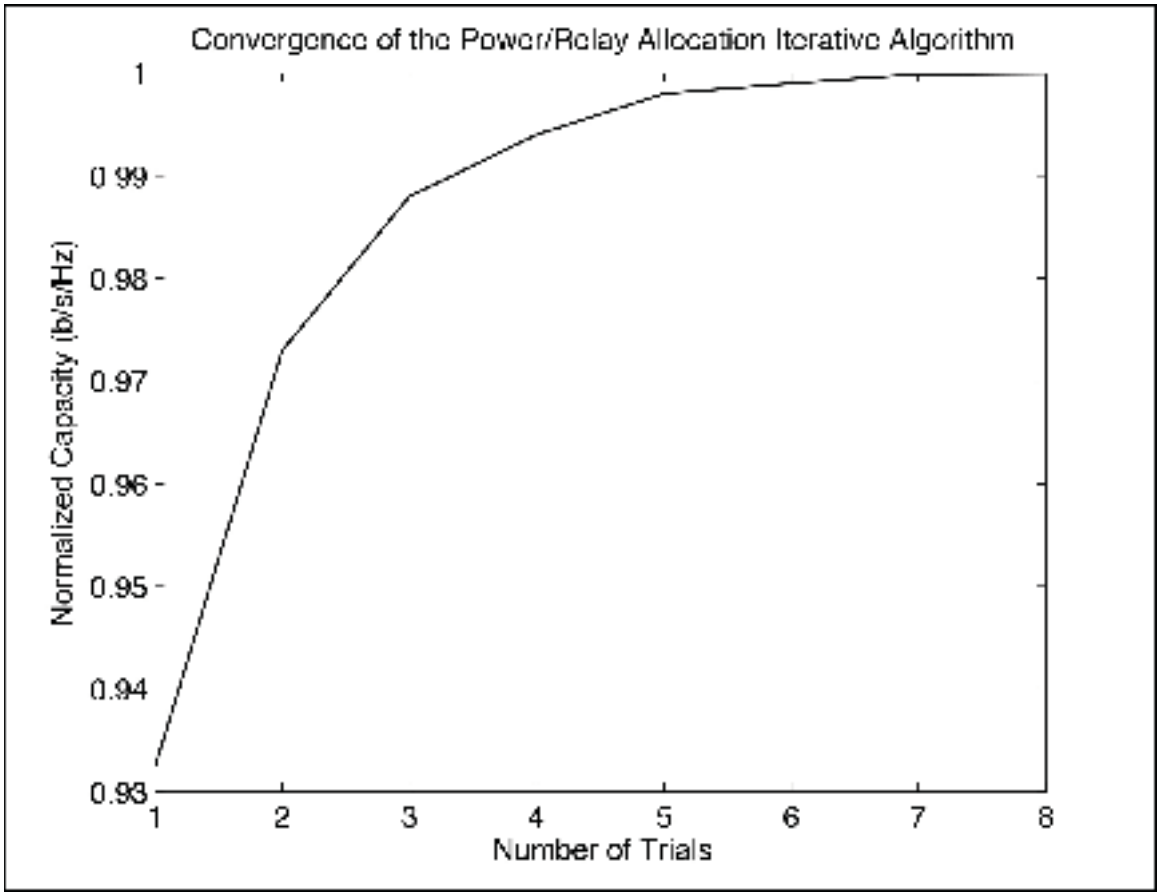

Figure 2.6 Convergence of the selection heuristics.

with $\alpha = 3$, distance d m, and $L = 4$. Using $|h|^2$ from (2.36) and $\sigma_d^2 = \sigma_r^2 = 4.14 \times 10^{-17}$, and $N_{FFT} = 16$ subcarriers, we calculate values for the channel gain to noise power ratios a_k, b_k and c_k defined in (2.3). For all of the calculations, the source-destination distance is set to 1000 meters. For all the considered scenarios, the algorithm described in Section 2.2.2 reaches 99% of the achievable capacity in a total of 3 trials. Extensive simulations show that the heuristic

described in section 2.2.1 converges to a maximal value after setting up to 6 subcarriers to *not relay*, or $\mu_k = 0$, as shown on Fig. 2.6.

2.4.1.1 Capacity vs Relay Power Budget

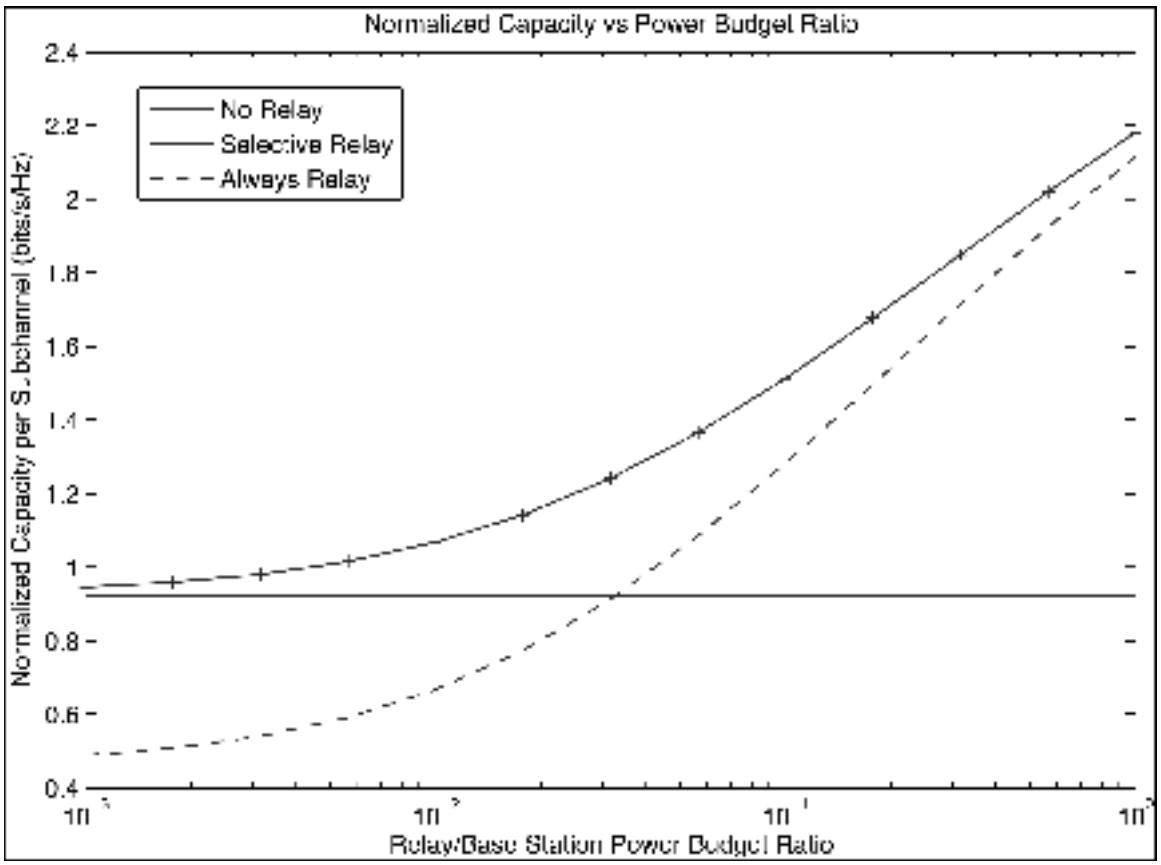

Figure 2.7 Capacity vs. relay/base station power ratio.

We first measure the impact of modifying the relay power budget on the overall capacity of the system. We position the relay at an equal distance of $d = 500$ m from both the source and destination, and we calculate the capacity for systems where relaying occurs in all subcarriers, and for systems with selective subcarriers relaying, using the algorithm described in Section 2.2.2. The results are shown in Fig. 2.7.

The non-relaying link is used as a reference performance against which we compare our algorithm, and the numerical results for this link are represented as the unitary capacity “No relay" curve in Fig. 2.7. The “Always Relay" system improves capacity over the reference “No Re-

lay" scheme with high relay power budgets, i.e. when $P_R > 0.04P_S$. For lower power budgets, it is always better to not relay, at least in some of the subcarriers. Under high power relay budgets, it is always better to relay in all subcarriers, and our selective relay method tends to the “Always Relay" case. Similarly, under low power budgets, it is better not to relay at all, and our system tends to the “No Relay" case. When the relay power budget is between these extreme values, selective subcarrier relaying improves capacity over both comparative schemes.

2.4.2 Capacity vs Distance under High Relay Power Budget

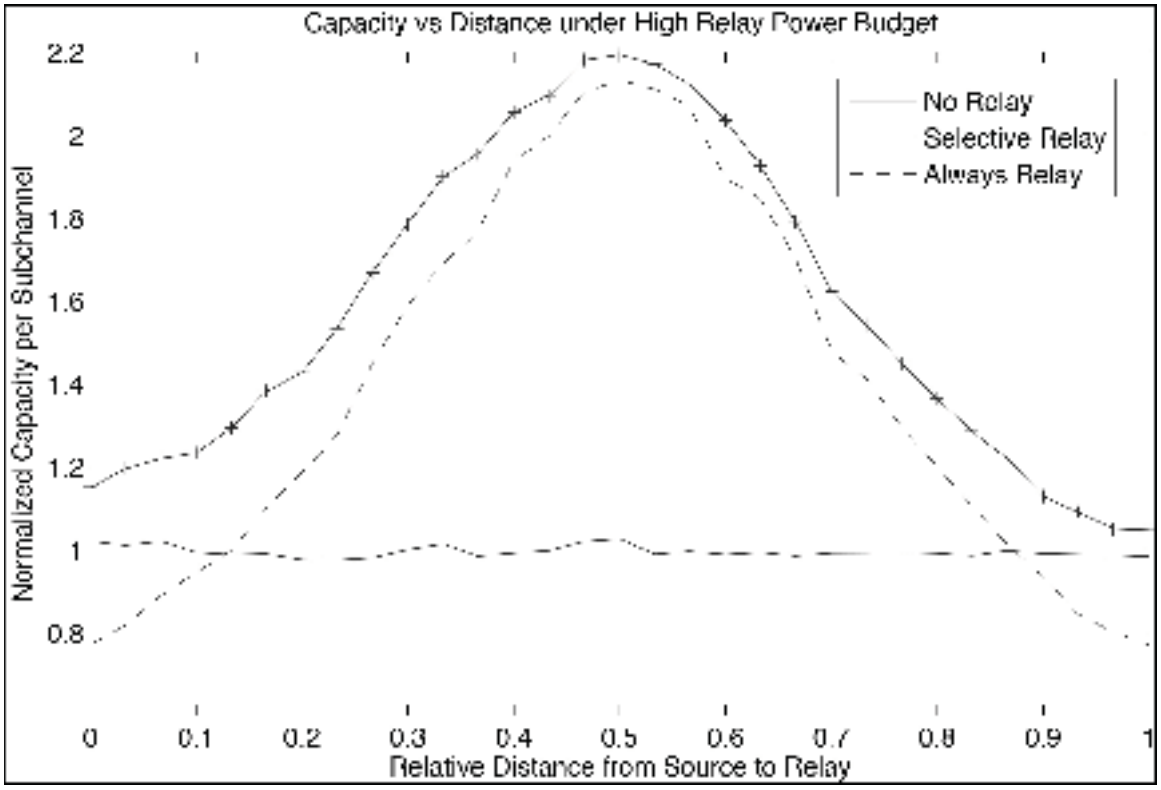

Figure 2.8 Capacity vs. distance for high relay power budget.

In this section, we set the relay power budget $P_S = P_R$ to values that maintain the comparative SNR $\rho_{0,k} = 0$ dB, and we place the relay between the source and destination, and calculate the capacity for several distances to source relatively to the source-destination destination. The results are shown in Fig. 2.8. The “Always Relay" scheme improves capacity for all positions except when the relay is located close to either the source or destination. In these positions, the long-distance channels dominate the relaying signal to noise ratios, and make it hard to

compensate for the 0.5 loss in capacity created by the half duplex relaying scheme performed on all subcarriers.

Using the proposed selective subcarrier relaying, we obtain better capacity for any relay position, but when the relay is located close to the destination, we simply do not relay in any subcarrier, and obtain a capacity equivalent to the “No Relay" case. The offset observed when the relay and source are co-located is explained by the small capacity increase obtained with using the full P_R in a few subcarriers, so that their capacity is improved, even considering the 0.5 half duplex cost.

The symmetry of these curves can be explained from the symmetry of the amplify-and-forward SNR in (2.3), where a_k increases as b_k decreases when the relay is moved towards the source. Also, in this particular case, we impose equal source and relay power budgets, suggesting that, on average, the allocated source and relay powers are equal, keeping the symmetry property about relay distance.

2.4.2.1 Capacity vs Distance under Low Relay Power Budget

As we have seen in Section 2.4.1.1, the achievable capacity should be higher in the selective relaying scheme for low relay power budgets. As in the previous section, we calculate the capacity for different relative distances with $P_R = 0.04P_S$. Figure 2.9 shows that the selective subcarrier relaying scheme improves capacity over all distances, but when the relay is located close to the source, the capacity is equal to the capacity of the “No Relay" scheme. The “Always Relay" scheme only improves capacity in a limited portion of positions, close to the destination and degrades capacity for other positions. These results show how that the selective relaying schemes presented in this paper improve capacity over all non-selective algorithms presented in the litterature in the studied scenario. It also shows that a naive implementation of relays depicted in the “Always Relay" scheme can actually worsen overall capacity performances over a point-to-point communication link with no relay.

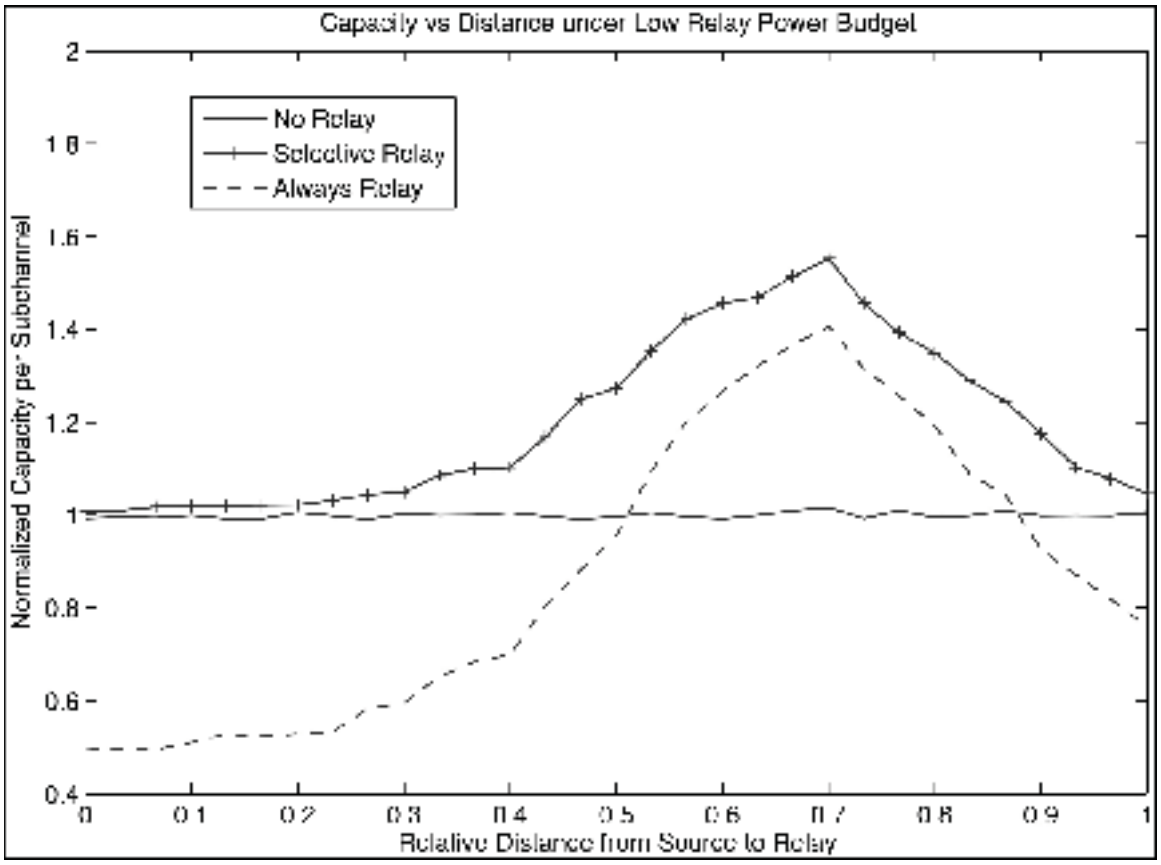

Figure 2.9 Capacity vs. distance for low relay power budget.

2.4.3 Decode-and-Forward Numerical Results

We demonstrate the performance of our selective DF subcarrier pairing and PA technique through simulation for different source-relay and relay-destination distances, and different source and relay power budgets. It is assumed that all the three nodes are located on a line. The distance between source and destination (d_0) is always 1000 m, and location of the relay is indicated by $\frac{d_r}{d_0}$ where d_r is source-relay distance. We consider an OFDM modulation with $N_{FFT} = 16$, subcarrier separation of 10 kHz, and $\sigma_r^2 = \sigma_d^2 = 4.47 \times 10^{-17}$. Channel complex gains h_i are picked from a Rayleigh fading channel with the following distribution [Hammerstrom and Wittneben (2006)]:

$$h_i = \mathcal{CN}\left(0, \frac{1}{L(1+d)^{\alpha}}\right) \tag{2.37}$$

where the path loss exponent $\alpha = 3$, distance d m, and the number of taps $L = 4$. Source power budget is selected such that for all subcarriers we have the average SNR of 0 dB at destination. Finally, given $|h|^2, \sigma_r^2, \sigma_d^2, N_{FFT}$ and subcarrier separation, the channel gains to noise power ratios a_i, b_i and c_i are calculated as described in section 2.2.

2.4.4 Convergence

We study the convergence of the iterative process described in section 2.3.2. As it will be shown later in this section, the distance and power budgets play a major role in the selection and power allocation decisions, so we performed simulations scenarios for different relay power budgets of $P_R = P_S$, $0.1P_S$ and $0.04P_S$, and for relays positioned either at midpoint between source and relay, or at a relative distance $\beta \sim U[0, 1]$. The average ratio of subcarriers used for relaying for these scenarios is shown on table 2.3. We also show the convergence rate of these scenarios on Fig. 2.10.

Table 2.3 Relaying Subcarriers Ratio

Relay Power Budget	**% Relaying Subcarriers**	
	$d_r = 0.5d_0$	$d_r = \beta d_0$
P_S	92.75	67.5
$0.1 \cdot P_S$	74.44	49.94
$0.04 \cdot P_S$	57.31	40.44

Analyzing the results on Fig. 2.10, we first find that the iterative process converges to the optimal solution for every considered scenario and even the first step is very close to the optimal. An important observation is that the convergence time increases when the ratio of relaying subcarriers is close to 50%. This is a situation where the number of pairing and selection combinations is large, and it takes more trials to reach the optimal solution.

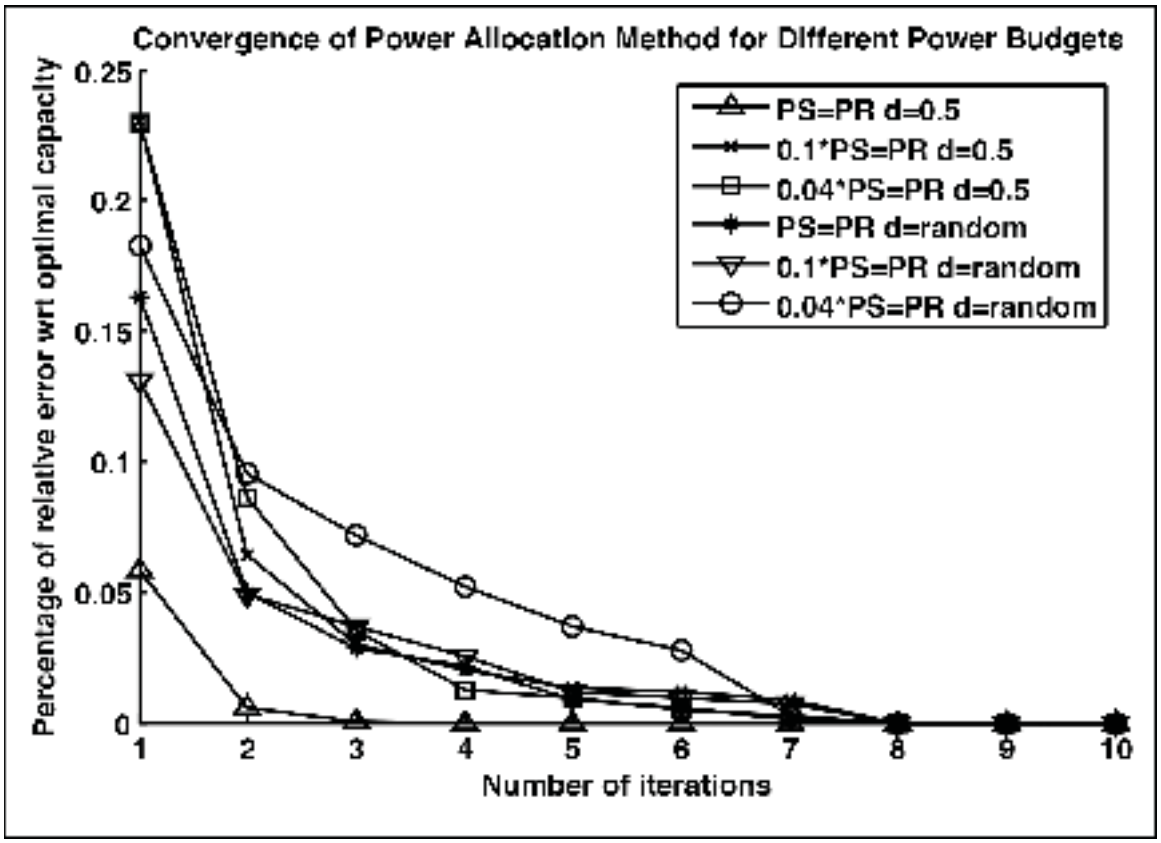

Figure 2.10 Convergence of the power allocation technique.

2.4.5 Pairing and Selection Performance

We consider the performance of the pairing and selection parts of the process described in section 2.3.2. We performed simulations for a power budget of $P_R = 0.1 \cdot P_S$, with several positions for the relay node. The resulting capacity for scenarios where pairing and selection are activated or not are shown in Fig. 2.11. Analyzing the result, we observe that selection plays an important role in cooperative capacity, and that any scenario without considering selection will worsen capacity for some positions of the relay. For instance, the *always relay* curves of Fig. 2.11 fall below the reference "$1\,B/S/Hz$" non-relaying capacity for several relay positions. Pairing is mainly useful when a lot of relaying occurs. Overall, it appears clearly with the results that pairing and selection using the method described in section 2.3.2 improves capacity over non-selective and non-pairing schemes for every considered relay position.

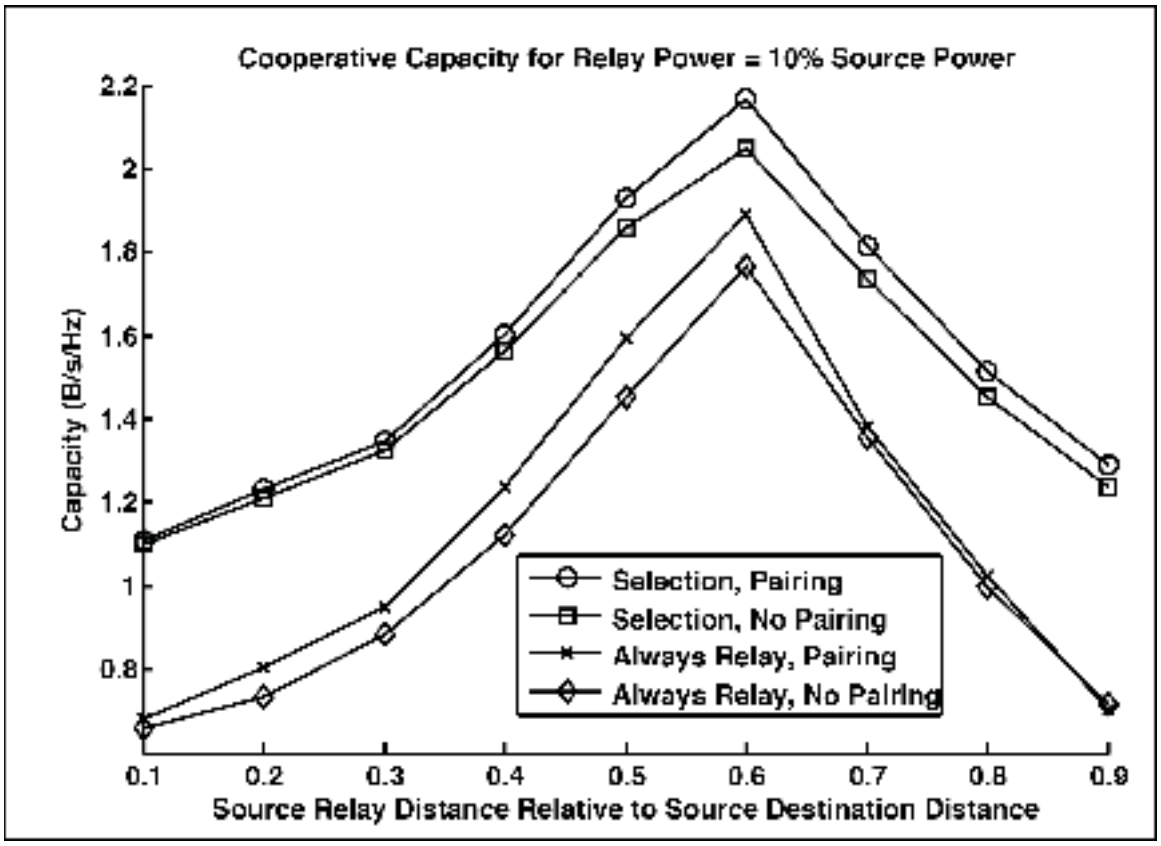

Figure 2.11 Performance of the pairing and selection processes.

2.4.5.1 Power Allocation

We study the performance of the power allocation part of the process described in section 2.3.2 for several relay node positions, and show the resulting capacity for relay power budget $P_R = P_S$ on Fig. 2.12 and $P_R = 0.1 \cdot P_S$ on Fig. 2.13. We will first compare observations between these figures:

Location of the Peak Capacity: In the equal power budget case, the peak occurs at the midpoint between source and relay.

When the relay power ratio is less, the peak capacity with regards to position moves towards the destination, because the maximal capacity occurs when the source-relay and relay-destination links have the same level of SNR.

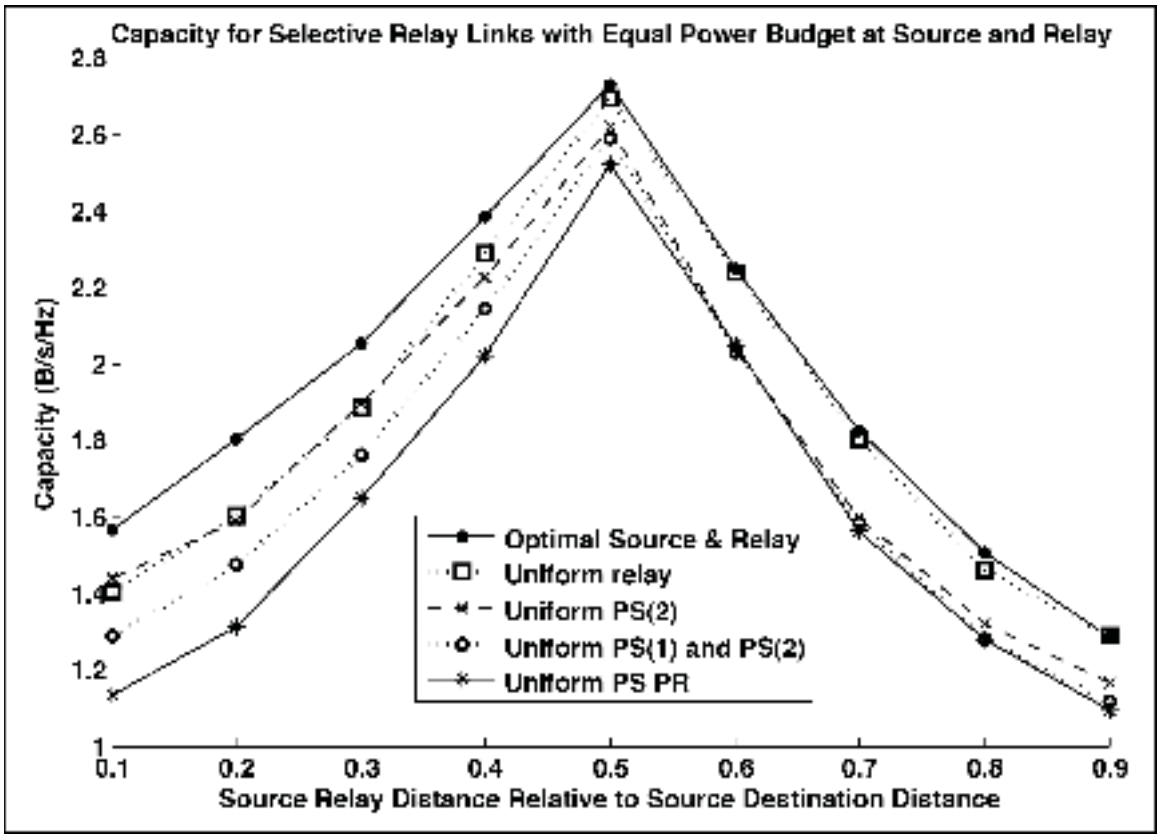

Figure 2.12 Capacity for equal power budgets at source and relay.

Capacity Close to the Destination: The capacity obtained for both scenarios when the relay is close to destination is similar, because the min function in (2.21) is dominated by the source-relay link, which is weaker than the relay-destination link.

Capacity Elsewhere: The capacity obtained in the equal power scenario is much higher compared to the reduced relay power, because more power is available at the relay, and in turn, more subcarriers will be used for relaying. For instance, at distance $d_r = 0.5d_0$, table 2.3 shows an average of 92.75% relaying subcarriers for the equal power scenario and 74.4% for the reduced relay power scenario.

Now, we analyze the performance of different power allocation schemes for both relay power budget scenarios in Fig. 2.12 and 2.13. We use uniformly distributed power as a reference to which we compare optimal power allocation.

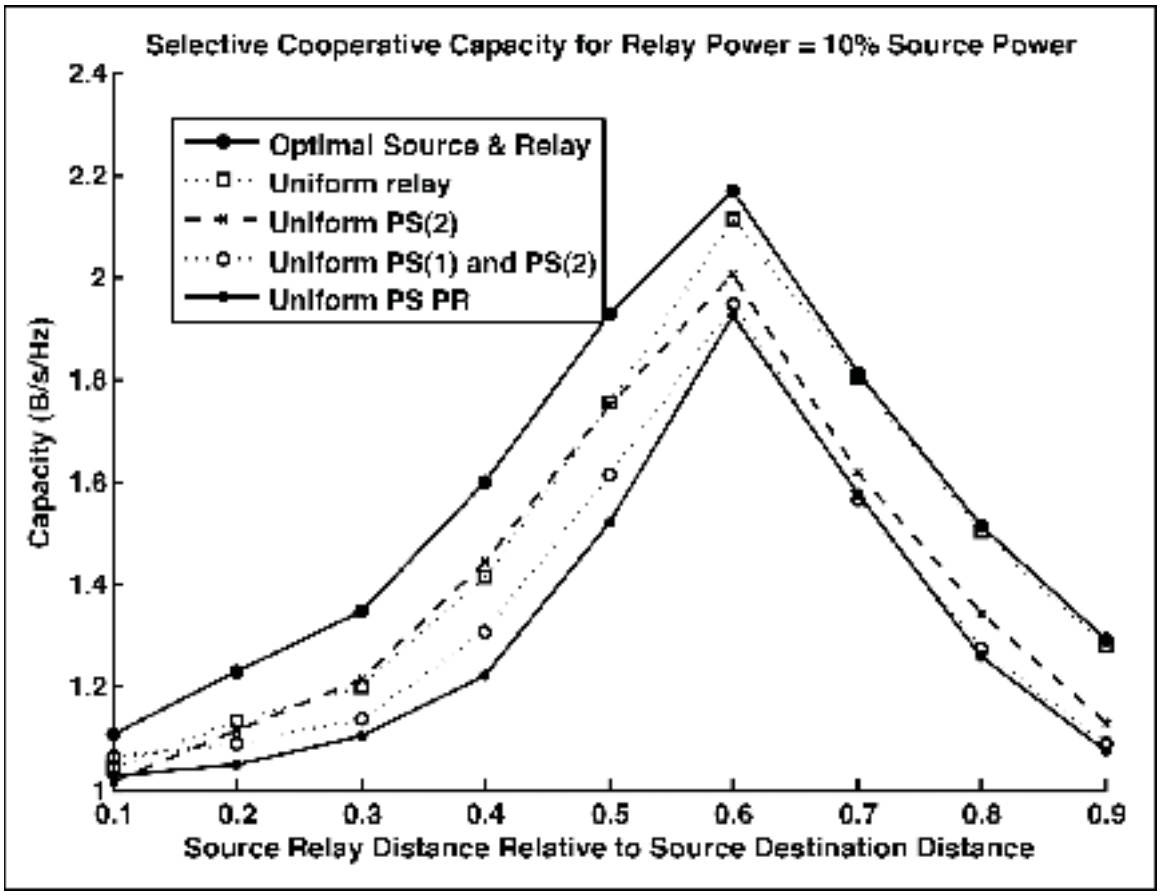

Figure 2.13 Capacity for reduced relay power budget.

Performance Gain: It is observed that our power allocation technique improves capacity for any considered relay position and relay power budget scenario.

Source Power Importance: It can be seen that *uniform relay* curves offer better performances than all uniform source power curves for most considered positions of the relay. This is because the source power allocation has an impact on both direct and relay links, which is not the case for relay power allocation.

Impact of the source power in time slot 2 vector $p_S^{(2)}$: Recent research in the field [Ying *et al.* (2007) and Vandendorpe *et al.* (2008b)] did not include the $p_S^{(2)}$ optimization. In our scenario, we associate these schemes to the *uniform* $p_S^{(2)}$ curves, which show considerably less capacity than our *optimal source and relay* method.

2.5 Conclusion

We have studied the capacity of a selective cooperative relaying wireless communication scheme using OFDM modulation under power constraints for both the base station and the relay station. We have developed a scheme for subcarrier relay selection and power allocation that outperforms nonselective relaying schemes over a range of relay power budgets, and converges in a few iterations.

We have also presented algorithms for decode-and-forward relaying schemes permitting the relay to pair source-transmitted and relay-transmitted subcarriers. We have developed a method for optimizing the capacity of cooperative systems operating under this signalling scheme. We have analytically demonstrated that our method maximizes instantaneous rates using CSI, for several individual power budgets and relay location scenarios. Numerical results show that our method outperforms systems using similar solutions to the most recent research in the field. Also, adding pairing and selection processes to our iterative power allocation problem greatly improves capacity performance, without considerably increasing the computational complexity.

CHAPTER 3

BLIND MULTI-SOURCES DETECTION AND LOCALIZATION FOR COGNITIVE RADIO

3.1 Introduction

In recent years, cognitive wireless communication networks have emerged as a way to improve frequency spectrum use by offering unlicensed secondary users the opportunity to momentarily occupy spectrum holes in licensed bands [Haykin (2005)]. When occupying licensed spectrum bands, the cognitive radio must not cause any perceptible harmful effect for every primary receiver. Radio scene analysis is an important advance associated with cognitive radios [Haykin (2005); Bhargava and Hossain (2007)] because the knowledge it offers allows the radio to adapt to the changing radio frequency environment. With extensive knowledge on both the location and class of all local users, the cognitive radio can efficiently reuse spectrum holes and avoid causing any harmful interference on primary users [Haykin (2005)]. Cognitive radios must also adapt to presumably non-cooperative legacy primary user networks and secondary user competitors seeking to occupy the spectrum as well.

Secondary users attempting to efficiently reuse spectrum holes left free by single-carrier linear digital (SCLD) primary users can use orthogonal frequency division modulation (OFDM) schemes to occupy spectrum bands efficiently [Haykin (2005), Cabric and Brodersen (11-14 Sept. 2005)]. In order to determine whether sources are primary or secondary users, the cognitive radio must then classify incoming signals through modulation classification (MC). Recently proposed OFDM-SCLD blind MC algorithms require carrier and timing recovery [Akmouche (1999)], or estimation of signal-to-noise ratio (SNR) [Wang and Ge (23-26 Sept. 2005)], before the recognition algorithm applied. The classification algorithm proposed in [Punchihewa *et al.* (3-7 Sept. 2007)] does not require the preprocessing tasks, such as symbol timing estimation, carrier and waveform recovery, and signal and noise power estimation. However, it requires the knowledge of presence or absence of signals to avoid identifying noise input as single carrier. This knowledge is not available for uncooperative radios like primary

users or competing secondary users. Also, authors did not investigate the classifier's performance with multiple received signals.

The MC algorithm proposed in [Punchihewa *et al.* (3-7 Sept. 2007)] requires the presence of a single signal source to perform classification correctly. If these requirements are not satisfied, the MC algorithm can misclassify the signal sources. In order to overcome this issue, our original contribution is to combine the number of sources estimation provided by the MUSIC [Godara (2004)] algorithm to the MC algorithm described in [Punchihewa *et al.* (3-7 Sept. 2007)] to ensure the cognitive radio's knowledge on the location of primary and secondary users.

In order to extend the spatial reuse, the location of other users has to be known so the cognitive radio can avoid disturbing them. Several localization techniques have been proposed, but may require cooperation from mobile users through the use of a beacon signal [Bulusu *et al.* (Oct. 2000)] or pseudo-noise sequence [Caffery and Stuber (May 1998)]. Angle of arrival estimation (AoA) is an efficient way to measure users location and may not require cooperation from sources [Godara (2004)]. The multiple signal classification (MUSIC) algorithm has been proven efficient for AoA [Bulusu *et al.* (Oct. 2000)] and estimating the number of present sources [Hu *et al.* (1999b)]. In this paper, we show how we can combine these localization techniques to classification and detection to effectively identify spectral spectrum holes.

The rest of the chapter is organised as follows: Signal models and the proposed localization and classification algorithms are introduced in Sections 3.2 and 3.3, respectively. Simulation results for the proposed algorithm are discussed in Section 3.4. Finally, conclusions are drawn in Section 3.5.

3.2 Signal Model

The signal model considered in this chapter includes wireless transmissions from primary and secondary users through an additive white gaussian noise (AWGN) channel and the receiver consists of a uniform linear array.

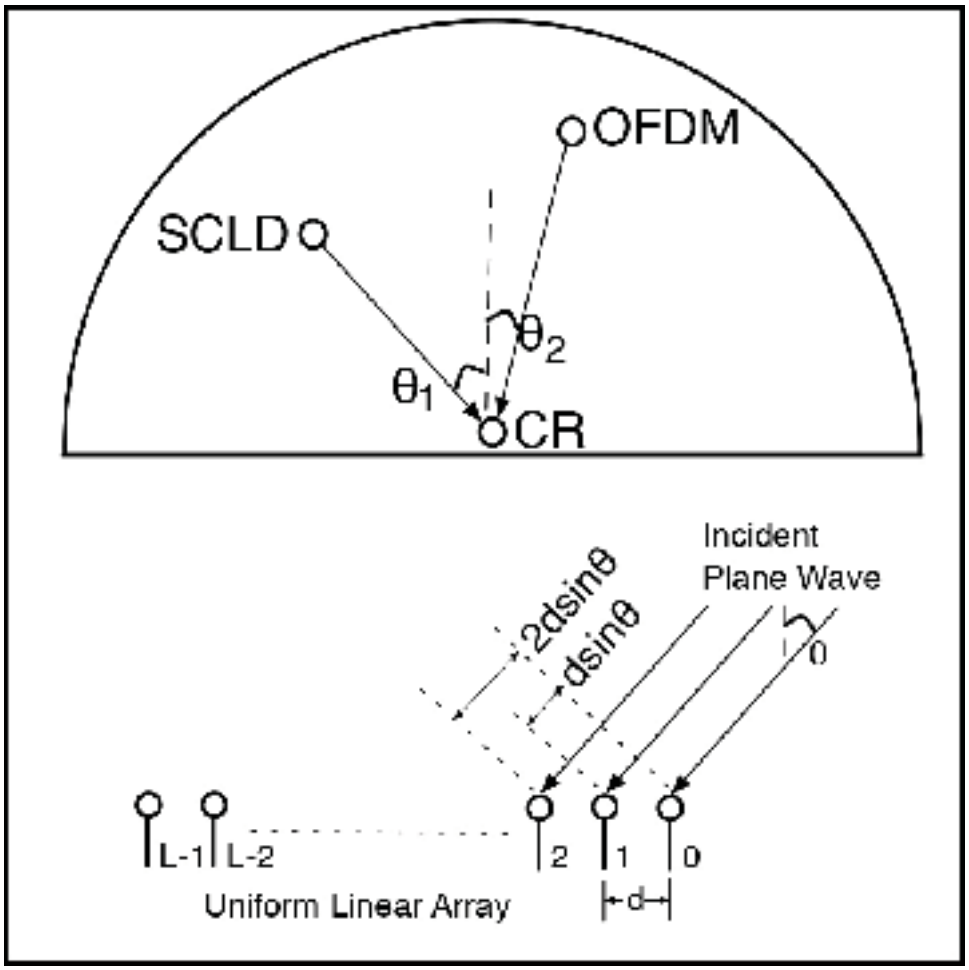

Figure 3.1 Angles of arrival measurement setup.

3.2.1 Primary and Secondary Users Signals

The noiseless received SCLD and OFDM modulated signals $s_{SCLD}(t)$ and $s_{OFDM}(t)$ are defined as follows [Punchihewa *et al.* (3-7 Sept. 2007)]:

$$s_{SCLD}(t) = \alpha\, e^{j\phi} e^{j2\pi\Delta f_c t} \sum_{p=-\infty}^{\infty} s_p g(t - pT - \epsilon T) \tag{3.1}$$

$$s_{OFDM}(t) = \alpha\, e^{j\phi} e^{j2\pi\Delta f_c t} \sum_{k=0}^{K-1} \sum_{p=-\infty}^{\infty} s_{k,p} e^{j2\pi\Delta f_K (t - pT - \epsilon T)} g(t - pT - \epsilon T) \tag{3.2}$$

where α is the attenuation factor, ϕ is the initial phase, Δf_c is the carrier frequency offset, s_p and $s_{k,p}$ represent the symbols transmitted within the p^{th} period, and the p^{th} period and k^{th} subcarrier, respectively. Function *g(t)* is the pulse shape, *T* is the symbol period, and $0 \leq \epsilon \leq 1$ is the timing offset. For OFDM modulation scheme, Δf_K is the frequency separation between adjacent subcarriers, *K* is the total number of subcarriers and the symbol period is given by $T = T_{use} + T_{cp}$ where the useful symbol duration is $T_{use} = \Delta f_K^{-1}$ and the cyclic prefix is usually $T_{cp} = T_{use}/4$.

3.2.2 Received Signal

As shown in Fig. 3.1, the receiver is equipped with an array of L antennas with uniform distance *d*, which offers different channel lengths for each element of the antenna array. These differences in distances are shown in Fig. 3.1, as $ldsin(\theta)$, where l refers to the antenna's number and θ is the wave's angle of arrival from SCLD and OFDM sources located at an unknown distance from a cognitve receiver (CR). These effects can be accounted for using vector $\mathbf{a}(\theta)$:

$$\mathbf{a}(\theta) = [a_0(\theta), a_1(\theta), \cdots, a_{L-1}(\theta)] \tag{3.3}$$

with its elements defined as:

$$a_l(\theta) = e^{\frac{j2\pi ldsin(\theta)}{\lambda_0}}, \quad 0 \leq l \leq L-1 \tag{3.4}$$

where λ_0 is the received signal's wavelength.

The signal received at the antenna array level is defined by the L-sized vector **r**(t,θ):

$$\mathbf{r}(t, \theta) = \mathbf{a}(\theta)s(t) + \mathbf{n}(t) \tag{3.5}$$

with **n**(t) a L-sized vector with independent AWGN elements.

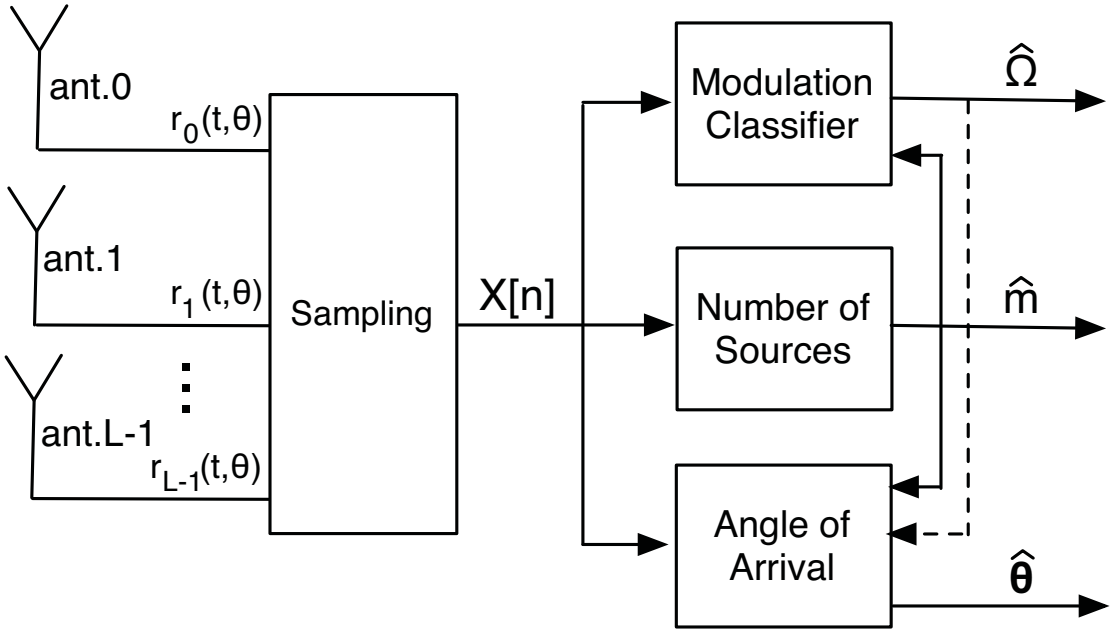

Figure 3.2 Block diagram for receiver system.

As shown in Fig. 3.2, for each snapshot n, N samples of **r**(t,θ) are saved in the received L x N matrix X[n]:

$$X[n] = [\mathbf{r}(t_0, \theta), \mathbf{r}(t_0 + t_s, \theta), \cdots, \mathbf{r}(t_0 + (N-1)t_s, \theta)] \tag{3.6}$$

3.3 Detection and Localization Algorithm

An important objective for cognitive systems is to detect spectrum holes [Haykin (2005)], and maximize the exploitation of these novel wireless communications opportunities. OFDM is a very efficient way for cognitive secondary user networks to fill those dynamic spectrum holes [Cabric and Brodersen (11-14 Sept. 2005)]. Therefore, when a secondary user detects OFDM transmissions in a band, a competitor secondary user network is most likely filling a significant portion of the available spectrum holes. On the other hand, if no OFDM transmission is detected, a larger number of spectrum holes can be expected. The primary objective of our algorithm is to provide AoA of primary sources in order to exploit spectrum holes when no OFDM sources are detected.

For each considered snapshot *n* of $X[n]$, the proposed system, shown in Fig. 3.2, operates as follows:

a. Determine the number of sources $\hat{m}$;

b. if $\hat{m} \geq 1$, evaluate the OFDM presence detector Ω;

c. if $\Omega = false$, calculate the AoA estimate $\hat{\Theta}$, for all primary users;

d. modify the cognitive radio's antenna array radiation pattern to minimize transmitted power for every $\Theta \approx \hat{\Theta}$[1].

We employ the MUSIC algorithm [Godara (2004)] to detect the number of sources and the AoA of incoming signals. The modulation classifier is based on results in [Punchihewa *et al.* (3-7 Sept. 2007)]. In the following, we describe the functionalities of each of these blocks, also shown in Fig. 3.2.

3.3.1 Number of Sources

The first objective of the algorithm is to determine the number of distinctive sources in order to provide presence of signal information to the MC block.

First, we calculate $\hat{C}$, the estimate of the L x L covariance matrix for a given snapshot $X[n]$. The elements $\hat{c}_{i,j}$ of $\hat{C}$ are defined as follows:

$$\hat{c}_{i,j} = \frac{1}{N-1} \sum_{k=1}^{N} (X_{i,k}[n] - \bar{X}_i[n])(X_{j,k}[n] - \bar{X}_j[n]) \tag{3.7}$$

where

$$\bar{X}_i[n] = \frac{1}{N} \sum_{k=1}^{N} X_{i,k}[n] \tag{3.8}$$

[1]The 4^{th} element of the algorithm will be considered as future work.

Then, the covariance matrix $\hat{C}$ is decomposed in eigenvalues matrix Λ and eigenvectors matrix Q:

$$\hat{C} = Q\Lambda Q^{-1} \tag{3.9}$$

for which we consider that the diagonal elements of Λ are arranged in descending order, and the corresponding eigenvectors in Q are ordered accordingly. The diagonal elements of Λ are then stored in L-elements vector $\boldsymbol{\lambda}$. These eigenvalues are separated in two groups [Zhang *et al.* (Oct 1989)], the signal subspace: $\boldsymbol{\lambda}_s$

$$\boldsymbol{\lambda}_{ss} = [\lambda(0)\,\lambda(1)\,\cdots\,\lambda(\hat{m}-1)] \tag{3.10}$$

and the noise subspace $\boldsymbol{\lambda}_{ns}$

$$\boldsymbol{\lambda}_{n} = [\lambda(\hat{m})\,\lambda(\hat{m}+1)\,\cdots\,\lambda(L-1)] \tag{3.11}$$

The objective of the algorithm is to estimate the threshold shift Γ that separates these two groups.

$$\Gamma = \frac{\psi Ps}{\left(1+\sqrt{\frac{Ps}{L}}\right)^2} \tag{3.12}$$

where

$$Ps = \frac{\lambda(0)-\lambda(L-1)}{L} \tag{3.13}$$

and ψ is a constant depending on the quality of the data [Hu *et al.* (1999b)]. The number of sources $\hat{m}$ is then estimated with:

$$\hat{m} = \begin{cases} 0 & \text{if } \hat{\mathbf{m}} = \emptyset \\ \max(\hat{\mathbf{m}}) & \text{otherwise} \end{cases} \tag{3.14}$$

where $\emptyset$ represents the empty set and

$$\hat{\mathbf{m}} = \{\forall\, i \in \{0, 1, 2, \ldots, L-1\} : \lambda(i-1) - \lambda(i) > \Gamma\} \tag{3.15}$$

As discussed in section 3.1, in order to avoid misclassification of noise-only inputs, the MC algorithm requires at least one input signal to be present. Therefore, we only invoke the MC algorithm when $\hat{m} \neq 0$.

3.3.2 Blind Detection and Classification

We classify OFDM against single-carrier linear digital (SCLD) with the lowest order non-zero cyclic cumulants (CC), second-order/ one conjugate, as in [Punchihewa *et al.* (3-7 Sept. 2007)]. The input signal for the classification algorithm is a snapshot *n* of $X[n]$ for which the *number of sources* block has detected the presence of at least one source. We consider $r = r_0$, the first row of the received signal $X[n]$, representing the input signal from antenna 0. We calculate the estimate $\hat{c}_{r_\Omega}(\beta;\tau)_{2,1}$ of the second order, one conjugate CC of *r* at cycle frequency (CF) β and delay τ as:

$$\hat{c}_{r_\Omega}(\beta;\tau)_{2,1} = \frac{1}{U}\sum_{u=0}^{U-1} r_\Omega(u+\tau)\cdot r_\Omega^H(u)e^{-2j\pi\beta u} \tag{3.16}$$

where *U* is the total number of time samples in the received signal vector r and Ω represents the unknown class of signal *r*:

$$\Omega = \begin{cases} 1 & \text{if at least one OFDM source is present} \\ 0 & \text{if only SCLD sources are present} \end{cases} \tag{3.17}$$

Under the assumption that there is no aliasing, the second-order/ one-conjugate CC at CF β and delay τ for SCLD and OFDM signals are given as [Punchihewa *et al.* (3-7 Sept. 2007)]:

$$\begin{aligned} c_{r_{SCLD}}(\beta;\tau)_{2,1} &= \alpha^2 c_{s,2,1}\rho^{-1}e^{-j2\pi\beta\epsilon\rho}e^{-j2\pi\rho^{-1}\Delta f_c T\tau} \\ &\quad\cdot\sum_u g(u+\tau)g^H(u)e^{-j2\pi\beta u} + c_w(\beta;\tau)_{2,1} \end{aligned} \tag{3.18}$$

$$c_{r_{OFDM}}(\beta;\tau)_{2,1} = \alpha^2 c_{s,2,1} D^{-1} e^{-j2\pi\beta\epsilon D} e^{-j2\pi(\rho K)^{-1}\Delta f_c T_u \tau} \cdot \Xi_K(\tau) \sum_u g(u+\tau) g^H(u) e^{-j2\pi\beta u} + c_w(\beta;\tau)_{2,1} \tag{3.19}$$

where

$$\begin{aligned} \Xi_K(\tau) &= \sum_{k=0}^{K-1} e^{-j2\pi(\rho K)^{-1} k\tau} \\ &= e^{j\pi(\rho K)^{-1}(K-1)\tau} \cdot \frac{\sin(\pi\tau\rho^{-1})}{\sin(\pi\tau(\rho K)^{-1})} \end{aligned} \tag{3.20}$$

here, ρ represents the oversampling factor, $C_w(\beta;\tau)_{2,1}$ represents the noise CC, and *D* represents the total number of samples in one OFDM symbol period. The classification of OFDM against SCLD is based on the existence of a significant peak located at a non-zero delay value of the estimated second-order/ one-conjugate CC magnitude. Classification of OFDM against SCLD is performed in two steps. First, we locate a non-zero peak in the estimated second-order/ one-conjugate CC magnitude at delay τ_{peak}, with $0 < \tau_{peak} < U$, and at CF $\beta = 0$. Then, using the cyclostationarity test developed by Dandawate [Dandawate and Giannakis (Sep 1994)], we check whether or not $\beta = 0$ is indeed a CF for delay $\tau = \tau_{peak}$. If $\beta = 0$ is found to be a CF for delay $\tau = \tau_{peak}$, the signal is classified as OFDM, otherwise the signal is classified as SCLD.

3.3.3 Angle of Arrival

Using the number of sources, and the eigenvectors Q calculated in the *number of sources* block, we employ the MUSIC algorithm to estimate the angle of arrival for all of these sources. First, we obtain $Q_{ns} \subseteq Q$, the noise subspace eigenvectors matrix by keeping the eigenvectors that

are associated with the noise eigenvalues $\boldsymbol{\lambda}_{ns}$:

$$Q = [\mathbf{v}_0\, \mathbf{v}_1\, \cdots\, \mathbf{v}_{L-1}] \tag{3.21}$$

$$Q_{ns} = [\mathbf{v}_{\hat{m}}\, \mathbf{v}_{\hat{m}+1}\, \cdots\, \mathbf{v}_{L-1}] \tag{3.22}$$

Then we estimate the angle of arrival $\hat{\theta}$:

$$\hat{\theta} = \underset{\vartheta \in (-\pi/2, \pi/2]}{argmax} \left(\frac{1}{\mathbf{a}^H(\vartheta)\, Q_{ns}\, Q_{ns}^H\, \mathbf{a}(\vartheta)} \right) \tag{3.23}$$

where $\mathbf{a}(\vartheta)$ is defined in (3.3) and (3.4).

3.4 Simulation Results and Analysis

In this section, we illustrate the performance of each part of the algorithm through extensive simulations.

3.4.1 Simulation Setup

For all simulations conducted in this chapter, we select the parameters defined in section 3.2.1 as follows: $\alpha = 1$, $\epsilon = 0.75$ and $\phi \sim U(-\pi, \pi)$. We generate baseband SCLD signals using $g(t)$ as a raised cosine filter with roll-off factor 0.35, 40 kHz bandwidth and $\Delta f_c = 16$ kHz. We select baseband OFDM signals parameters as $g(t)$ is a raised cosine window with roll-off factor 0.025, 800 kHz bandwidth, $\Delta f_c = 320$ kHz, $K = 128$. We select the data symbols $\{s_p\}$ and $\{s_{k,p}\}$ by choosing independent and identically distributed samples from M-ary phase shift keying (MPSK) constellations. Regarding the propagation and reception parameters defined in Section 3.2.2, we select $L = 15$, $d/\lambda_0 = 0.5$ and N=12800. These parameters could represent an antenna array with 15 elements, separated by a half-wavelength distance, and installed on a cognitive base station using 12800 signal samples to detect nearby radios.

3.4.2 Simulation of the Number of Sources Detector

This simulation illustrates the performance of the *number of sources* detector, described in Section 3.3.1. We investigate several combinations of primary and secondary user scenarios. For each scenario, we estimate the number of signals $\hat{m}$ and evaluate the average estimation error $\bar{e}$ as:

$$\bar{e} = \frac{\sum_{v=1}^{V} |\hat{m}_v - m_v|}{\mathrm{V}} \tag{3.24}$$

for which we conduct $V = 100$ trials. Our results, illustrated in Fig. 3.3, show that the *number of sources* estimation algorithm obtains low estimation errors for all scenarios even with SNR as low as -10 dB. In addition, except for the 7 PSK sources scenario, similar performance is obtained for SNR as low as -15 dB. However, the 7 PSK sources scenario, with sources located at angles $6\,^{\circ}$, $14\,^{\circ}$, $29\,^{\circ}$, $40\,^{\circ}$, $46\,^{\circ}$, $63\,^{\circ}$ and $74\,^{\circ}$, shows a significant estimation error for SNR below -10 dB. This deviation is due to the eigenvalues vector $\boldsymbol{\lambda}$ which does not show a clear threshold between the noise and signal subspaces $\boldsymbol{\lambda}_{ns}$ and $\boldsymbol{\lambda}_{ss}$ as the number of sources increases significantly. These results dominate the overall performance of the system and will hinder any AoA estimation for this particular scenario and SNR levels. Our algorithm offers near zero error average error for a 4 single carrier signals input, when SNR is as low as -17 dB, which significantly outperforms [Hu *et al.* (1999b)].

3.4.3 Simulation of the Modulation Classifier

We have investigated the performance of the MC algorithm described in 3.3.2 with several combinations of primary and secondary user scenarios. In Fig. 3.4, we show the probability of correct classification P_{CC} for those scenarios. We obtain $P_{CC} = 1$ for the whole examined SNR range for a scenario for which only noise is present. If the MC block is operated alone, this result would be incorrect because $\Omega = 0$ is supposed to represent SCLD, not noise only sources. Since our system combines the *number of sources* and MC blocks, we eliminate this misclassification. In addition, we have shown that our system is able to detect OFDM signals when there are also SCLD signals present, even at SNR = -3 dB. Whereas [Punchihewa *et al.* (3-7 Sept. 2007)] has considered only one SCLD or OFDM signal source. We observe a

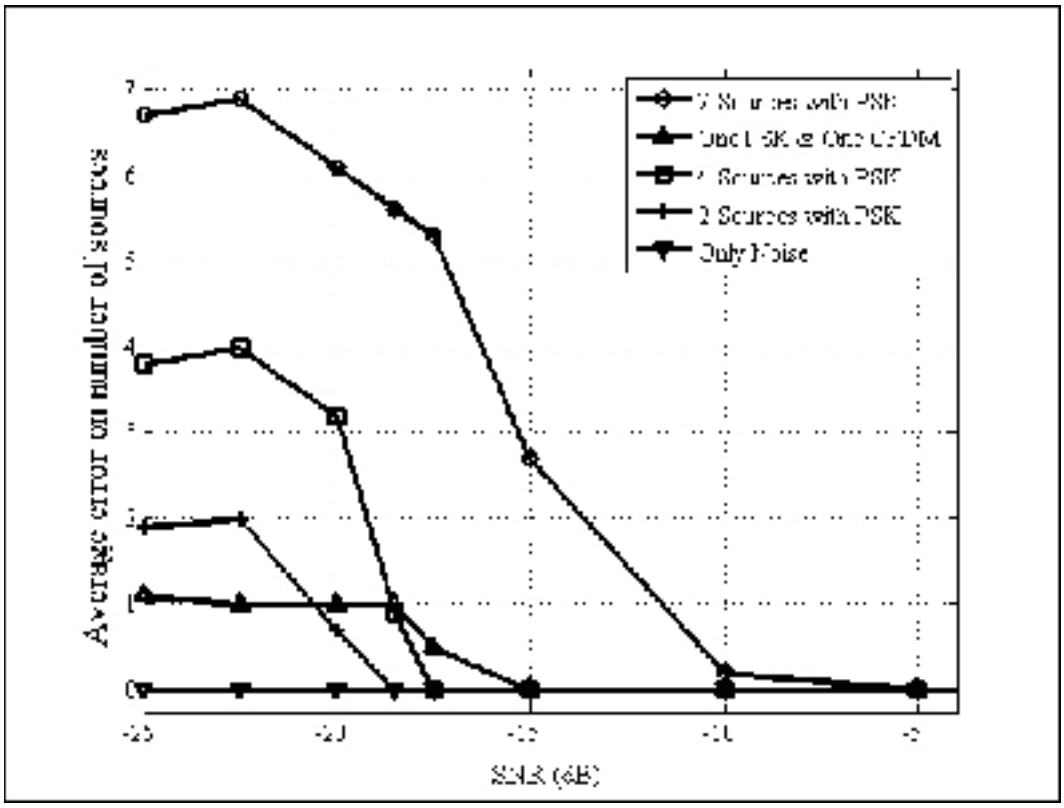

Figure 3.3 Average error on number of sources.

performance degradation when compared with a single OFDM source scenario because the presence of SCLD transmissions decreases the value of the CF determination statistic defined in section 3.3.2. This means that the SCLD transmissions have a similar effect to noise power as they increase the required SNR to effectively detect OFDM transmissions. Furthermore, the scenario with seven SCLD sources shows perfect classification results for the whole SNR range. The cognitive radio can use these classification results to find out all the available spectrum holes.

3.4.4 Performance of the Angle of Arrival Estimator

In Fig. 3.5, we illustrate a typical set of estimated angles with SNR = -8 dB. There, one can easily identify seven distinguished peaks corresponding to the seven distinct sources.

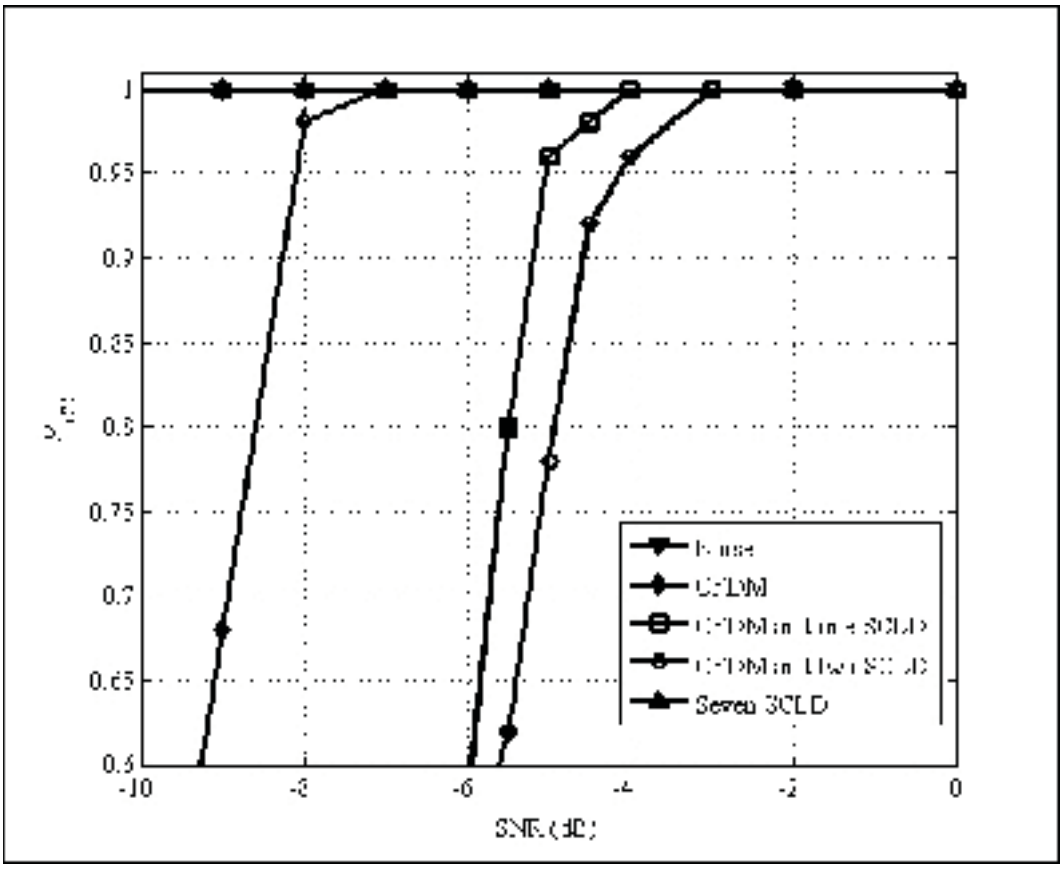

Figure 3.4 Performance evaluation of the MC block.

We then calculate the root mean square error (RMSE) of the AoA estimation for several combinations of primary and secondary user scenarios, with RMSE defined as:

$$\text{RMSE} = \sqrt{\frac{\sum_{v=1}^{V}(\hat{\theta}_v - \theta_v)^2}{V}} \tag{3.25}$$

where we measure the square error for each one of the V estimated angles θ_v. According to the results shown in Fig. 3.6, the AoA block estimates offers a maximum RMSE of 1° for SNR as low as -12 dB for all considered scenarios. From Fig. 3.6, one can notice that the RMSE of the AoA increases with the increase of the number of sources. This is caused by an error in the number of sources estimation, as discussed in 3.4.2.

By combining the number of sources, blind modulation classification and angle of arrival blocks results, the secondary user has cognition of the angle of arrival and class of all surround-

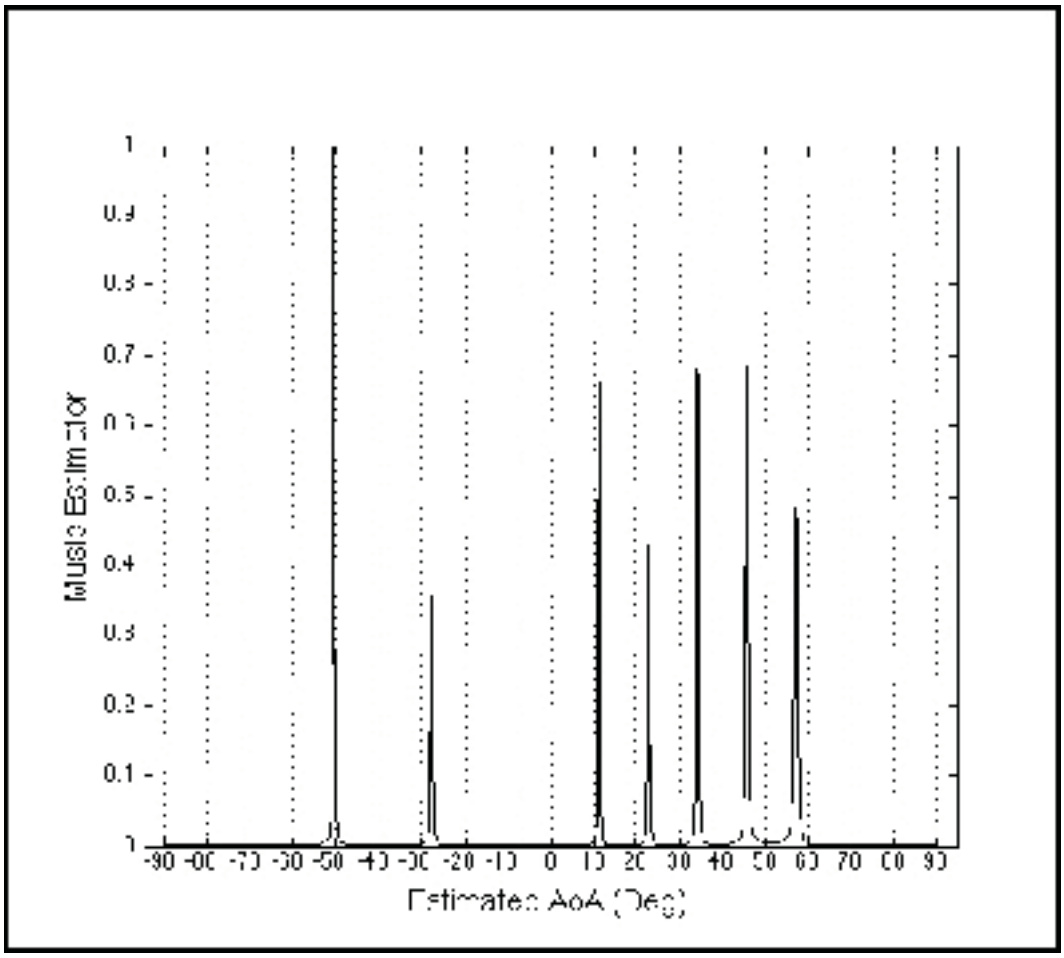

Figure 3.5 Estimation of the AOA for seven BPSK sources.

ing sources. This knowledge can then be exploited to occupy available dynamic spectrum holes without interfering with primary users, through advanced beamforming techniques.

3.5 Conclusion

In this chapter, we presented an algorithm for blind detection and localization of primary and secondary users for cognitive radio through modulation classification and angle of arrival estimation. The overall simulation results indicate that this system identifies and locates sources correctly for all considered scenarios, even at -4 dB SNR. In addition, we have shown the classification performance for several SCLD sources and for OFDM signal in presence of multiple SCLD sources. Cognitive radios employing the proposed system will identify available spec-

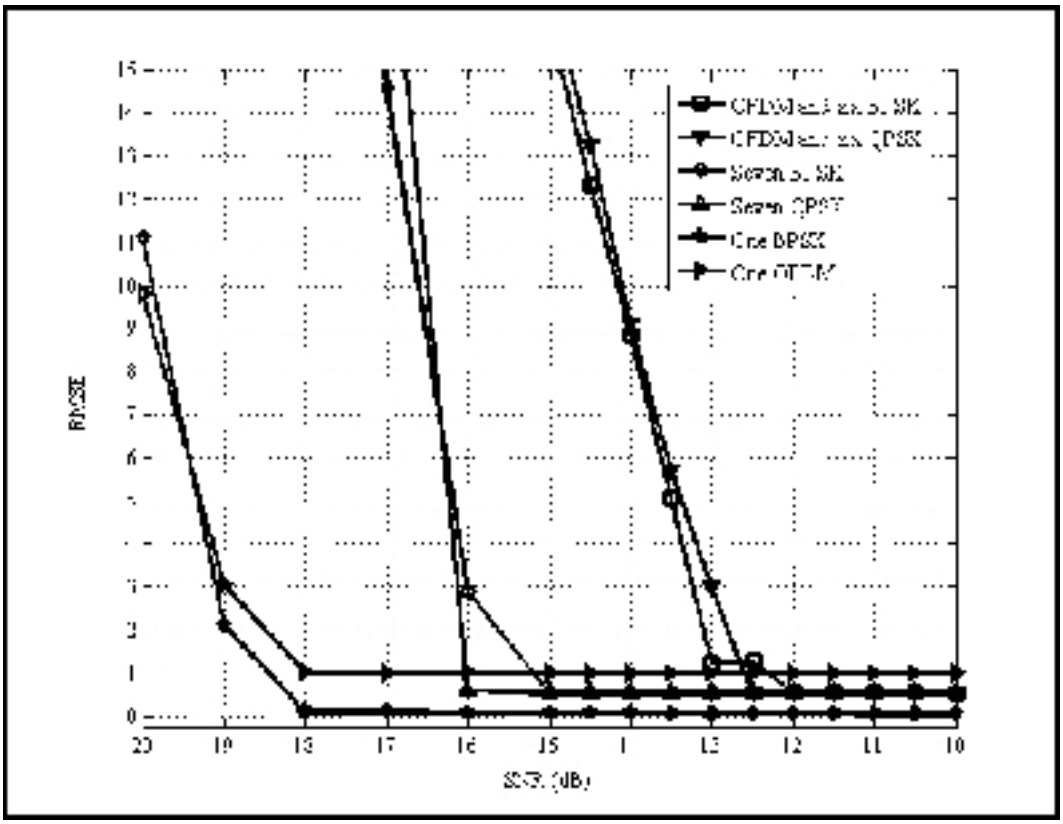

Figure 3.6 Root mean square error on the AOA estimation algorithm.

trum holes efficiently by avoiding frequency bands that are already filled by secondary user competitors, and exploit available spectrum holes by avoiding interference to primary users, employing information on their localization.

CHAPTER 4

REAL-TIME LOCALIZATION SOLVER WITH LINEAR COMPLEXITY RAY-TRACING UNDER NLOS CONDITIONS

4.1 Introduction

The recent development of high-end, low cost mobile devices running location-based applications and including global positioning system (GPS) receivers has attracted increasingly important research for real-time localization solvers (RTLS). However, new RTLS methods are required for indoors environments, where no direct link between the mobile and the GPS satellites is available.

Even though some localization-specific hardware can significantly improve the effectiveness of this task, we aim at developing software localization methods based on existing wireless communication technology, such as 4G cellular and 802.11, without adding any hardware. Recently developed devices under these technologies enable the estimation of channel parameters with sufficient precision to effectively estimate the mobile station's (MS) location within a few meters precision [Pahlavan and Levesque (2005)].

Several classical RTLS methods use known channel models and estimate one or several of its features. Channel features that are mostly used for localization are the received signal strength (RSS), time-of-arrival (TOA), and the angle of arrival (AOA). Roughly speaking, RSS offers low-cost, yet inaccurate estimates of distance and AOA requires antenna arrays and advanced front-end hardware at the base station level, which are not available in general [Pahlavan and Levesque (2005)].

TOA can be used under many technologies at relatively low cost, offering very accurate estimates on distance, though under non-line-of-sight (NLOS) conditions, the lack of knowledge for the shape of obstacles significantly increases the error on distance estimation [Pahlavan and Levesque (2005)]. When confronted with such challenges, one popular approach aims at identifying NLOS channels and to ignore them until the mobile moves in line-of-sight (LOS),

[Heidari *et al.* (2009)], [Chan *et al.* (2006)], [Morelli *et al.* (2007)]. Other methods consist in considering single-bounce reflection NLOS channels [Seow and Tan (2008)], but ignoring any paths that experienced multiple scattering on obstacles. These solutions are limited to certain scatterers geometries and require a large number of deployed base stations to cover one floor of a building with a large number of scatterers.

Site-specific RTLS use additional knowledge acquired by either conducting a campaign of channel measurements at several locations of the environment or from a map of the scatterers. The former method, also known as fingerprinting, can provide good positioning performance [Nerguizian *et al.* (2006)], and the latter can be used when field test measurements are not available. Most in-building base stations and wireless router installers usually need the map of the building to properly install their hardware, so this map is generally easy to obtain for any service provider, as it is already used in commercial RTLS solutions [Cisco Systems Inc. (2010)].

In this chapter, we present a site-specific RTLS method based on ray-tracing (RT) modelling on a map of scatterers for positioning mobile stations using distances based TOA estimates, and solving the position to less than the estimated distance error when the distance from three base stations is used. We also performed extensive field trials in corridors of *École de technologie supérieure*, and obtained less than 5 meters error for more than 85% of the tested locations when the distance estimation has a 5 meters quantization step size. To the author's knowledge, this is the first real-time ray tracing algorithm for in-building mobile localization, and a detailed discussion on related research is conducted in section 4.2.

The rest of the chapter is the following: in section 4.3, we formally define the localization problem in our case and show the different blocks in our system model. In section 4.4, we then show how we employ ray tracing methods to perform the RTLS task and discuss on the complexity of our method. Finally, in section 4.5, we show the precision and computational complexity that our method can reach using data gathered in extensive field tests we have conducted.

4.2 Related Research

4.2.1 NLOS Mitigation

Most solutions proposed in the literature for reducing the positioning errors caused by NLOS channels can be described as mitigation: the detection and elimination of measurements obtained from NLOS paths. Several authors have proposed mitigation techniques: [Heidari *et al.* (2009)] use a binary hypothesis test based on a hybrid function of root mean square (RMS) delay spread and RSS features, [Chan *et al.* (2006)] use a residual on measurements from all base stations to only keep those that result from LOS channels, and [Morelli *et al.* (2007)] use hidden Markov models on the whole channel impulse response data. In these methods, the information obtained from NLOS paths is eliminated, and not used for localization purposes.

In [Seow and Tan (2008)], a method similar to NLOS mitigation is proposed, but adding information from paths that experience single-bounce scattering on obstacles to the localization solution, while eliminating every path experiencing higher order scattering. This added information was shown to improve performances, but extending this work to higher order scattering would significantly increase computational complexity.

In [Chen *et al.* (2012)], an estimate on the distance error caused by NLOS measurements is produced using a network of sensors. The results are supported by extensive simulation results, based upon an exponential propagation model.

Using prior information on the error caused by NLOS paths lowers the Cramer-Rao lower bound on positioning [Qi *et al.* (2006); Sieskul *et al.* (2009)]. By using the map of scatterers (which is readily available to most service providers), an acceptable positioning accuracy can be maintained even in heavily obstructed areas, while keeping a low density of sensors.

4.2.2 Scatterers Map Solutions

In outdoors, urban scenarios, several RTLS have successfully included scatterers maps, but could not be easily exported to the kind of scatterers geometries that indoor environments

experiment: [Kikuchi *et al.* (2006)] uses ray tracing software to generate a database of AOA and *degree of scattering* channel features at every point on a 10m tile of an urban map. The RTLS then finds the closest point in this database to measured features from MS. In [Coco *et al.* (2004)], a similar tile database is generated, using ray tracing, including Universal Theory of Diffraction formulae, and the RTLS then finds an electromagnetic source's position by finding its closest match in the database. [Tsalolikhin *et al.* (2011)] creates a partition of the floor plan instead of generating a tiles database. Each partition encloses a set of locations with similar TOA and AOA distributions. The RTLS then measures TOA and AOA from a MS, and finds the partition with the closest joint AOA-TOA distribution in the database as a solution. Our method follows a similar partitioning philosophy, which we adapted for indoor environments.

Indoors ray tracing methods have attracted much less attention in the RTLS literature, but the *ELVIS* RTLS [Kaya *et al.* (2007)] proposes using a joint AOA-TOA estimate to back trace the signal's path from the BS to the MS. Our method is partially inspired from this method, but it drops the need for a costly AOA estimator and only uses TOA measurements. Moreover, our proposed technique comprises a preprocessing step which simplifies the real-time computational complexity, thus allowing its use in complicated scattering environments.

4.2.3 Fast and Precise Radio Ray Tracing

In this section, we discuss advances in radio ray tracing modelling that are useful for our system, but are not related directly to RTLS. The computational complexity of these methods have been an issue for several years [Huschka (1994)].

Hoppe et al. have developed a large number of radio ray tracing methods for indoors [Rautiainen *et al.* (2007)] and urban microcells [Hoppe *et al.* (1999)] environments. These models are shown to be accurate in extensive field tests and use preprocessing of the database to quicken the ray tracing query process. The ray tree concept developed in section 4.4 of this chapter is partially based on their work.

Fuschini et al. [Fuschini *et al.* (2008)] have developed 3D urban ray tracing models and assembled specialized hardware to measure their accuracy. Among other results, they have shown

that path gains and delay spreads can be modelled accurately using RT. Similar results have been obtained for urban environments in [Son and Myung (1999)]. The concept of *ray tubes* presented in this chapter, which concatenates several rays with similar properties in order to simplify ray tracing is used extensively in our model.

The *method of regions* [Kimpe *et al.* (1999)] used for indoors radio ray tracing represents regions that intersect several ray tubes obtained from reflections on walls, and is part of our model. Indoor ray tracing models have also been proven to be accurate through extensive measurements [Athanasiadou and Nix (2000), Browne *et al.* (2002)].

In summary, no indoor real-time localization method has been developed that compensates for the radio-waves NLOS paths without requiring on-field propagation losses measurements.

4.2.4 Proposed TOA RTLS with Ray Tracing

The *proposed* RTLS solution for indoor environments uses existing wireless communication infrastructures with relatively scarce base stations, and is shown to be accurate even with wireless channels experiencing perturbations from a large density of scatterers. The method presented in this chapter first performs extensive ray-tracing pre-processing tasks, partly based on the fast ray tracing methods described in this section to create partitions as in [Tsalolikhin *et al.* (2011)], but in regions sharing the same quantized TOA. The second task in our system is performed by a RTLS that queries sets of partitions in the database to estimate the MS' position.

4.3 System Model

In this chapter, we estimate a mobile station's (MS) two dimensional (2D) position using uplink channels, from the MS to several base stations (BS). We first describe how we estimate the time of arrival from the channel's impulse response (CIR) and we then show an optical approximation to model the reflections of electromagnetic waves on walls.

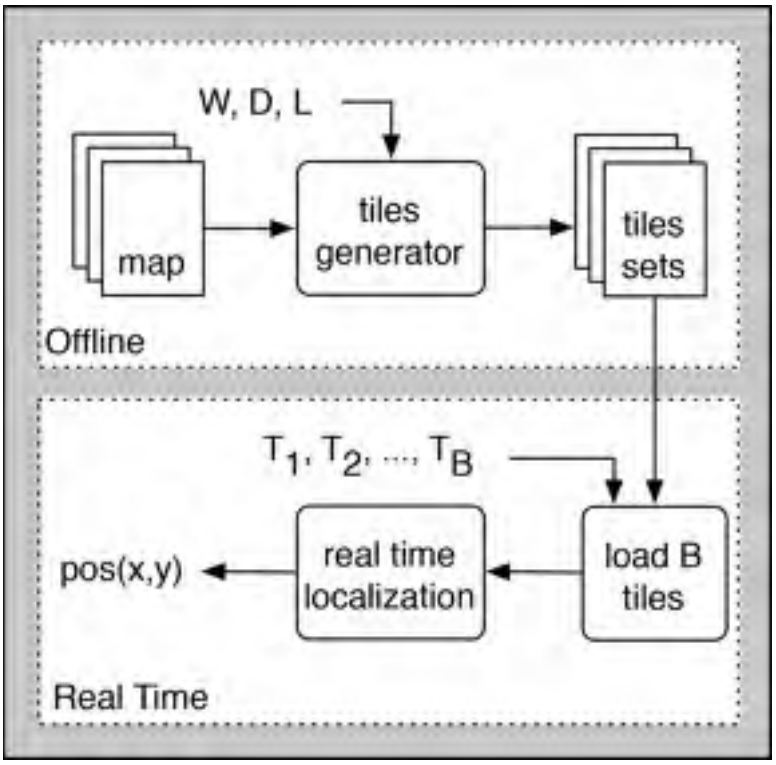

Figure 4.1 System model block diagram.

The system model is shown on Fig. 4.1. Map files are first preprocessed to generate tiles sets files. These tiles sets files are then used for real-time localization. The different blocks for this system are described in the following sections.

4.3.1 Map File

The geometry of walls is available in *shapefile* format, possibly extracted from the architectural plans of a commercial, industrial or residential building. The type of materials and fine geometry of walls, as well as any information on furniture are not required in our reflective geometric system, as opposed to electromagnetic propagation simulators. The algorithms presented in this chapter consider the walls as two-dimensional impenetrable obstacles by all radio waves composing the wireless channel. This ray-optical reflective model is acceptable for modeling the TOA of radiowaves with a wavelength smaller than 30 cm and transmitted power smaller than 100 mW studied in this chapter, and we leave the inclusion of transmissions, diffractions and diffuse scattering of radio waves as future work.

4.3.2 Tiles Generator

The tiles generator is the main part of our system, and we define some of its parameters in table 4.1:

Table 4.1 System Definitions

W	Bandwidth (Hz)
D	Propagation Depth
L	Number of bins in Channel Impulse Response
T_i	TOA Bin Index for Base Station i
B	Number of base stations in system

The objective of the tile generator function is then to take a map and a base station position, and to trace all the areas that have in common a distance from the base station. In the LOS area surrounding the base station, each tile set has a single ring-shaped tile, and as the range is increased further, tiles sets are created from a collection of parts from several rings. The distance is estimated from the channel impulse response, for LOS and NLOS conditions.

4.3.2.1 LOS Distance Estimation

Time of arrival (TOA) is a well known feature used in mobile positioning, and in this section we derive an extension of the time of arrival estimation to non direct path.

The wideband channel impulse response is represented by [Pahlavan and Levesque (2005)]:

$$h(\tau) = \sum_{i=1}^{L} \beta_i e^{j\phi_i} \delta(\tau - \tau_i) \tag{4.1}$$

where each multipaths i out of a total of L significantly strong paths has gain β_i, phase ϕ_i and delay τ_i. The TOA is the delay $\tau_{1,w}$ of the first multipath reaching the receiver from a transmitter and is estimated from the CIR of a channel with bandwidth w. In this chapter, we

consider quantized delay bins, i.e.:

$$\tau_{k,w} = \frac{k}{w},\ k \in 0, 1, \ldots, N_{bins} \tag{4.2}$$

where N_{bins}/w is the delay spread of one channel h.

A common method for estimating $\hat{\tau}_{1,w}$ is to identify the delay τ at which $h(\tau)$ crosses a pre-determined threshold:

$$\tau_{1,w} = \{\min \tau \,|\, h(\tau) > threshold\} \tag{4.3}$$

The distance between the transmitter and receiver nodes, calculated from TOA estimations is then:

$$\hat{d}_w = c\hat{\tau}_{1,w} \tag{4.4}$$

4.3.2.2 NLOS First Specular Path

Under LOS conditions, event though multiple paths between MS and BS constitute the radio channel, the direct path is the strongest and shortest one, thus easing the distance estimation using the technique defined in section 4.3.2.1. Figure 4.2 b) shows these longer and weaker multi paths *mp*.

Under NLOS conditions, however, an obstacle such as a wall blocks the direct path, so the first detected path can be created from radio waves that were reflected or diffracted on obstacles, or transmitted through them. Figure 4.2 c) shows two paths with similar length and most probably similar strength, thus making the selection of the correct paths (figure 4.2 d), here for three correct paths) more difficult.

Several techniques have been demonstrated to identify the shortest path in NLOS conditions [Richter (2005)], [Botteron *et al.* (2004)] and [Pahlavan *et al.* (2006)]. Therefore, we assume it is possible to always find the correct first path.

4.3.2.3 NLOS Path Identification

Path rays are traced emerging from the base station *bs* at an angle α and reaching a distance $c\tau$, thereby creating a pair labelled $p_{\alpha,\tau}$. Figure 4.2 a) shows the geometry for the shortest path *sp* and its destination point $p_{x,y}$ in the LOS case. The channel follows several paths for the LOS case (b) and the NLOS case (c). The overal objective is to identify the shortest path for every base station in a considered environment (d).

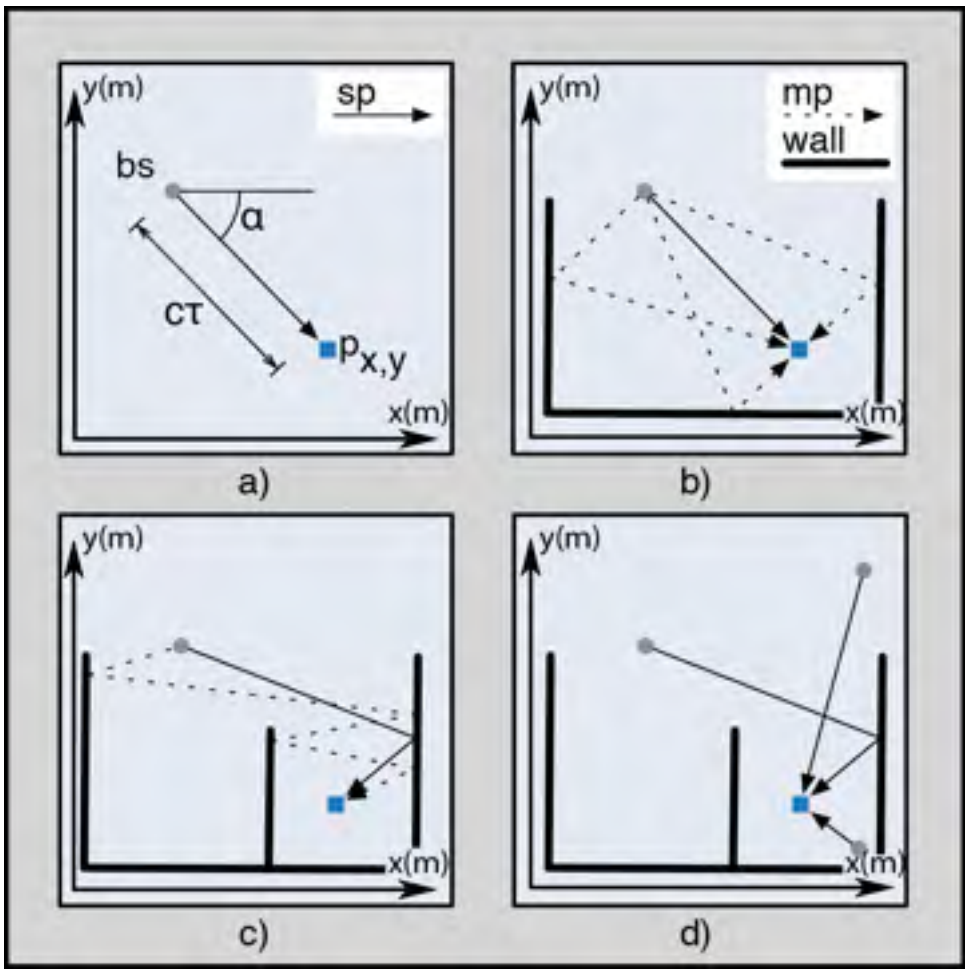

Figure 4.2 Identifying the closest path to $p_{x,y}$.

Definition 4.1. *The set of all angular and delay pairs*

$$\mathcal{A}^T \equiv \{p_{\alpha,\tau} \,|\, 0 < \alpha < 2\pi, 0 < \tau < \tau_{\max}\}$$

Definition 4.2. *The set of all positions on the floor:*

$$\mathcal{S}^T \equiv \{p_{x,y} \,|\, 0 < x < x_{\max}, 0 < y < y_{\max}\}$$

with $(0, 0)$ and $(x_{\max},\ y_{\max})$ being the lower left and upper right corners of the floor plan, respectively.

Identifying the correct path then consists in defining a mapping function f between sets $\mathcal{A}^T$ and $\mathcal{S}^T$:

$$f : \mathcal{A}^T \to \mathcal{S}^T \tag{4.5}$$

One important challenge in this task is the fact that for every location $p_{x,y} \in \mathcal{S}^T$, there are several possible paths, each of which passing on different walls, requiring a lot of calculations. Using simple assumptions, this problem can be greatly simplified.

Proposition 1. *NLOS paths have only been created from reflections on walls, and not from diffraction or diffusion.*

Lemma 1. *Some positions $p_{x,y}$ can be unreachable with purely specular interactions with walls.*

Definition 4.3. *The area covering all areas only reachable with specular reflections is defined as set $\mathcal{S} \subseteq \mathcal{S}^T$.*

Lemma 2. *$f : \mathcal{A}^T \to \mathcal{S}$ is a surjective mapping, because every location is linked to at least one ray emerging from the receiver.*

Proposition 2. *Only the shortest path is detected at receiver level and it is always detected.*

Lemma 3. *For a given position $p_{x,y}$, there are many ray-generated points $p_{\alpha,\tau}$ resulting from many paths, but we need only to consider the closest one (i.e. the one with $\tau_{\min}$).*

Definition 4.4. *The set of ray points that cover closest locations is defined as $\mathcal{A} \subseteq \mathcal{A}^T$.*

Lemma 4. *$f : \mathcal{A} \to \mathcal{S}^T$ is an injective mapping, because every ray traced from the receiver can be linked to at most one location.*

We now have enough lemmae to pose the following theorem:

Theorem 1. *By reducing the set of ray pairs $p_{\alpha,\tau}$ to $\mathcal{S}$ and the set of positions $p_{x,y}$ to $\mathcal{A}$, a bijective function can be created that links the two sets:*

$$f : \mathcal{A} \leftrightarrow \mathcal{S} \tag{4.6}$$

Defining a bijective mapping function in this manner greatly reduces the complexity of the NLOS path identification at the cost of additional simple sets operations. RTLS methods that do not exhibit the bijective property (such as fingerprinting techniques) can potentially experiment a higher probability of error. First, several signal patterns can point to the same location, and secondly some locations on the map could be unresolvable.

In the rest of the chapter, function f will be called the tiles generator, and we will describe it in more detail in section 4.3.3.

4.3.3 Tiles Generator Function

The tile generator function quantizes a measured TOA to one out of L equal-sized delay bins smaller than the delay spread of a site.

The tile generator takes a base station position and a map M, the delay quantization factor L, tree depth D and creates a bijective function f of a time of arrival plus tolerance and angle of arrival plus tolerance to create a set of tiles that represent all the positions at the end of the rays that satisfy these times and angles. All these combinations are then saved in one file for each base station, to be used later for real-time localization.

4.3.4 Loading Tiles & real-time Localization

During real-time localization, the TOAs are estimated and quantized by base stations, providing a set of time bin indexes $T_1, T_2, \ldots, T_B$. Then, for every time bin index, the corresponding tile set is loaded.

We then obtain a reduced tiles set by intersecting all the loaded sets. The transmitter's position can then be picked from any location in this reduced tiles set. This position follows a result similar to the geometric solution [Cafferty and Venkatraman (2004)] but using mirror images of base stations on the obstacles' surfaces. As future work, we could consider different probability density functions for the TOA within one quantized step and use linear estimators to further improve the positioning accuracy [Tseng and Feng (2012)].

We conduct a more detailed discussion on these mirror images in the next section.

4.4 Ray Tracing Computation

In this section, we derive detailed ray tracing computation methods for implementing the theoretical tiles generating and real-time localization functions developed in section 4.3. For every computational geometry function we present, a short discussion on its computational complexity is also provided.

4.4.1 Geometric Structures

The geometric structures used for the ray tracing method presented in this chapter are defined in table 4.2.

The geometric structures defined in table 4.2 are illustrated on Fig. 4.3 for LOS geometry and Fig. 4.4 for NLOS geometry. The TWVP in Fig. 4.4 is generated from the reflection on the leftmost wall of the VP shown on Fig. 4.3. Its ghost source is then a mirror image of the VP's receiver on this same wall.
The algorithm used for generating the visibility polygon is the point visibility in a polygon with holes, which is a classic computational geometry problem. This framework can be directly applied to generate the VP from a receiver which applies very well to ray tracing problems.

1: **procedure** VISIBILITY POLYGON($Receiver, Map$)
2: Asano's point visibility in the plane algorithm [Ghosh (2007)].

Complexity: $O(N \log N)$ [Ghosh (2007)].

Table 4.2 Definitions for Geometric Structures

Primitives	
Map	A non-winding polygon with holes obtained from maps (Fig. 4.1)
N	Number of vertices in a map
Wall	Any complete segment of a map
Wall Segment	A segment $\subseteq$ any one wall
Receiver	An isolated vertex representing the known exact location of a base station, the observer.
Generated Structures	
Ghost	An isolated vertex obtained from one or more reflections of a receiver on walls
Ray Tube	Triangle formed from one vertex on a ghost and the opposing segment on a wall
Ray Tree	Hierarchic ray tubes structure, defining rays from a receiver and bouncing on walls
Visibility Polygon (VP)	The area seen by a receiver
Through Wall VP (TWVP)	The area seen by a ghost through a wall
Ring	area comprised between two concentric circles centred on a receiver or ghost
Tile	A polygon which is the subset of a ring comprised of segments and circular arcs

The algorithm used for generating the Through-Wall Visibility polygon adds an intersection step to the VP algorithm and is based upon the reflection ray tubes presented in [Son and Myung (1999)].

1: **procedure** TWVP($Ghost, Wall, Map$)
2: Create viewport(Wall, Ghost Rays, map's boundary)
3: $NewMap \leftarrow$Intersect map with trapeze
4: Remove Wall from New map
5: Call Visibility Polygon with ghost and new map

The rays defining the viewport's sides in step 1 emerge from the ghost, pass by the wall's endpoints and reach the map's boundary.

Complexity: Step 2 involves intersecting a $N - edges$ map with a $k - edges$ viewport, which can be done in $O(k \log k + kN + N \log N)$ [Dévai (1995)]. In all cases, k has a value of either 4

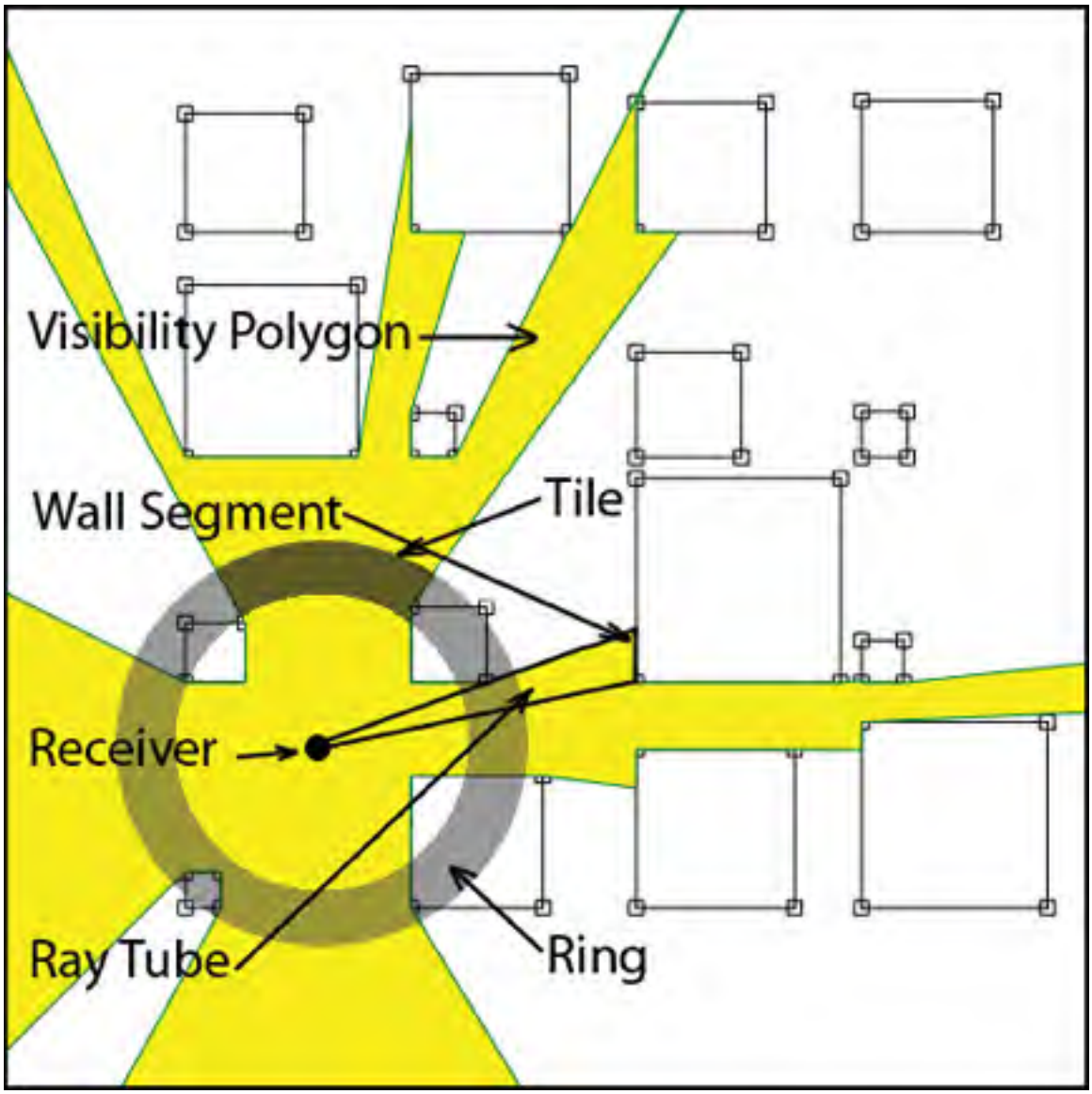

Figure 4.3 LOS Geometry.

or 5, therefore $k \ll N$ and the complexity reduces to $O(N \log N)$. The *new map* polygon has K edges, where $K \ll N$. Therefore, the overall TWVP complexity is $O\left(N \log N + K \log K\right) \propto O\left(N \log N\right)$, which is exactly of the same order as the VP algorithm.

4.4.2 Ray Tubes Tree

Classical ray tracing methods [Huschka (1994)] consist in calculating the power emitted by a transmitter as it radiates through its environment. While this method is very useful for cal-

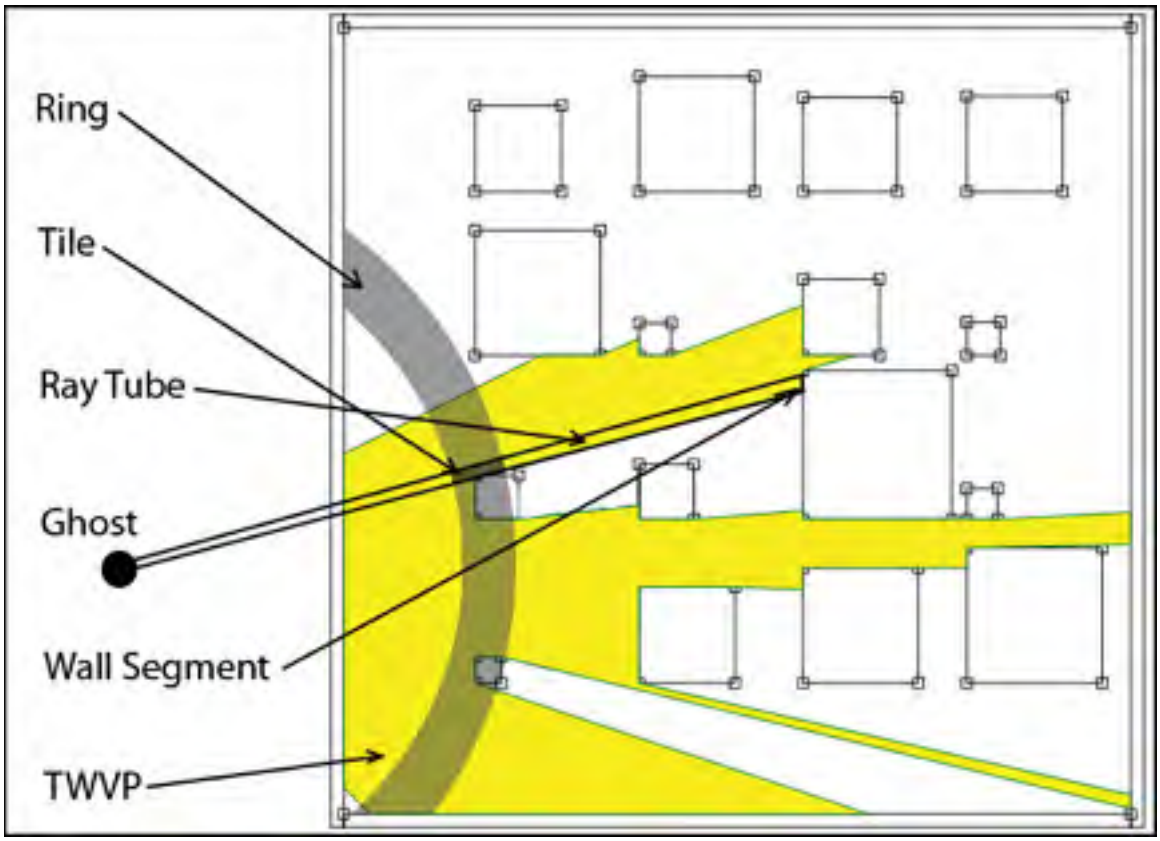

Figure 4.4 Reflective geometry.

culating the coverage from base stations, a reverse ray tracing method [Kaya *et al.* (2007)] originating from the receiver is preferable for TOA localization purposes. The ray tracing problem then consists in drawing all possible paths that a received signal can have taken.

Figure 4.5 shows that the reflective geometry from the receiver follows a *n-ary tree* structure rooted on the visibility polygon around the receiver and propagating one step every time an interaction occurs on a scatterer, or *ray tree* [Hoppe *et al.* (1999); Son and Myung (1999)]. Every non-root node represents a ray tube, for which a TWVP is generated; for every wall segment in the TWVP, a child ray tube node is generated, until a depth D is reached.

The ray tracing tree is created using the following method:

The algorithm for generating ray tubes nodes in the ray tubes tree is the following:

1: **procedure** NODE(SOURCE, WALL, MAP)

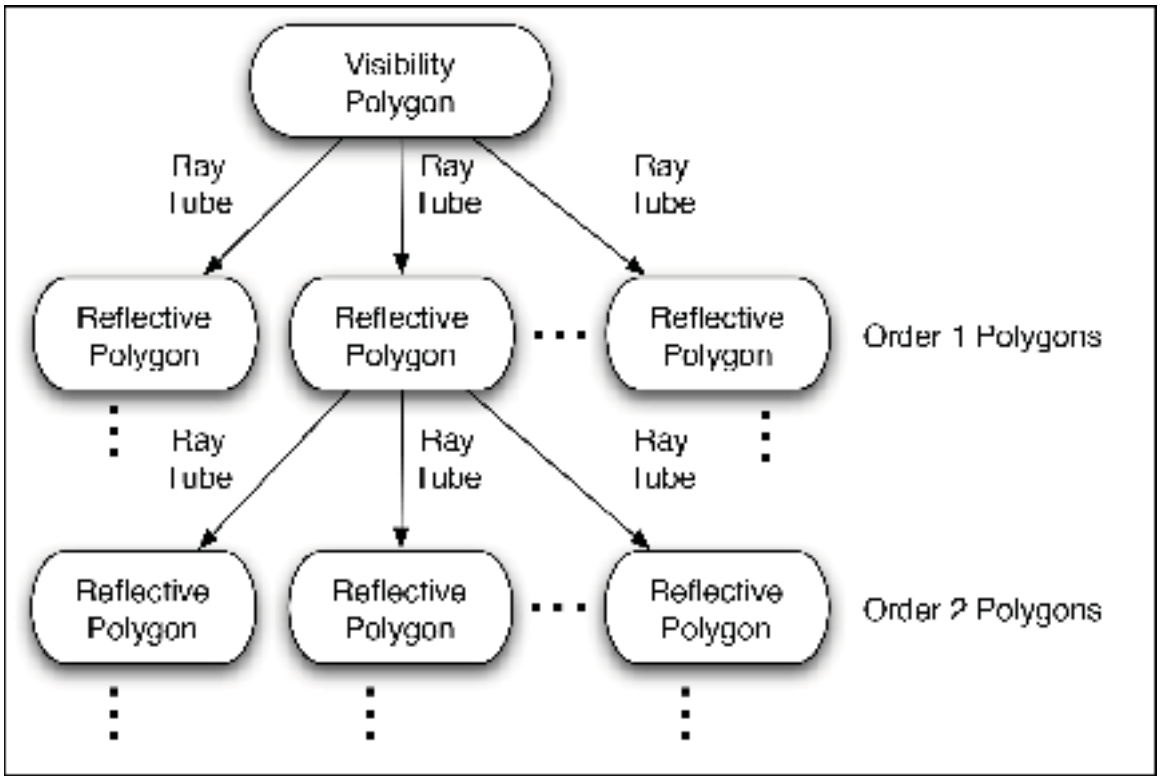

Figure 4.5 Ray tree structure.

2: Calculate $G \leftarrow$ Ghost(Source, Wall)

3: Calculate TWVP (G, Wall, Map)

4: Depth $d \leftarrow d + 1$

The recursive function of ray tubes for generating the ray tree is the following:

1: **procedure** RAY TREE GENERATION

2: Get Receiver R

3: Get Map M

4: Depth $d \leftarrow 0$

5: Calculate VP(R,M)

6: **for all** Wall $W_i \in$ VP **do**

7: d, G_i, $TWVP_i \leftarrow$ Node(R, W_i, M)

8: **if** $d < D$ **then**

9: **for all** Wall $W_{i,j} \in TWVP_i$ **do**

10: d, $G_{i,j}$, $TWVP_{i,j} \leftarrow$ Node (G_i, $W_{i,j}$, M)
11: **if** $d < D$ **then**
12: **for all** Wall $W_{i,j,k} \in TWVP_{i,j}$ **do**
13: d, $G_{i,j,k}$, $TWVP_{i,j,k} \leftarrow$ Node($G_{i,j}$, $W_{i,j,k}$, M)
14: ...

The complexity associated with this process is directly linked to $\sum_{d=1}^{D} N^{d+1} \log N$, the total number of nodes in the ray tree.

The total complexity is $O\left(\sum_{d=1}^{D} N^{d+1} \log N\right) = O\left(N^D \log N\right)$. Typically, from one depth level to the next, each wall generates polygons with no more than 2 walls, so this expression can be approximated with $O\left(2^D N \log N\right)$. As a comparison, the worst-case complexity for generating the *D-reflections-visibility-polygon* is $O(N^{2D} logN)$ [Aronov *et al.* (2006)].

4.4.3 Tiles Generation Algorithm

In a strictly LOS environment, regions of the floor sharing a common quantized TOA value would have a ring-shape as shown on Fig. 4.3. However, the presence of reflective scatterers in NLOS environments creates distortions in these rings, which become fractioned in curved polygons sets, defined as tiles in table 4.2. Using the ray tree structure developed in section 4.4.2, we can draw tiles sets by intersecting rings centred on ghosts with every TWVP in the tree:

1: **procedure** TILES GENERATION(RAY TREE RT)
2: RL $\leftarrow$ List of L rings with increasing radii
3: PS $\leftarrow$ The set of TWVP polygons from RT
4: **for all** Ring $R_i \in$ RL with increasing radii **do**
5: $PS^i \leftarrow$ Set of polygons $\in PS$ intersecting R_i
6: **for all** Polygons $P_{i,j}$ in PS^i **do**
7: $Tile_{i,j} \leftarrow$ Intersect $P_{i,j}$ with R_i
8: Tile Set $T^i \leftarrow Tile_{i,j}$
9: Save T^i to file

10: Remove T^i from PS^i

The intersection or difference of two polygons with a total of N vertices, and k intersecting edges have a $O(N \log N + k)$ time complexity [O'Rourke (1998)]. Since $k \ll N$ in our case, we skip this factor and the combined intersection and difference operations have a $O(2N \log N)$ time complexity. We perform this task for every TWVP intersecting a ring, which has a worst case complexity of $O\left(N^{D+1}L\right)$ then the overall upper bound is $O(N^{D+2}2L \log N)$. Typically, the number of nodes in the ray tree is less than $O\left(2^D\right)$, and most TWVPs have less than 10 vertices in regular indoors geometries similar to ones we have experimented in our field trials, so the typical time complexity for generating tiles is $O\left(66L \cdot 2^D\right)$.

The space complexity for tiles sets files is the number of vertices used to represent the curved polygons generated in procedure TILES GENERATION. An upper bound on the number of vertices is to have N vertices for every TWVP associated with every node in the ray tree. The polygon-polygon intersection has a $O(N)$ space complexity [O'Rourke (1998)]. Then, the space complexity per file is $O(L \cdot N^{D+2})$ vertices. Using a similar argument to the time complexity above, the typical space complexity is $O\left(10L \cdot 2^D\right)$.

4.4.4 RTLS from Tiles

For every measured and quantized TOA T_i at receiver points i, the RTLS seeks its corresponding Tile Set T_i and calculates the intersection between all tiles sets to generate the final solution space S. Figure 4.6 illustrates an example of tiles sets for different quantized TOA. Since we assume no knowledge on the TOA within the quantized value, every position in S is equiprobable. The RTLS then returns region S and a randomly picked point in S as its final result.

1: **procedure** REAL-TIME LOCALIZATION($T_1, T_2, \ldots, T_B$)
2: **for all** Requested times of arrival T_i **do**
3: Load tile set T_i of tiles set list i.
4: Polygons set S $\leftarrow$ Intersection of all loaded tiles sets
5: Pick any point at random from S

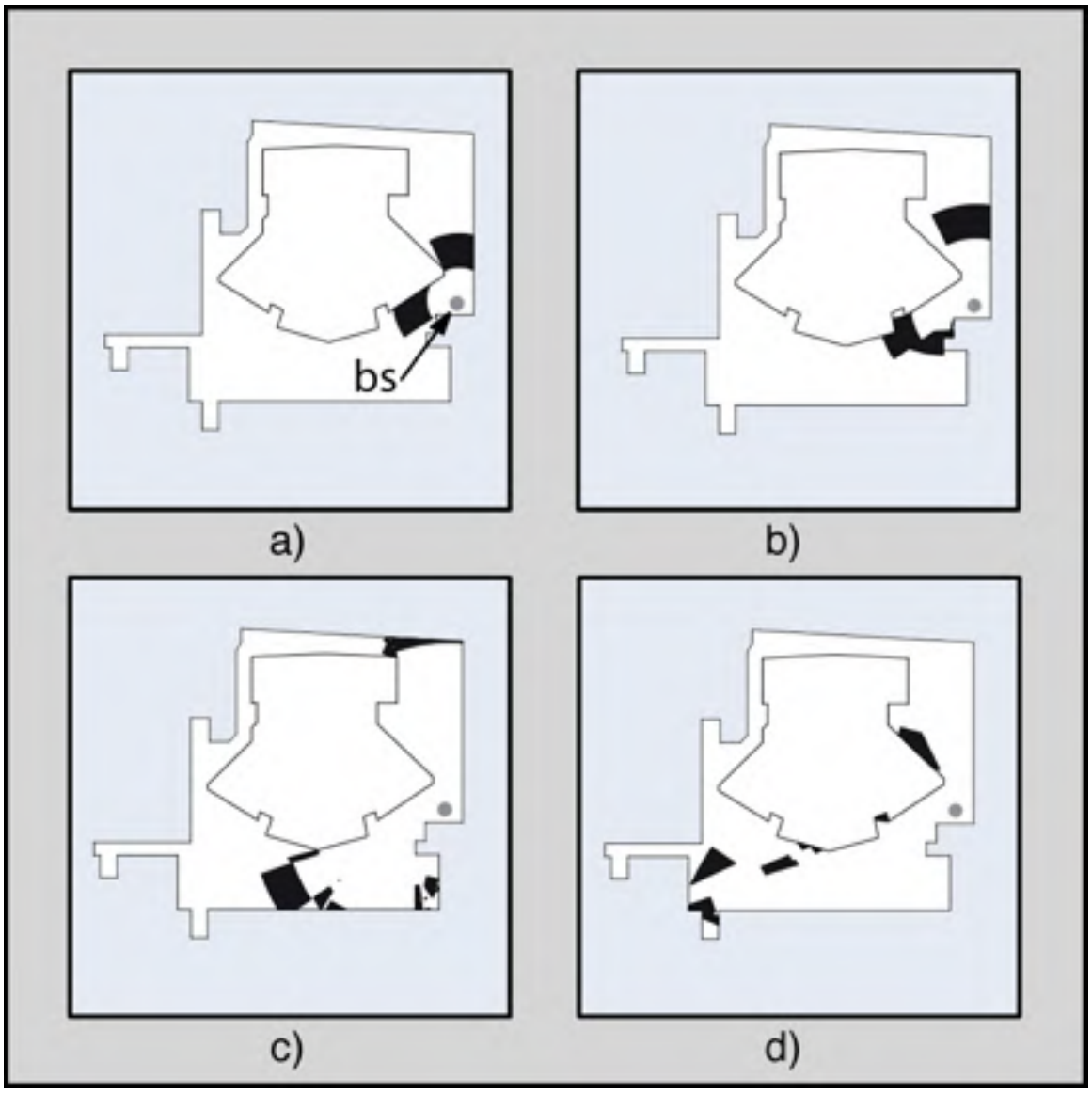

Figure 4.6 Example of tiles generated for TOA bin indexes 2, 3, 6 and 9.

Complexity: the number of polygons in one of the L tile sets of a file generated from a ray tree with depth D has an upper bound of $O(L \cdot N^{D+2})$ vertices, which happens if all the vertices of the largest possible ray tree are concentrated in a single tile set. Since vertices are divided fairly evenly among the L tiles sets, and since most polygons have less than 10 vertices each, the typical complexity per tiles set is $O(\frac{10 \cdot 2^{D+2}}{L} + K)$ with bias K representing the minimal number of vertices per tile, which occurs when rings are very thin.

The joint intersection of B tiles sets has a worst case time complexity of

$O\left((B-1)\left[(L \cdot N^{D+2} \log \cdot N^{D+2}\right]\right)$

and since $L \ll N^{D+2}$, the expression can be reduced to $O\left((B-1)(LN^{D+2})\frac{D+2}{\log_N 2}\right)$.

The typical time complexity is $O\left((B-1)\left[\frac{10}{L} \cdot 2^{D+2} + K\right] \log\left[\frac{10}{L} \cdot 2^{D+2} + K\right]\right)$.

4.5 Measurements

Our objective is to measure the limits in accuracy of our ray tracing model shown in section 4.4 when tested with field measurements. Our tests involve channel sounding experiments [Heidari *et al.* (2009)] performed at the first floor of *École de Technologie Supérieure*, in the corridors surrounding an amphitheater room. The floorplan is shown in Fig. 4.7.

4.5.1 Tests Setup

We have placed an emitter antenna at 24 randomly picked different locations and a receiver antenna at 5 different locations, as shown on Fig. 4.7. The tx locations illustrate the path that a pedestrian could have followed in the ETS corridors and the rx positions illustrate possible Wi-Fi router positions. For all these $tx - rx$ combinations, we have measured the channel frequency response following the test equipment and parameters defined in table 4.3.

4.5.2 Channel Impulse Response

For all frequency response measurements done following the methods defined in section 4.5.1, we used the chirp-z transform to extract the channel impulse response:

$$h(n) = h(\tau)|_{\tau=n\Delta t} = \frac{1}{N}\sum_{k=0}^{N-1} W(k)H(k)e^{j2\pi n\Delta t \times k\Delta f} \tag{4.7}$$

with $N = 1601$, $\Delta t = 187.5ps$, $\Delta f = 936.9kHz$,

Table 4.3 Field Trial Specifications

Hardware	
Vector Network Analyzer	Agilent HP8753ES
Low Noise Amplifier	Mini Circuit ZRL-1150LN
Low Noise Amplifier	Mini Circuit ZX60-1215LN+
Amplifier	Mini Circuit ZX60-24+
60m Coaxial Cable	AIR802 CA600
Channel Sounding Parameters	
Bandwidth	800 MHz to 1.4 GHz
Power	10 dBm
Number of points	1601
Time index size	1 ns
Ray Tracing Parameters	
Ray Tree Depth (D)	8
Last Ring's Radius	130m
Number of Rings (L)	13, 26 and 130

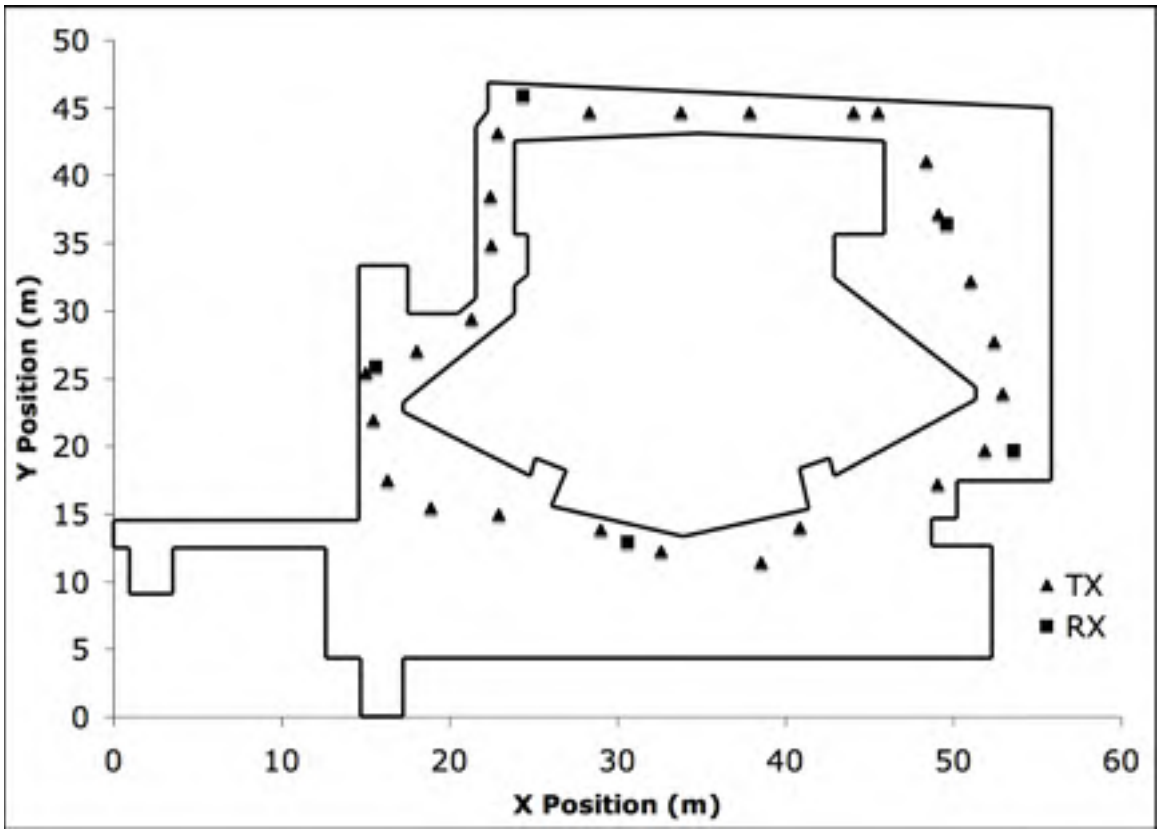

Figure 4.7 Transmitters and receivers positions.

4.5.3 Experimental Specular Time-Of-Arrival

For all channel impulse responses extracted in the previous section, the first specular path's time of arrival is estimated. In LOS situations, this task is a straightforward application of Eq. 4.3. For NLOS situations, we assume that the correct multi path element can be picked by a method described in section 4.3.2.2. We have therefore selected the correct multi path component in the channel impulse response and applied Eq. 4.3 on it to obtain the time-of arrival.

The TOA at every receiver i is then quantized in one out of L equally-sized bins to obtain T_i. For every transmitter, we have then measured the positioning error of our RTLS for all possible combinations of three TOA estimations T_i: $[(1,2,3),(1,2,4),(1,2,5)\ldots(3,4,5)]$.

4.5.4 Accuracy

The root-mean-square complementary cumulative distribution function for the localization position error is illustrated in Fig. 4.8. The *trilateration* scenario involves classical trilateration without considering the effect of walls on the result. The *ideal* curves show the limit on localization accuracy when the time of arrival selects the correct time bin for three different ring width sizes (130/L = 10m, 5m and 1m). The *experimental* curves show the localization accuracy for the process described in section 4.5.3 for the same ring width sizes.
A single CIR measurement was considered for estimating the TOA at every base stations, and no super-resolution [Pahlavan and Levesque (2005)] was used. Using several CIR samples to estimate the TOA, super-resolution algorithms or others could at least improve localization performances and produce CDF curves similar to those shown on Fig. 4.8, but shifted leftwise.

Comparing our algorithm to the trilateration method, we can see a 10-fold accuracy improvement using the additional information provided by NLOS multipath bounces on scatterers.

Another important observation is that our three-way intersection method improves the accuracy from any single TOA estimate. For example, three TOA measurements quantized in 5 meters bins have more than 98 % probability of positioning the MS with less than 5 meters error in

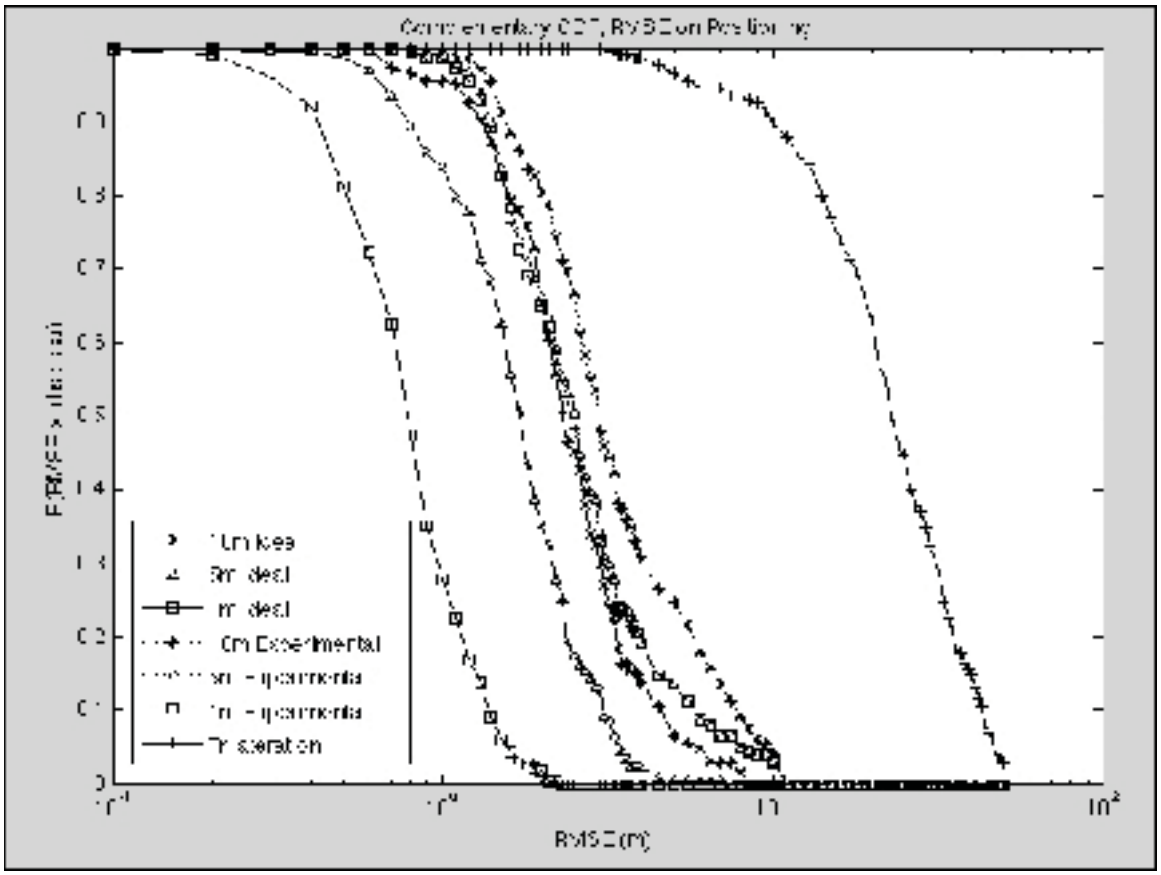

Figure 4.8 Positioning error.

the ideal curve. For the experimental curve, this probability drops to 80 %, which could be compensated by more advanced TOA estimation techniques. Obstacles with various shapes and positions result in positioning results with different accuracy, whose distribution can be observed on the positioning error CDF curves on Fig. 4.8.

4.5.5 Complexity

The theoretical complexity expressions defined in section 4.4 are tested experimentally here. In Fig. 4.9, the time complexity for the tiles generation pre-processing task is measured for several ray tree depths. It is found to be between 2^D and 3^D, which is close to the theoretical typical complexity.

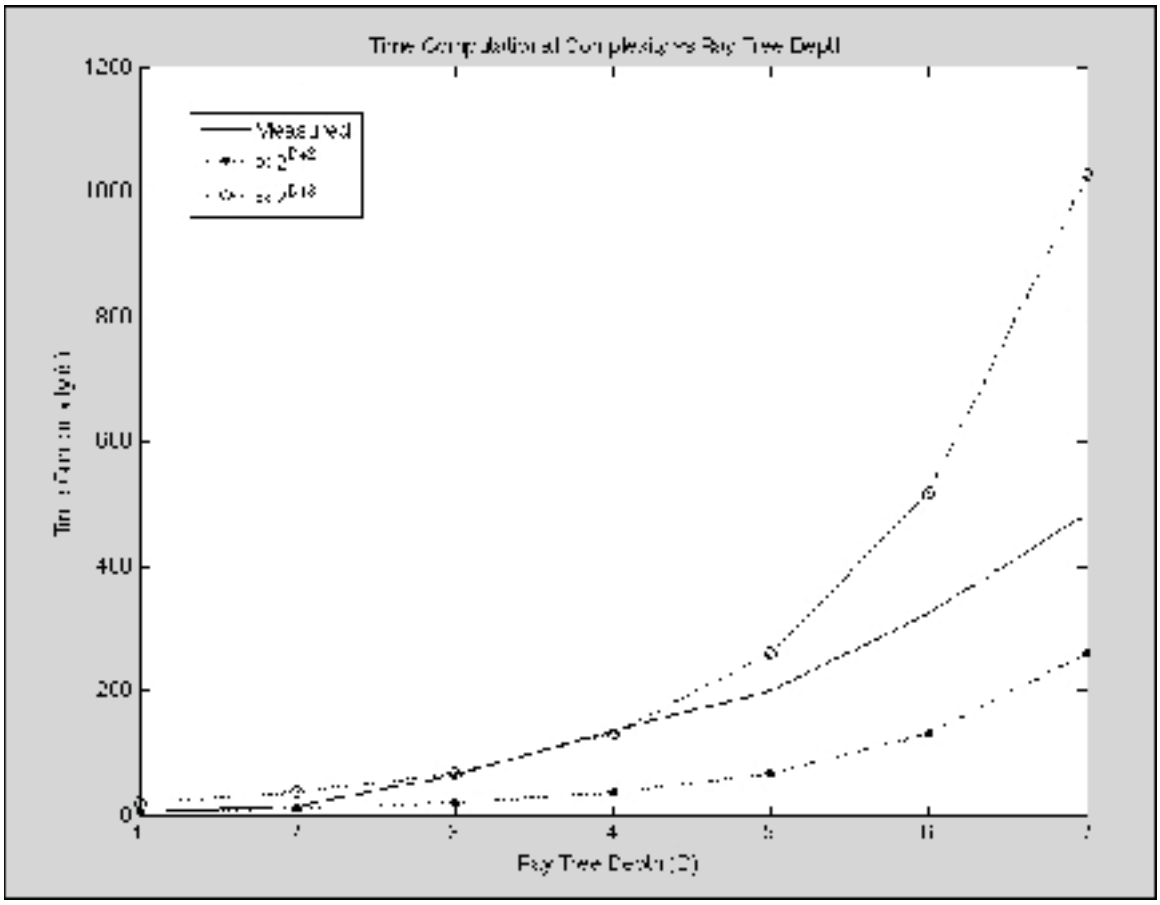

Figure 4.9 Ray tree creation time complexity.

Real-time complexity was measured and the results are shown on Fig. 4.10. The time complexity of the RTLS method is inversely proportional to the number of rings used until it reaches bias K, which is 0.6 in our case.

Figure 4.11 illustrates the space complexity per ring and time complexity in the same plot. The objective of this plot is to show how the number of vertices per ring commands the RTLS time complexity for a wide range of ring step size L values.

4.5.6 Area Coverage

Using a purely specular reflection propagation model can leave some points of the considered area untouched by rays. On Fig. 4.12, a), we can see the LOS area around a receiver, on b), a small spot represents the area simultaneously in LOS of three receiver points, on c) the

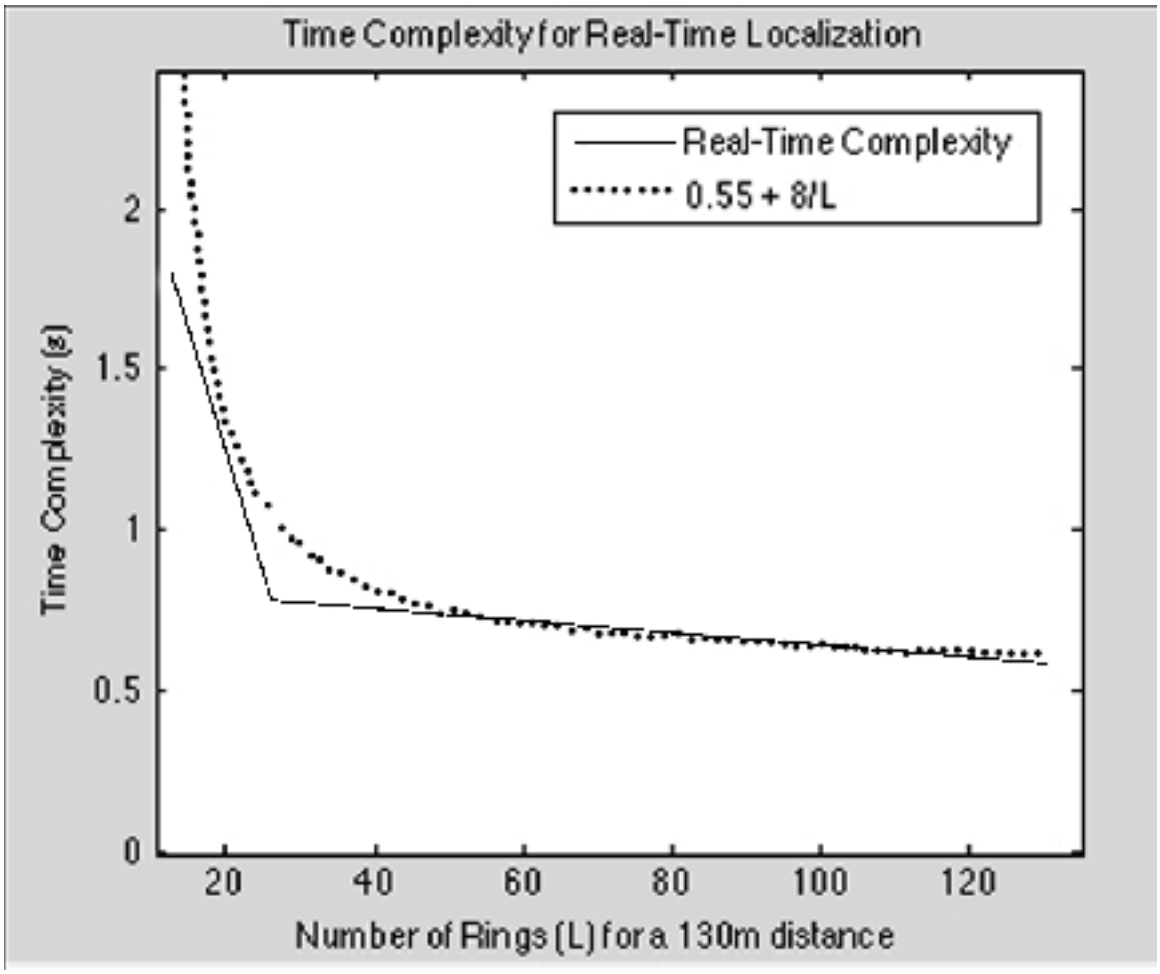

Figure 4.10 RTLS time complexity.

area seen in LOS and reflections around the same receiver, and d) the area seen in LOS and reflections from the same three receivers simultaneously.

Fig. 4.12 shows the area covered by (a) LOS and one base station, (b) LOS intersection of 3 base stations, (c) reflective visibility of one base station and (d) the area covered by the intersection of the reflective visibility of the same 3 base stations. This figure illustrates how NLOS methods can increase the area coverage over LOS methods. Our model includes specular reflections on walls, but no diffraction or diffusion. Therefore, some locations on the floorplan that are only reachable with these electromagnetic scattering effects are not covered, as discussed in section 4.3.2.3. Nevertheless, the area covered by the intersection of three LOS areas used for localization can be smaller than one meter-squared like for Fig. 4.12 b). By adding

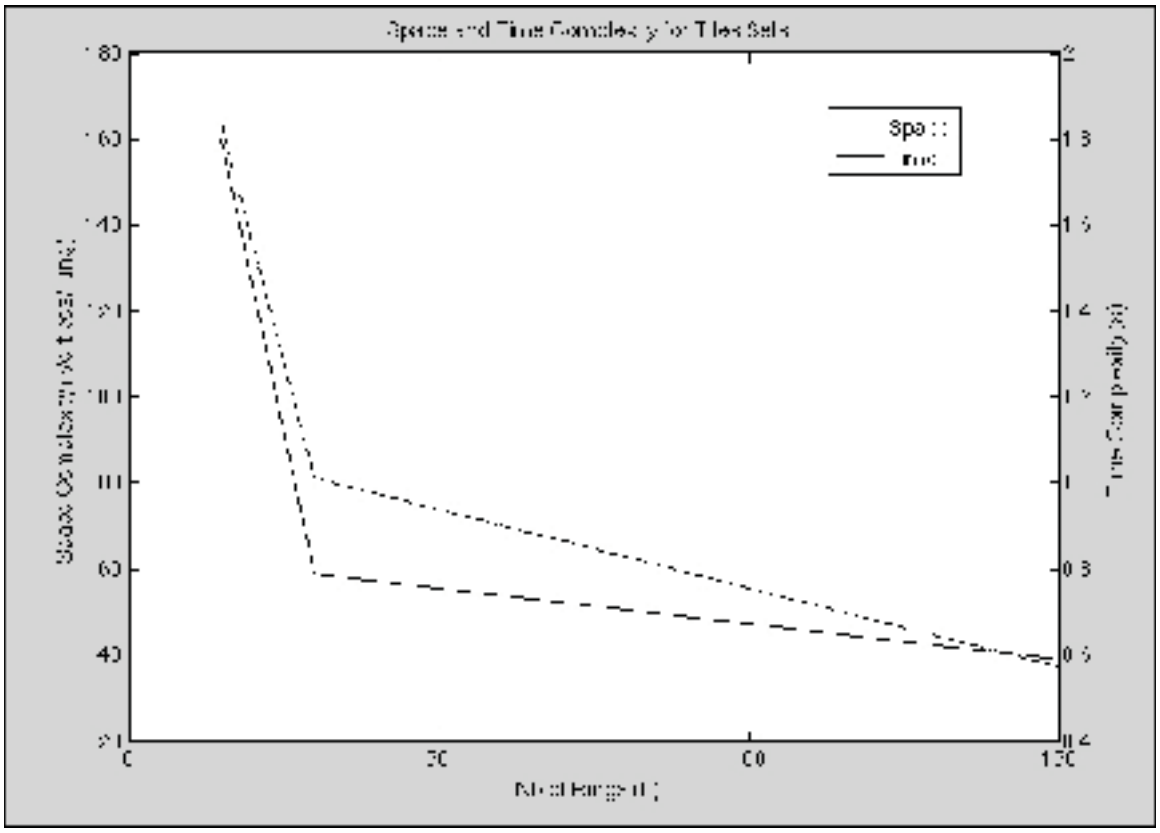

Figure 4.11 Tiles Complexity.

specular reflections, the three-way intersection covered area increases to more than 80% of the floorplan as shown on Fig. 4.12 d).

We have calculated the area covered for all *tx-rx* combinations in this scenario and the results are summarized in table 4.4.

Since the average distance between base stations is 28.7 m, we consider that this deployment scenario has a higher base stations density than any commercial 802.11 or indoor cellular networks. For this optimistic scenario, a NLOS mitigation technique that eliminates any NLOS path will end up with an average joint three base stations coverage of 1.9% in our scenario with 5 base stations. In comparison, our method using multiple order reflections on walls has a 82.3 % coverage ratio. When a MS is located outside the covered area, large localization errors

Table 4.4 Map Characteristics

Total Area Number of Base Stations	1620 m^2 5	
	Mean	Std
Distance Between Base Stations (m)	28.7	7.9
LOS Area Coverage per BS (%)	25.34	11.4
Total Area Coverage per BS (%)	97.9	1.8
LOS Three-way Intersection Area Coverage (%)	1.9	3.3
Total Three-way Intersection Area Coverage (%)	82.3	19.4

occur. These results clearly show that TOA RTLS methods based on LOS hypothesis are less suitable than our method in indoors environments involving a high scatterers density.

4.6 Conclusion

In this chapter, an indoor RTLS for dense scatterers environments is presented which uses scatterers maps and ray tracing techniques to define zones having common TOA to base stations with known locations.

The simulation and field trials shown in this chapter illustrate how using ray tracing methods on a scatterers map in TOA RTLS can significantly increase the coverage area and accuracy when compared with LOS methods. In our experimental test setup at ETS, the coverage area increased from 1.9% to 82.3% using the proposed technique while the accuracy was improved by a 10-fold factor. This task can be accomplished in real-time by saving pre-processed tiles sets files.

As discussed in section 4.3.2.2, in this chapter, we have assumed that the right multi-path element is picked in the CIR, using known signal processing methods. A logical next step in developing a realistic application would be to implement these methods and expect a decrease in accuracy for the realistic TOA estimation of the first CIR peak is prone to more errors than the ideal scenario we have used in this work. On the other hand, no drop in coverage is expected, as the CIR peak estimation process does not decrease the channel delay spread.

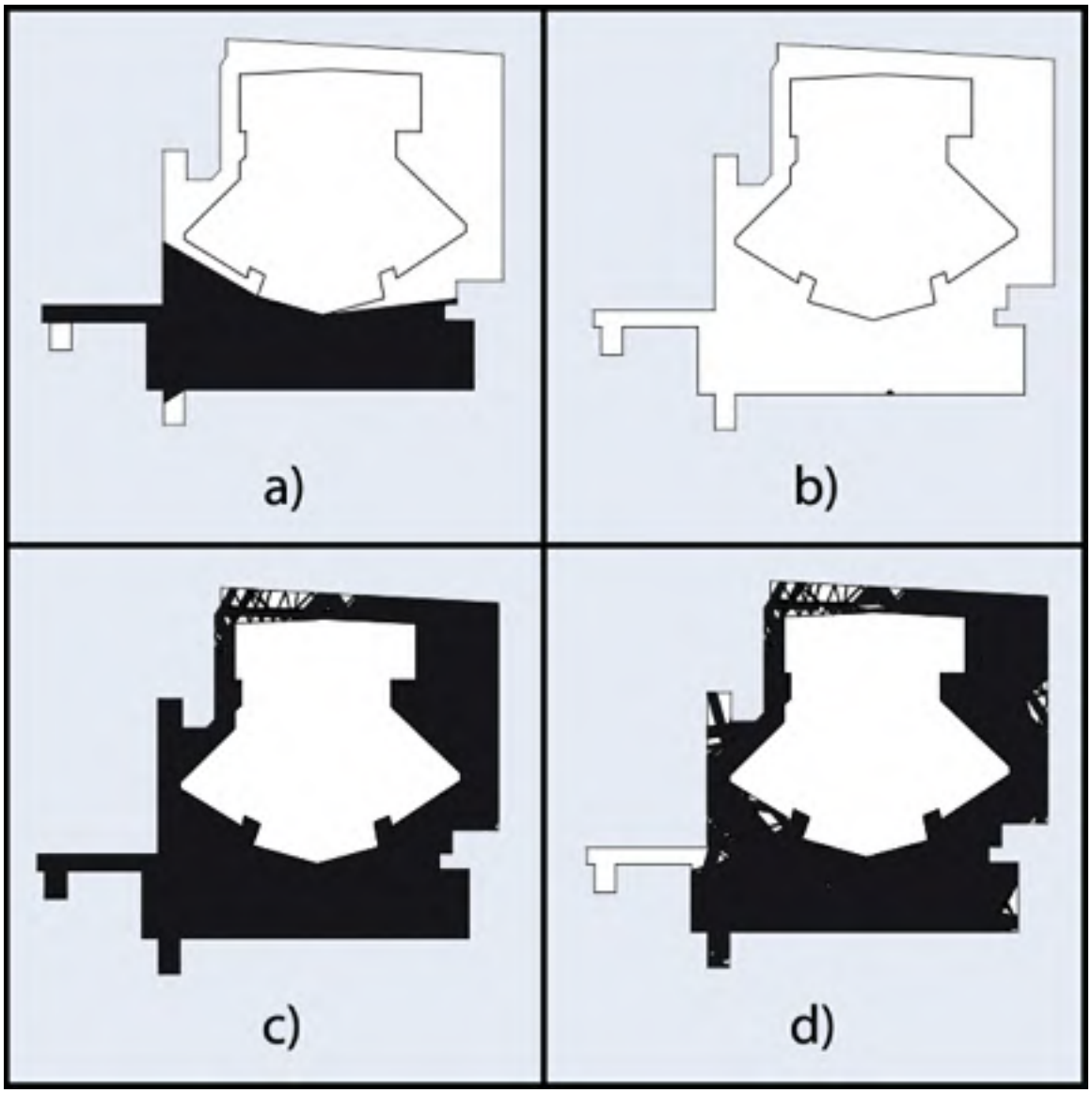

Figure 4.12 Coverage for different visibility and base stations combinations.

Improving our ray tree structure pose some important challenges such as adding diffraction, transmission through walls, diffuse scattering and 3D geometries while maintaining the real-time properties. The regularity of the scatterers surfaces like walls, floors and ceilings mean that ray tubes can be used for many of these model improvements [Son and Myung (1999)].

CONCLUSION

The deployment of cognitive radio devices by the wireless communication industry offers fundamental performance improvements on communication capacity, localization accuracy and coverage.

We have proposed selective relaying schemes for amplify-and-forward and decode-and-forward which achieve near optimal power and subcarrier allocation with perfectly known channel state information. Even in the cognitive radio context with advanced spectrum sensing mechanisms implemented, continuously estimating the changing channel gains in all frequency bands can prove to be a difficult challenge to tackle. An extension of our work could include optimization algorithms for selective relaying and non-relaying subcarriers with only partial channel state information.

Cognitive radios can opportunistically access spectrum holes to increase their link capacity, and significantly increase the number of users and services they can support. By using cooperative communication under low transmission power bounds, not only can mobile cognitive radios transmit in licensed bands without interfering with primary users, but they can also reduce their power consumption. In this work. we have shown how OFDM power and subcarrier resources can be allocated in order to maximize the capacity of wireless communication links.

Cognitive radios can be used for opportunistic access of the radio spectrum by detecting spectrum holes left unused by licensed primary users. We introduce a spectrum holes detection approach, which combines blind modulation classification, angle of arrival estimation and number of sources detection. We perform eigenspace analysis to determine the number of sources, and estimate their angles of arrival (AOA). In addition, we classify detected sources as primary or secondary users with their distinct second-order/ one-conjugate cyclostationarity features. Extensive simulations carried out indicate that the proposed system identifies and locates individual sources correctly, even at -4 dB SNR.

In environments involving a high density of scatterers, several wireless channels experience non-line-of-sight(NLOS) condition, which considerably increases the localization error, even

when the AOA estimate is accurate. We present a real-time localization solver (RTLS) for time-of-arrival (TOA) estimates using ray-tracing methods on the map of the geometry of walls and compare its performance with classical TOA trilateration localization methods. Extensive simulations and field trials for such indoor environments show that our method increases the coverage area from 1.9% of the floor to 82.3 % and the accuracy by a 10-fold factor when compared with trilateration.

As mentioned in section 4.3.2.2, the ideal first path is used as the input time-of-arrival metric in our system. A logical further step to implement our RTLS to practical systems would be to include a non-line-of-sight first path estimation method. Commercial three-dimensional radio ray tracing software is already available for solving the ray-optical approximation to the Maxwell equations including diffraction on edges, transmissions through obstacles and diffusion on rough surfaces. Expanding our RTLS software to include all these elements, while maintaining its real-time property would then be an obvious next step in implementing our RTLS algorithm in commercial RTLS products. Nevertheless, the ray-tracing pre-rendering philosophy and computational geometry basis on which this work is rooted will provide a useful framework for developing a robust RTLS with limited complexity.

In general, this thesis opens the path for a significant amount of future research in order to reach a cognitive radio system capable of jointly localizing, identifying and avoiding to interfere with primary users, in any wireless channel propagation condition. Results presented in this thesis show that steps on this path have been taken, especially in marginally solving each part of this problem, but solving them jointly would be an important step in developing a realistic cognitive radio system using spatial spectrum holes.

Cognitive radios in general are not as widely implemented in commercial applications as its predecessor software-defined radio. Even though current service providers could try to block changes in spectrum access regulations for several years, if a technology capable of opportunistically accessing the radio spectrum without interfering with primary users is developed, it is of my opinion that pressure will be too strong to let some 90 % of its spectrum be wasted by licensed users. Until cognitive radios are indeed widely deployed, the algorithms presented

in this thesis can be adapted for their implementation in other cooperative communication and localization systems.

BIBLIOGRAPHY

Aguado, F., F.P. Fontan, and A. Formella. may 1997. "Indoor and outdoor channel simulator based on ray tracing". In *Vehicular Technology Conference, 1997, IEEE 47th*. p. 2065 -2069 vol.3.

Aguado Agelet, F., A. Formella, J.M. Hernando Rabanos, F. Isasi de Vicente, and F. Perez Fontan. nov 2000. "Efficient ray-tracing acceleration techniques for radio propagation modeling". *Vehicular Technology, IEEE Transactions on*, vol. 49, n. 6, p. 2089 -2104.

Akmouche, W. 1999. "Detection of multicarrier modulations using 4th-order cumulants". *in Proc. IEEE MILCOM*, vol. 1, p. 432-436 vol.1.

Alavi, B. and K. Pahlavan. sept. 2003a. "Bandwidth effect on distance error modeling for indoor geolocation". In *Personal, Indoor and Mobile Radio Communications, 2003. PIMRC 2003. 14th IEEE Proceedings on*. p. 2198 - 2202 vol.3.

Alavi, B. and K. Pahlavan. march 2003b. "Modeling of the distance error for indoor geolocation". In *Wireless Communications and Networking, 2003. WCNC 2003. 2003 IEEE*. p. 668 -672 vol.1.

Alavi, B. and K. Pahlavan. apr 2006. "Modeling of the TOA-based distance measurement error using UWB indoor radio measurements". *Communications Letters, IEEE*, vol. 10, n. 4, p. 275 - 277.

Alavi, B., K. Pahlavan, N.A. Alsindi, and Xinrong Li. sept. 2005. "Indoor Geolocation Distance Error Modeling using UWB Channel Measurements". In *Personal, Indoor and Mobile Radio Communications, 2005. PIMRC 2005. IEEE 16th International Symposium on*. p. 481 -485.

Aronov, B., A. R. Davis, T. K. Dey, S. P. Pal, and D. C. Prasad. 2006. "Visibility with Multiple Reflections". *Discrete & Computational Geometry*, vol. 20, n. 1, p. 61–78.

Athanasiadou, G. and A.R. Nix. jul 2000. "A novel 3-D indoor ray-tracing propagation model: the path generator and evaluation of narrow-band and wide-band predictions". *Vehicular Technology, IEEE Transactions on*, vol. 49, n. 4, p. 1152 -1168.

Atia, M., A. Noureldin, and M. Korenberg. 2012. "Dynamic Online-Calibrated Radio Maps for Indoor Positioning In Wireless Local Area Networks". *Mobile Computing, IEEE Transactions on*, vol. PP, n. 99, p. 1.

Bakanoglu, K., D. Gundiiz, and E. Erkip. nov. 2007. "Dynamic Resource Allocation For The Broadband Relay Channel". In *Signals, Systems and Computers, 2007. ACSSC 2007. Conference Record of the Forty-First Asilomar Conference on*. p. 458 -462.

Bansal, G., O. Duval, and F. Gagnon. may 2010. "Joint Overlay and Underlay Power Allocation Scheme for OFDM-Based Cognitive Radio Systems". In *Vehicular Technology Conference (VTC 2010-Spring), 2010 IEEE 71st*. p. 1 -5.

Bhargava, V. K. and Ekram Hossain, 2007. *Cognitive Wireless Communication Networks*. New York: Springer-Verlag,.

Biglieri, E., J. Proakis, and S. Shamai. oct 1998. “ Fading channels: information-theoretic and communications aspects ”. *Information Theory, IEEE Transactions on*, vol. 44, n. 6, p. 2619 -2692.

Bishop, A. N., Baris Fidan, Kutluyil Dogancay, Brian D.O. Anderson, and Pubudu N. Pathirana. 2008. “ "Exploiting geometry for improved hybrid AOA/TDOA-based localization" ”. *"Signal Processing"*, vol. 88, n. 7, p. 1775–1791.

Bladel, J. G. V., 2007. *Electromagnetic Fields (IEEE Press Series on Electromagnetic Wave Theory)*. Wiley-IEEE Press.

Boostanimehr, H., O. Duval, V.K. Bhargava, and F. Gagnon. may 2010. “ Selective Subcarrier Pairing and Power Allocation for Decode-and-Forward OFDM Relay Systems ”. In *Communications (ICC), 2010 IEEE International Conference on*. p. 1 -5.

Botteron, C., A. Host-Madsen, and M. Fattouche. april 2004. “ Cramer-Rao bounds for the estimation of multipath parameters and mobiles’ positions in asynchronous DS-CDMA systems ”. *Signal Processing, IEEE Transactions on*, vol. 52, n. 4, p. 862 - 875.

Boyd, S. and Lieven Vandenberghe, March 2004. *Convex Optimization*. Cambridge University Press.

Browne, D., J. Medbo, H. Asplund, and Jan-Erik Berg. 2002. “ A simple approach to site sensitive modeling of indoor radio propagation ”. In *Vehicular Technology Conference, 2002. VTC Spring 2002. IEEE 55th*. p. 384 - 388 vol.1.

Bulusu, N., J. Heidemann, and D. Estrin. Oct. 2000. “ GPS-less low-cost outdoor localization for very small devices ”. *IEEE Trans. on Wireless Commun.*, vol. 7, n. 5, p. 28-34.

Cabric, D. and R.W. Brodersen. 11-14 Sept. 2005. “ Physical layer design issues unique to cognitive radio systems ”. *in Proc, IEEE PIMRC*, vol. 2, p. 759-763 vol. 2.

Cabric, D., S.M. Mishra, and R.W. Brodersen. nov. 2004. “ Implementation issues in spectrum sensing for cognitive radios ”. In *Signals, Systems and Computers, 2004. Conference Record of the Thirty-Eighth Asilomar Conference on*. p. 772 - 776 Vol.1.

Cafferty, J. J. and Saipradeep Venkatraman, aug 2004. *Signal Processing for Mobile Communications Handbook*, chapter 21. CRC, éd. 1.

Caffery, J, J. and G.L. Stuber. May 1998. “ Subscriber location in CDMA cellular networks ”. *IEEE Trans. Veh. Technol.*, vol. 47, n. 2, p. 406-416.

Caire, G., G. Taricco, and E. Biglieri. jul 1999. “ Optimum power control over fading channels ”. *Information Theory, IEEE Transactions on*, vol. 45, n. 5, p. 1468 -1489.

Cesbron, F. and R. Arnott. aug 1998. “Locating GSM mobiles using antenna array”. *Electronics Letters*, vol. 34, n. 16, p. 1539 -1540.

Chan, Y.-T., Wing-Yue Tsui, Hing-Cheung So, and Pak chung Ching. jan. 2006. “Time-of-arrival based localization under NLOS conditions”. *Vehicular Technology, IEEE Transactions on*, vol. 55, n. 1, p. 17 - 24.

Chen, H., Gang Wang, Zizhuo Wang, H.C. So, and Vincent. Poor. january 2012. “Non-Line-of-Sight Node Localization Based on Semi-Definite Programming in Wireless Sensor Networks”. *Wireless Communications, IEEE Transactions on*, vol. 11, n. 1, p. 108 -116.

Chen, Z., H.L. Bertoni, and A. Delis. jan. 2004. “Progressive and approximate techniques in ray-tracing-based radio wave propagation prediction models”. *Antennas and Propagation, IEEE Transactions on*, vol. 52, n. 1, p. 240 - 251.

Cisco Systems Inc. June 2010. *Cisco Wireless Control System Configuration Guide*, éd. Software Release 7.0. <http://www.cisco.com>.

Clarke, A. 2002. “A Reaction Diffusion Model for Wireless Indoor Propagation”. Master of science in computer science, University of Dublin, 63 p.

Coco, S., A. Laudani, and L. Mazzurco. march 2004. “A novel 2-D ray tracing procedure for the localization of EM field sources in urban environment”. *Magnetics, IEEE Transactions on*, vol. 40, n. 2, p. 1132 - 1135.

Cordeiro, C., Kiran Challapali, Dagnachew Birru, and Sai Shankar N. 2005. “IEEE 802.22: the first worldwide wireless standard based on cognitive radios”. In *in Proc. IEEE Int. Symp. New Frontiers Dynamic Spectr. Access Networks*. p. 328–337.

Cover, T. and A.E. Gamal. sep 1979. “Capacity theorems for the relay channel”. *Information Theory, IEEE Transactions on*, vol. 25, n. 5, p. 572 - 584.

Dandawate, A. and G.B. Giannakis. Sep 1994. “Statistical tests for presence of cyclostationarity”. *IEEE Trans. Signal Processing*, vol. 42, n. 9, p. 2355-2369.

Degli-Esposti, V., F. Fuschini, E. M. Vitucci, and G. Falciasecca. jan. 2007. “Measurement and Modelling of Scattering From Buildings”. *Antennas and Propagation, IEEE Transactions on*, vol. 55, n. 1, p. 143 -153.

del Coso, A. and C. Ibars. 28 - november 1, 2005. “Capacity of Decode-and-forward Cooperative Links with Full Channel State Information”. In *Signals, Systems and Computers, 2005. Conference Record of the Thirty-Ninth Asilomar Conference on*. p. 1514 - 1518.

Del Coso, A. and C. Ibars. april 2009. “Linear Relaying for the Gaussian multiple-access and broadcast channels”. *Wireless Communications, IEEE Transactions on*, vol. 8, n. 4, p. 2024 -2035.

Denis, B., L. Ouvry, B. Uguen, and F. Tchoffo-Talom. sept. 2005. "Advanced Bayesian filtering techniques for UWB tracking systems in indoor environments". In *Ultra-Wideband, 2005. ICU 2005. 2005 IEEE International Conference on*.

Dévai, F. L. 1995. "On the Complexity of Some Geometric Intersection Problems". *Journal of Computing and Information*, vol. 1, p. 333–352.

Dobre, O., A. Abdi, Y. Bar-Ness, and W. Su. april 2007. "Survey of automatic modulation classification techniques: classical approaches and new trends". *Communications, IET*, vol. 1, n. 2, p. 137 -156.

Durgin, G., T.S. Rappaport, and D.A. de Wolf. jun 2002. "New analytical models and probability density functions for fading in wireless communications". *Communications, IEEE Transactions on*, vol. 50, n. 6, p. 1005 -1015.

Duval, O., A. Punchihewa, F. Gagnon, C. Despins, and V.K. Bhargava. 30 2008-dec. 4 2008. "Blind Multi-Sources Detection and Localization for Cognitive Radio". In *Global Telecommunications Conference, 2008. IEEE GLOBECOM 2008. IEEE*. p. 1 -5.

Duval, O., Z. Hasan, E. Hossain, F. Gagnon, and V. Bhargava. april 2010. "Subcarrier selection and power allocation for amplify-and-forward relaying over OFDM links". *Wireless Communications, IEEE Transactions on*, vol. 9, n. 4, p. 1293 -1297.

Duval, O., G. Gagnon, and F. Gagnon. 2012. "Real-Time Localization Solver with Linear Complexity Ray-Tracing Under NLOS Conditions". *Submitted to Wireless Communications, IEEE Transactions on*.

El-Kafrawy, K., M. Youssef, A. El-Keyi, and A. Naguib. sept. 2010. "Propagation Modeling for Accurate Indoor WLAN RSS-Based Localization". In *Vehicular Technology Conference Fall (VTC 2010-Fall), 2010 IEEE 72nd*. p. 1 -5.

Farhadi, G. and N.C. Beaulieu. may 2008. "Ergodic Capacity Analysis of Wireless Relaying Systems In Rayleigh Fading". In *Communications, 2008. ICC '08. IEEE International Conference on*. p. 3730 -3735.

Fuschini, F., H. El-Sallabi, V. Degli-Esposti, L. Vuokko, D. Guiducci, and P. Vainikainen. march 2008. "Analysis of Multipath Propagation in Urban Environment Through Multidimensional Measurements and Advanced Ray Tracing Simulation". *Antennas and Propagation, IEEE Transactions on*, vol. 56, n. 3, p. 848 -857.

Gentile, C., A. Judson Braga, and Alfred Kik. January 2008. "A comprehensive evaluation of joint range and angle estimation in indoor ultrawideband location systems". *EURASIP J. Wirel. Commun. Netw.*, vol. 2008, p. 36:1–36:11.

Gezici, S., Zhi Tian, G.B. Giannakis, H. Kobayashi, A.F. Molisch, H.V. Poor, and Z. Sahinoglu. july 2005. "Localization via ultra-wideband radios: a look at positioning aspects for future sensor networks". *Signal Processing Magazine, IEEE*, vol. 22, n. 4, p. 70 - 84.

Ghosh, S., 2007. *Visibility Algorithms in the Plane*. New York, NY, USA : Cambridge University Press.

Godara, L. C., 2004. *Smart Antennas*. CRC.

Goldsmith, A. and P.P. Varaiya. nov 1997. "Capacity of fading channels with channel side information". *Information Theory, IEEE Transactions on*, vol. 43, n. 6, p. 1986 -1992.

Grubisic, S., W.P. Carpes, C.B. Lima, and P. Kuo-Peng. april 2006. "Ray-tracing propagation model using image theory with a new accurate approximation for transmitted rays through walls". *Magnetics, IEEE Transactions on*, vol. 42, n. 4, p. 835 -838.

Gui, B. and Leonard J. Cimini, Jr. 2008. "Bit loading algorithms for cooperative OFDM systems". *EURASIP J. Wirel. Commun. Netw.*, vol. 2008, n. 2, p. 1–9.

Gunduz, D. and E. Erkip. april 2007. "Opportunistic cooperation by dynamic resource allocation". *Wireless Communications, IEEE Transactions on*, vol. 6, n. 4, p. 1446 -1454.

Haeberlen, A., Eliot Flannery, Andrew M. Ladd, Algis Rudys, Dan S. Wallach, and Lydia E. Kavraki. 2004. "Practical robust localization over large-scale 802.11 wireless networks". In *Proceedings of the 10th annual international conference on Mobile computing and networking*. (New York, NY, USA 2004), p. 70–84. ACM.

Hammerstrom, I. and A. Wittneben. june 2006. "On the Optimal Power Allocation for Nonregenerative OFDM Relay Links". In *Communications, 2006. ICC '06. IEEE International Conference on*. p. 4463 -4468.

Hammerstrom, I. and A. Wittneben. August 2007. "Power Allocation Schemes for Amplify-and-Forward MIMO-OFDM Relay Links". *Wireless Communications, IEEE Transactions on*, vol. 6, n. 8, p. 2798-2802.

Hasna, M. and M.-S. Alouini. April 2003. "Optimal power allocation for relayed transmissions over Rayleigh fading channels". In *Vehicular Technology Conference, 2003. VTC 2003-Spring. The 57th IEEE Semiannual*. p. 2461-2465 vol.4.

Haykin, S. 2005. "Cognitive radio: brain-empowered wireless communications". *Select Areas Commun., IEEE J.*, vol. 23, n. 2, p. 201–220.

Heidari, M., N.A. Alsindi, and K. Pahlavan. july 2009. "UDP identification and error mitigation in toa-based indoor localization systems using neural network architecture". *Wireless Communications, IEEE Transactions on*, vol. 8, n. 7, p. 3597 -3607.

Hoppe, R., G. Wölfle, and F.M. Landstorfer. 1999. "Fast 3-D Ray Tracing for the Planning of Microcells by Intelligent Preprocessing of the Data Base". In *of the Database," in 3rd European Personal and Mobile Communications Conference (EPMCC*.

Hoppe, R., P. Wertz, F. M. Landstorfer, and G. Wölfle. 2003. "Advanced ray-optical wave propagation modelling for urban and indoor scenarios including wideband properties". *European Transactions on Telecommunications*, vol. 14, n. 1, p. 61–69.

Host-Madsen, A. and J. Zhang. june 2005. "Capacity bounds and power allocation for wireless relay channels". *Information Theory, IEEE Transactions on*, vol. 51, n. 6, p. 2020 -2040.

Hsu, C.-N., Hsuan-Jung Su, and Pin-Hsun Lin. jan. 2011. "Joint Subcarrier Pairing and Power Allocation for OFDM Transmission With Decode-and-Forward Relaying". *Signal Processing, IEEE Transactions on*, vol. 59, n. 1, p. 399 -414.

Hu, J. and T.M. Duman. nov. 2007. "Frequency Selective Fading Relay Channels: Information Rates and Turbo Coding". In *Global Telecommunications Conference, 2007. GLOBECOM '07. IEEE.* p. 1653 -1657.

Hu, O., Fuchun Zheng, and M. Faulkner. 1999a. "Detecting the number of signals using antenna array: a single threshold solution". In *Signal Processing and Its Applications, 1999. ISSPA '99. Proceedings of the Fifth International Symposium on*. p. 905 -908 vol.2.

Hu, O., Fuchun Zheng, and M. Faulkner. 1999b. "Detecting the number of signals using antenna array: a single threshold solution". *in Proc. ISSPA*, vol. 2, p. 905-908 vol.2.

Humphrey, D. and M. Hedley. may 2008. "Super-Resolution Time of Arrival for Indoor Localization". In *Communications, 2008. ICC '08. IEEE International Conference on*. p. 3286 -3290.

Huschka, T. sep 1994. "Ray tracing models for indoor environments and their computational complexity". In *Personal, Indoor and Mobile Radio Communications, 1994. Wireless Networks - Catching the Mobile Future., 5th IEEE International Symposium on*. p. 486 -490 vol.2.

Iskander, M. and Zhengqing Yun. mar 2002. "Propagation prediction models for wireless communication systems". *Microwave Theory and Techniques, IEEE Transactions on*, vol. 50, n. 3, p. 662 -673.

Issariyakul, T. and V. Krishnamurthy. feb. 2009. "Amplify-and-Forward Cooperative Diversity Wireless Networks: Model, Analysis, and Monotonicity Properties". *Networking, IEEE/ACM Transactions on*, vol. 17, n. 1, p. 225 -238.

Ize, T., P. Shirley, and S. Parker. sept. 2007. "Grid Creation Strategies for Efficient Ray Tracing". In *Interactive Ray Tracing, 2007. RT '07. IEEE Symposium on*. p. 27 -32.

Ji, Z., Bin-Hong Li, Hao-Xing Wang, Hsing-Yi Chen, and T.K. Sarkar. apr 2001. "Efficient ray-tracing methods for propagation prediction for indoor wireless communications". *Antennas and Propagation Magazine, IEEE*, vol. 43, n. 2, p. 41 -49.

Jia, T. and R.M. Buehrer. sept. 2011. "A Set-Theoretic Approach to Collaborative Position Location for Wireless Networks". *Mobile Computing, IEEE Transactions on*, vol. 10, n. 9, p. 1264 -1275.

Jingmei, Z., Zhang Qi, Shao Chunju, Wang Ying, Zhang Ping, and Zhang Zhang. May 2004. "Adaptive optimal transmit power allocation for two-hop non-regenerative wireless relaying system". In *Vehicular Technology Conference, 2004. VTC 2004-Spring. 2004 IEEE 59th*. p. 1213-1217 Vol.2.

Jose, J., Lei Ying, and S. Vishwanath. oct. 2009. "On the stability region of amplify-and-forward cooperative relay networks". In *Information Theory Workshop, 2009. ITW 2009. IEEE*. p. 620 -624.

Jourdan, D., D. Dardari, and M. Win. april 2008. "Position error bound for UWB localization in dense cluttered environments". *Aerospace and Electronic Systems, IEEE Transactions on*, vol. 44, n. 2, p. 613 -628.

Kanatas, A., I.D. Kountouris, G.B. Kostaras, and P. Constantinou. feb 1997. "A UTD propagation model in urban microcellular environments". *Vehicular Technology, IEEE Transactions on*, vol. 46, n. 1, p. 185 -193.

Kaya, A., L. Greenstein, D. Chizhik, R. Valenzuela, and N. Moayeri. march 2007. "Emitter Localization and Visualization (ELVIS): A Backward Ray Tracing Algorithm for Locating Emitters". In *Information Sciences and Systems, 2007. CISS '07. 41st Annual Conference on*. p. 376 -381.

Kaya, A., L.J. Greenstein, and W. Trappe. august 2009. "Characterizing indoor wireless channels via ray tracing combined with stochastic modeling". *Wireless Communications, IEEE Transactions on*, vol. 8, n. 8, p. 4165 -4175.

Keller, J. B. September 1978. "Rays, waves and asymptotics". *Bulletin of the American Mathematical Society*, vol. 84, n. 5, p. 727–750.

Kikuchi, S., Akira Sano, and Hiroyuki Tsuji. January 2006. "Blind mobile positioning in urban environment based on ray-tracing analysis". *EURASIP J. Appl. Signal Process.*, vol. 2006, p. 154–154.

Kimpe, M., H. Leib, O. Maquelin, and T.H. Szymanski. jan/feb 1999. "Fast computational techniques for indoor radio channel estimation". *Computing in Science Engineering*, vol. 1, n. 1, p. 31 -41.

Klukas, R. and M. Fattouche. feb 1998. "Line-of-sight angle of arrival estimation in the outdoor multipath environment". *Vehicular Technology, IEEE Transactions on*, vol. 47, n. 1, p. 342 -351.

Kouyoumjian, R. and P.H. Pathak. nov. 1974. "A uniform geometrical theory of diffraction for an edge in a perfectly conducting surface". *Proceedings of the IEEE*, vol. 62, n. 11, p. 1448 - 1461.

Kuhn, H. W. 1955. "The Hungarian method for the assignment problem". *Naval Research Logistic Quarterly*, vol. 2, p. 83–97.

Laneman, J. and G.W. Wornell. 2000. "Energy-efficient antenna sharing and relaying for wireless networks". In *Wireless Communications and Networking Confernce, 2000. WCNC. 2000 IEEE*. p. 7 -12 vol.1.

Laneman, J., D.N.C. Tse, and G.W. Wornell. Dec. 2004. "Cooperative diversity in wireless networks: Efficient protocols and outage behavior". *Information Theory, IEEE Transactions on*, vol. 50, n. 12, p. 3062-3080.

Lawton, M. and J.P. McGeehan. nov 1994. "The application of a deterministic ray launching algorithm for the prediction of radio channel characteristics in small-cell environments". *Vehicular Technology, IEEE Transactions on*, vol. 43, n. 4, p. 955 -969.

Li, G. and Hui Liu. nov. 2006. "Resource Allocation for OFDMA Relay Networks With Fairness Constraints". *Selected Areas in Communications, IEEE Journal on*, vol. 24, n. 11, p. 2061 -2069.

Li, L. and A.J. Goldsmith. mar 2001. "Capacity and optimal resource allocation for fading broadcast channels .I. Ergodic capacity". *Information Theory, IEEE Transactions on*, vol. 47, n. 3, p. 1083 -1102.

Li, X. and K. Pahlavan. jan. 2004. "Super-resolution TOA estimation with diversity for indoor geolocation". *Wireless Communications, IEEE Transactions on*, vol. 3, n. 1, p. 224 - 234.

Li, Y., Wenbo Wang, Jia Kong, Wei Hong, Xing Zhang, and Mugen Peng. May 2008. "Power Allocation and Subcarrier Pairing in OFDM-Based Relaying Networks". In *Communications, 2008. ICC '08. IEEE International Conference on*. p. 2602-2606.

Liang, Y. and V.V. Veeravalli. sept. 2005. "Gaussian Orthogonal Relay Channels: Optimal Resource Allocation and Capacity". *Information Theory, IEEE Transactions on*, vol. 51, n. 9, p. 3284 - 3289.

Liang, Y. and G. Kramer. oct. 2007. "Rate Regions for Relay Broadcast Channels". *Information Theory, IEEE Transactions on*, vol. 53, n. 10, p. 3517 -3535.

Liang, Y., V.V. Veeravalli, and H.V. Poor. oct. 2007. "Resource Allocation for Wireless Fading Relay Channels: Max-Min Solution". *Information Theory, IEEE Transactions on*, vol. 53, n. 10, p. 3432 -3453.

Louveaux, J., R.T. Duran, and L. Vandendorpe. 31 2008-april 4 2008. "Efficient algorithm for optimal power allocation in OFDM transmission with relaying". In *Acoustics, Speech and Signal Processing, 2008. ICASSP 2008. IEEE International Conference on*. p. 3257 -3260.

Luo, F.-L., 2011. *Digital Front-End in Wireless Communications and Broadcasting: Circuits and Signal Processing*. Cambridge University Press.

Ma, Y., Na Yi, and R. Tafazolli. july 2008. "Bit and Power Loading for OFDM-Based Three-Node Relaying Communications". *Signal Processing, IEEE Transactions on*, vol. 56, n. 7, p. 3236 -3247.

Marina, N., A. Kavcic, and N.T. Gaarder. july 2008. "Capacity theorems for relay channels with ISI". In *Information Theory, 2008. ISIT 2008. IEEE International Symposium on*. p. 479 -483.

Mitilineos, S., G.K. Roumeliotis, K.S. Mougiakos, C.N. Capsalis, and S. Thomopoulos. june 2009. "Positioning accuracy enhancement using localization error modeling". In *World of Wireless, Mobile and Multimedia Networks Workshops, 2009. WoWMoM 2009. IEEE International Symposium on a*. p. 1 -5.

Mitola, J. 2000. "An Integrated Agent Architecture for Software Defined Radio". PhD thesis, Royal Inst. Technol.(KTH).

Morelli, C., M. Nicoli, V. Rampa, and U. Spagnolini. april 2007. "Hidden Markov Models for Radio Localization in Mixed LOS/NLOS Conditions". *Signal Processing, IEEE Transactions on*, vol. 55, n. 4, p. 1525 -1542.

Mouhamadou, M., G. Neveux, and P. Vaudon. july 2006. "Simulation of Smart Antenna System using ADS Co-Simulate with Matlab: Direction of Arrival estimation and Interference Canceller". In *Antennas and Propagation Society International Symposium 2006, IEEE*. p. 4545 -4548.

Nabar, R. U., H. Bolcskei, and F. W. Kneubuhler. 2004. "Fading relay channels: performance limits and space-time signal design". *Selected Areas in Communications, IEEE Journal on*, vol. 22, n. 6, p. 1099–1109.

Nasif, A., 2009. *Opportunistic Spectrum Access Using Localization Techniques*. George Mason University.

Nerguizian, C., C. Despins, and S. Affes. march 2006. "Geolocation in mines with an impulse response fingerprinting technique and neural networks". *Wireless Communications, IEEE Transactions on*, vol. 5, n. 3, p. 603 - 611.

Ng, K. H., E. K. Tameh, A. Doufexi, M. Hunukumbure, and A. R. Nix. may 2007. "Efficient Multielement Ray Tracing With Site-Specific Comparisons Using Measured MIMO Channel Data". *Vehicular Technology, IEEE Transactions on*, vol. 56, n. 3, p. 1019 -1032.

Ng, K., E.K. Tameh, and A.R. Nix. sept. 2004. "An advanced multi-element microcellular ray tracing model". In *Wireless Communication Systems, 2004, 1st International Symposium on*. p. 438 - 442.

O'Rourke, J., 1998. *Computational Geometry in C*. éd. 2nd. New York, NY, USA : Cambridge University Press.

Pabst, R., B.H. Walke, D.C. Schultz, P. Herhold, H. Yanikomeroglu, S. Mukherjee, H. Viswanathan, M. Lott, W. Zirwas, M. Dohler, H. Aghvami, D.D. Falconer, and G.P. Fettweis. Sept. 2004. "Relay-based deployment concepts for wireless and mobile broadband radio". *Communications Magazine, IEEE*, vol. 42, n. 9, p. 80-89.

Pahlavan, K. and A.H. Levesque, 2005. *Wireless information networks*. Wiley series in telecommunications and signal processing. John Wiley.

Pahlavan, K., Ferit O. Akgul, Mohammad Heidari, Ahmad Hatami, John M. Elwell, and Robert D. Tingley. dec. 2006. "Indoor geolocation in the absence of direct path". *Wireless Communications, IEEE*, vol. 13, n. 6, p. 50 -58.

Patwari, N., J.N. Ash, S. Kyperountas, III Hero, A.O., R.L. Moses, and N.S. Correal. july 2005. "Locating the nodes: cooperative localization in wireless sensor networks". *Signal Processing Magazine, IEEE*, vol. 22, n. 4, p. 54 - 69.

Pischella, M. and J.-C. Belfiore. may 2008. "Power control in distributed cooperative OFDMA cellular networks". *Wireless Communications, IEEE Transactions on*, vol. 7, n. 5, p. 1900 -1906.

Prasant, S. P. and Dilip Sarkar. 2003. "On multiple connectedness of regions visible due to multiple diffuse reflections". *Computer Research Repository*.

Proakis, J. G., 2000. *Digital Communications*. McGraw-Hill Series in Electrical and Computer Engineering. McGraw-Hill.

Punchihewa, A., O.A. Dobre, S. Rajan, and R. Inkol. sept. 2007. "Cyclostationarity-based Algorithm for Blind Recognition of OFDM and Single Carrier Linear Digital Modulations". In *Personal, Indoor and Mobile Radio Communications, 2007. PIMRC 2007. IEEE 18th International Symposium on*. p. 1 -5.

Punchihewa, A., O. A. Dobre, S. Rajan, and R. Inkol. 3-7 Sept. 2007. "Cyclostationarity-based Algorithm for Blind Recognition of OFDM and Single Carrier Linear Digital Modulations". *in Proc. PIMRC*, p. 1-5.

Qi, Y., H. Kobayashi, and H. Suda. march 2006. "Analysis of wireless geolocation in a non-line-of-sight environment". *Wireless Communications, IEEE Transactions on*, vol. 5, n. 3, p. 672 - 681.

Qi, Z., Zhang Jingmei, Shao Chunju, Wang Ying, Zhang Ping, and Hu Rong. May 2004. "Power allocation for regenerative relay channel with Rayleigh fading". In *Vehicular Technology Conference, 2004. VTC 2004-Spring. 2004 IEEE 59th*. p. 1167-1171 Vol.2.

Rankov, B. and Armin Wittneben. february 2007. "Spectral efficient protocols for half-duplex fading relay channels". *Selected Areas in Communications, IEEE Journal on*, vol. 25, n. 2, p. 379 -389.

Rautiainen, T., R. Hoppe, and G. Wölfle. sept. 2007. "Measurements and 3D Ray Tracing Propagation Predictions of Channel Characteristics in Indoor Environments". In *Personal, Indoor and Mobile Radio Communications, 2007. PIMRC 2007. IEEE 18th International Symposium on*. p. 1 -5.

Rhee, W. and J.M. Cioffi. 2000. "Increase in capacity of multiuser OFDM system using dynamic subchannel allocation". In *Vehicular Technology Conference Proceedings, 2000. VTC 2000-Spring Tokyo. 2000 IEEE 51st*. p. 1085 -1089 vol.2.

Richter, A. May 2005. "Estimation of Radio Channel Parameters: Models and Algorithms". PhD thesis, TU Ilmenau, Ilmenau, Germany.

Sack, J.-R. and J. Urrutia, 2000. *Handbook of computational geometry*. Amsterdam, The Netherlands, The Netherlands : North-Holland Publishing Co.

Saleh, A. and R. Valenzuela. february 1987. "A Statistical Model for Indoor Multipath Propagation". *Selected Areas in Communications, IEEE Journal on*, vol. 5, n. 2, p. 128 -137.

Samet, H. and Robert E. Webber. May 1988. "Hierarchical Data Structures and Algorithms for Computer Graphics". *IEEE Comput. Graph. Appl.*, vol. 8, n. 3, p. 48–68.

Seow, C. K. and Soon Yim Tan. may 2008. "Non-Line-of-Sight Localization in Multipath Environments". *Mobile Computing, IEEE Transactions on*, vol. 7, n. 5, p. 647 -660.

Sieskul, B., Feng Zheng, and T. Kaiser. nov. 2009. "On the Effect of Shadow Fading on Wireless Geolocation in Mixed LoS/NLoS Environments". *Signal Processing, IEEE Transactions on*, vol. 57, n. 11, p. 4196 -4208.

Siriwongpairat, W., T. Himsoon, Weifeng Su, and K.J.R. Liu. april 2006. "Optimum threshold-selection relaying for decode-and-forward cooperation protocol". In *Wireless Communications and Networking Conference, 2006. WCNC 2006. IEEE*. p. 1015 -1020.

Son, H.-W. and Noh-Hoon Myung. aug 1999. "A deterministic ray tube method for microcellular wave propagation prediction model". *Antennas and Propagation, IEEE Transactions on*, vol. 47, n. 8, p. 1344 -1350.

Tayebi, A., J. Gomez, F. M. Saez de Adana, and O. Gutierrez. mar. 2009. "The application of ray-tracing to mobile localization using the direction of arrival and received strength in multipath indoor environments". *Progress in Electromagnetics Research*, vol. 91, p. 1–15.

Tsalolikhin, E., I. Bilik, and N. Blaunstein. march 2011. "A Single-Base-Station Localization Approach Using a Statistical Model of the NLOS Propagation Conditions in Urban Terrain". *Vehicular Technology, IEEE Transactions on*, vol. 60, n. 3, p. 1124 -1137.

Tseng, P. and K. Feng. 2012. "Geometry-Assisted Localization Algorithms for Wireless Networks". *Mobile Computing, IEEE Transactions on*, vol. PP, n. 99, p. 1.

Ullmo, D. and H.U. Baranger. may 1999. "Wireless propagation in buildings: a statistical scattering approach". *Vehicular Technology, IEEE Transactions on*, vol. 48, n. 3, p. 947 -955.

Van Bilsen, A. and Egbert Stolk. jun 2008. "Solving Error Problems in Visibility Analysis for Urban Environments by Shifting From a Discrete to a Continuous Approach". *International Conference on Computational Sciences and Its Applications ICCSA*, p. 523–528.

Van Der Meulen, E. C. 1971. "Three-terminal communication channels". *Adv. Appl. Probab.*, vol. 3, p. 120–154.

Vandendorpe, L., R.T. Duran, J. Louveaux, and A. Zaidi. May 2008a. "Power Allocation for OFDM Transmission with DF Relaying". *Communications, 2008. ICC '08. IEEE International Conference on*, p. 3795-3800.

Vandendorpe, L., R.T. Duran, J. Louveaux, and A. Zaidi. May 2008b. "Power Allocation for OFDM Transmission with DF Relaying". *Communications, 2008. ICC '08. IEEE International Conference on*, p. 3795-3800.

Wagen, J.-F. and Karim Rizk. September 2003. "Radiowave propagation, building databases, and GIS: anything in common? A radio engineer's viewpoint". *Environment and Planning B: Planning and Design*, vol. 30, n. 5, p. 767-787.

Wahl, R., O. Staebler, and M.J. Gallardo. july 2007. "Requirements for Indoor Building Databases to increase the Accuracy of the Propagation Results". In *Mobile and Wireless Communications Summit, 2007. 16th IST*. p. 1 -4.

Walfisch, J. and H.L. Bertoni. dec 1988. "A theoretical model of UHF propagation in urban environments". *Antennas and Propagation, IEEE Transactions on*, vol. 36, n. 12, p. 1788 -1796.

Wang, B. and Lindong Ge. 23-26 Sept. 2005. "A novel algorithm for identification of OFDM signal". *in Proc. WiMob*, vol. 1, p. 261-264.

Wölfle, G., B.E. Gschwendtner, and F.M. Landstorfer. may 1997. "Intelligent ray tracing-a new approach for field strength prediction in microcells". In *Vehicular Technology Conference, 1997, IEEE 47th*. p. 790 -794 vol.2.

Wölfle, G., Philipp Wertz, and Friedrich M. Landstorfer. 1999. "Performance, Accuracy and Generalization Capability of Indoor Propagation Models in Different Types of Buildings".

Wong, C. Y., R.S. Cheng, K.B. Lataief, and R.D. Murch. oct 1999. "Multiuser OFDM with adaptive subcarrier, bit, and power allocation". *Selected Areas in Communications, IEEE Journal on*, vol. 17, n. 10, p. 1747 -1758.

Wonka, P., Michael Wimmer, and Dieter Schmalstieg. 2000. "Visibility Preprocessing with Occluder Fusion for Urban Walkthroughs". In *Rendering Techniques 2000 (Proceedings Eurographics Workshop on Rendering)*.

Yang, C.-F., Boau-Cheng Wu, and Chuen-Jyi Ko. jun 1998. “A ray-tracing method for modeling indoor wave propagation and penetration”. *Antennas and Propagation, IEEE Transactions on*, vol. 46, n. 6, p. 907 -919.

Yang, W. and Zhang Naitong. nov. 2005. “A New Semi-Deterministic Multipath Model for UWB Indoor Los Environments”. In *3G and Beyond, 2005 6th IEE International Conference on*. p. 1 -4.

Ying, W., Qu Xin-chun, Wu Tong, and Liu Bao-ling. April 2007. “Power Allocation and Subcarrier Pairing Algorithm for Regenerative OFDM Relay System”. *Vehicular Technology Conference, 2007. VTC2007-Spring. IEEE 65th*, p. 2727-2731.

Yousef, N. R. and Ali H. Sayed. 08 2002. “Method and Apparatus for Resolving Multipath Components for Wireless Location Finding, US Patent 7068742”.

Yu, K., Ian Sharp, and Y. Jay Guo, 2009. *Multipath Mitigation*, p. 249–287. John Wiley & Sons, Ltd. ISBN 9780470747988. doi: 10.1002/9780470747988.ch10. <http://dx.doi.org/10.1002/9780470747988.ch10>.

Yu, W. and R. Lui. july 2006. “Dual methods for nonconvex spectrum optimization of multicarrier systems”. *Communications, IEEE Transactions on*, vol. 54, n. 7, p. 1310 -1322.

Zhang, Q.-T., K.M. Wong, P.C. Yip, and J.P. Reilly. oct 1989. “Statistical analysis of the performance of information theoretic criteria in the detection of the number of signals in array processing”. *Acoustics, Speech and Signal Processing, IEEE Transactions on*, vol. 37, n. 10, p. 1557 -1567.

Zhang, Q.-T., K.M. Wong, P.C. Yip, and J.P. Reilly. Oct 1989. “Statistical analysis of the performance of information theoretic criteria in the detection of the number of signals in array processing”. *IEEE Trans. Signal Processing], IEEE Transactions on*, vol. 37, n. 10, p. 1557-1567.

Zhang, Y., Y. Hwang, and R.G. Kouyoumjian. sep 1998. “Ray-optical prediction of radio-wave propagation characteristics in tunnel environments. 2. Analysis and measurements”. *Antennas and Propagation, IEEE Transactions on*, vol. 46, n. 9, p. 1337 -1345.

Zhao, F., Wenbing Yao, C.C. Logothetis, and Yonghua Song. sept. 2006a. “Comparison of Super-Resolution Algorithms for TOA Estimation in Indoor IEEE 802.11 Wireless LANs”. In *Wireless Communications, Networking and Mobile Computing, 2006. WiCOM 2006.International Conference on*. p. 1 -5.

Zhao, Y., Jeffrey H. Reed, Shiwen Mao, and Kyung K. Bae. sept. 2006b. “Overhead Analysis for Radio Environment Mapenabled Cognitive Radio Networks”. In *Networking Technologies for Software Defined Radio Networks, 2006. SDR ’06.1st IEEE Workshop on*. p. 18 -25.

Zhao, Y., L. Morales, J. Gaeddert, K.K. Bae, Jung-Sun Um, and J.H. Reed. april 2007a. "Applying Radio Environment Maps to Cognitive Wireless Regional Area Networks". In *New Frontiers in Dynamic Spectrum Access Networks, 2007. DySPAN 2007. 2nd IEEE International Symposium on*. p. 115 -118.

Zhao, Y., David Raymond, Claudio da Silva, Jeffrey H. Reed, and Scott F. Midkiff. oct. 2007b. "Performance Evaluation of Radio Environment Map-Enabled Cognitive Spectrum-Sharing Networks". In *Military Communications Conference, 2007. MILCOM 2007. IEEE*. p. 1 -7.